The connective KO theory of the Eilenberg-MacLane space $K(\mathbb{Z}/2, 2)$

Donald M. Davis

Abstract. We compute $ko_*(K(\mathbb{Z}/2, 2))$ and $ko^*(K(\mathbb{Z}/2, 2))$, the connective KO-homology and -cohomology groups of the mod 2 Eilenberg-MacLane space $K(\mathbb{Z}/2, 2)$, using the Adams spectral sequence. The work relies heavily on work done several years earlier for the (complex) ku groups by the author and W.S.Wilson. We illustrate an interesting duality relation between the ko-homology and -cohomology groups. We deduce a new result about Stiefel-Whitney classes in Spin manifolds.

Contents

Date: February 15, 2026.

Key words and phrases. Adams spectral sequence, connective KO-theory, Eilenberg-MacLane space, Stiefel-Whitney classes.

2000 *Mathematics Subject Classification*: 55T15, 55N20, 55N15, 57R20.

1. Introduction and overview

Let $\mathbb{Z}_2 = \mathbb{Z}/2$ and let K_2 denote the Eilenberg-MacLane space $K(\mathbb{Z}_2, 2)$. In this paper, we use the Adams spectral sequence (ASS) to compute the connective KO-homology and -cohomology groups $ko_*(K_2)$ and $ko^*(K_2)$. The groups $ko_*(K_2)$ were initially studied long ago in [15] and more recently in [12] because of their close relationship with Stiefel-Whitney classes of Spin-manifolds, but only fragmentary results were obtained. A consequence of our work here is the following new result, which is discussed and proved in Section 17.

Theorem 1.1. *There exists an n-dimensional Spin manifold with the dual Stiefel-Whitney class $\overline{w}_{n-2} \neq 0$ if and only if n is a 2-power ≥ 8.*

Our work here draws heavily from the computation in [11] of the complex analogue $ku_*(K_2)$ and $ku^*(K_2)$, which in turn relied on the connective Morava K-theory groups $k(1)_*(K_2)$ and $k(1)^*(K_2)$ determined in [10]. Our primary focus in [11] was the ku-cohomology groups because of their product structure, but here our primary focus will be on the ko-homology groups, for historical reasons and because of the more familiar form of its ASS. We begin this introduction with a slight reformulation of results of [11] regarding $ku_*(K_2)$. This will enable us to describe the overall structure of $ko_*(K_2)$, and also to see the significant increase in complication of the ko result as compared with ku.

The ku-cohomology groups $ku^*(K_2)$ were a combination of suspensions of three basic types of summands, A_k, B_k, and $S_{k,\ell}$, $1 \leq k < \ell$. It was observed in [11, Section 7] that if $S_{k,\ell}$ is combined with two specific copies of B_k, we obtain something, which we now call $B_{k,\ell}$, that appears both in $ku^*(K_2)$ and, after switching to homology grading, in $ku_*(K_2)$. We denote by $\mathcal{B}_{k,\ell}$ the ko-homology analogue of this combination. The ku-homology analogue of A_k, which we denote by $\mathscr{A}_k$, was pictured when $k = 5$ in [11, Figure 4], which we repeat here as Figure 1.2. Short vertical lines indicate multiplication by 2, short diagonal lines are multiplication by $v \in ku_2$, and the long dashed lines, sometimes slightly curved, are exotic extensions ($\cdot 2$).

Figure 1.2. $\mathscr{A}_5$, the ku-homology analogue of A_5, from [11]

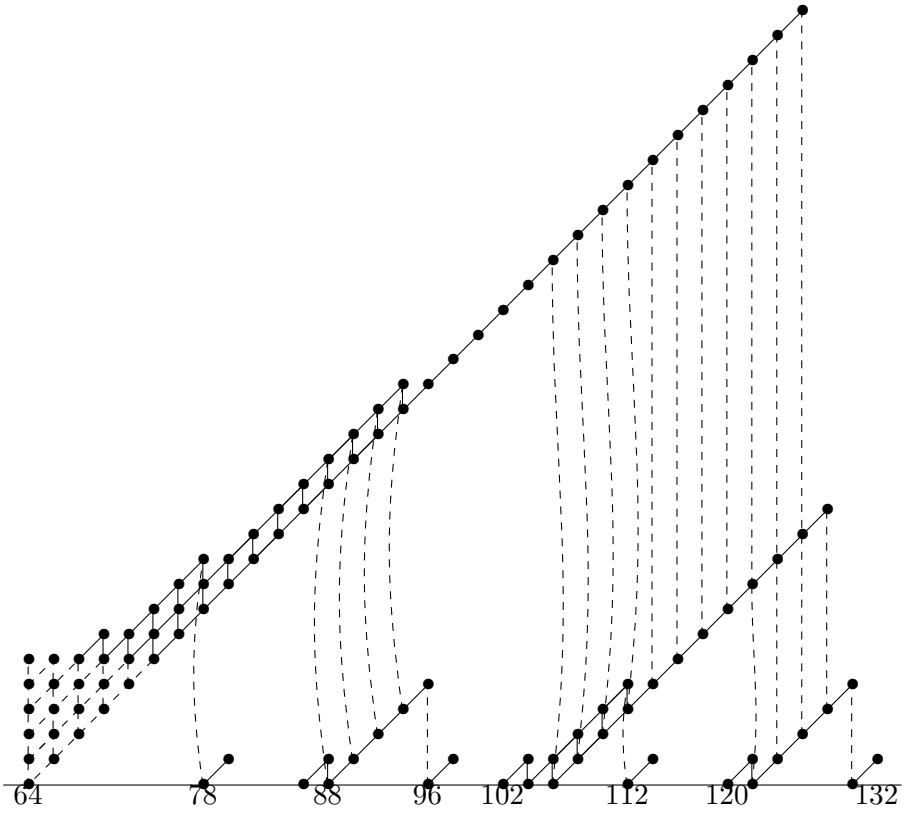

The iterative structure of the ku groups A_k and B_k can be seen by noting that the ku-homology analogue of B_4 is a desuspension of the portion of Figure 1.2 in grading ≥ 102, not including the upper edge, and $\mathscr{A}_4$ can be obtained from that by placing a triangle similar to the one in the lower left corner of the chart, but one level smaller, beneath the classes in grading 102 to 106. The ko-homology analogue of A_k, which we denote by $\mathcal{A}_k$, is much more complicated. We picture $\mathcal{A}_k$ for $1 \leq k \leq 6$ in Section 3, and in Section 4 state several results, 4.1, 4.8, 4.10, 4.18, and 4.21, which give a complete determination of all $\mathcal{A}_k$.

In the ku situation, each $B_{k,\ell}$ could be multiplied by any number of classes z_j, which just amounted to suspending by $\Sigma^{2^{j+2}+2}$ for each. In the ko analogue, multiplying $\mathcal{B}_{k,\ell}$ by z_j suspends by 2^{j+2} but also changes its form. We denote by $z^i\mathcal{B}_{k,\ell}$ the modified form of $\mathcal{B}_{k,\ell}$ after i such changes of form, but without the various $\Sigma^{2^{j+2}}$'s. So z^i can be thought of as a product of i different z_j's, each desuspended by 2^{j+2}. It turns out that $z^4\mathcal{B}_{k,\ell} = \Sigma^8\mathcal{B}_{k,\ell}$. We will describe and illustrate $z^i\mathcal{B}_{k,\ell}$ in Section 5.

We can now state the theorem which, along with the aforementioned descriptions of $\mathcal{A}_k$ and $z^i\mathcal{B}_{k,\ell}$, completely determines $ko_*(K_2)$. This will be proved in Section 11.

Theorem 1.3. *There is an isomorphism of ko_*-modules*

$$ko_*(K_2) \approx \bigoplus_{k\geq 1}\bigoplus_{i\geq 0} \Sigma^{2^{k+2}i}\mathcal{A}_k \oplus \bigoplus_{1\leq k<\ell}\bigoplus_{i,j\geq 0} \Sigma^{2^{k+2}i+2^{\ell+3}j} z^{\alpha(j)}\mathcal{B}_{k,\ell}$$

plus a trivial ko_*-module.

Here and elsewhere, $\alpha(j)$ denotes the number of 1's in the binary expansion of j. The trivial ko_*-module could be calculated, but is not of interest. It is discussed at the end of Section 11.

In Section 18, we determine the ko-cohomology groups, $ko^*(K_2)$, and discuss the following interesting duality theorem.

Theorem 1.4. *There is an isomorphism of ko_*-modules*

$$ko_*(K_2) \approx (ko^{*+6}(K_2))^\vee,$$

where $M^\vee = \mathrm{Hom}(M, \mathbb{Z}/2^\infty)$, the Pontryagin dual, localized at 2.

In the first seven sections, we describe our results in several ways. In Section 8, we outline the proof, which occupies the subsequent seven sections. At the end of the paper, we discuss the application to Stiefel-Whitney classes of Spin manifolds, and the adaptation to ko-cohomology groups of K_2.

We thank the referee for comments which led to improvement of exposition.

2. Charts, filtrations, and edges

Our computation of $ko_*(K_2)$ is merely a determination of the ASS with $E_2 = \mathrm{Ext}_{A(1)}(H^*K_2, \mathbb{Z}_2)$. (See Section 10.) However, the differentials and extensions in this spectral sequence are very complicated, and for ease in understanding and displaying them, we frequently increase filtrations of elements. We call the resulting diagrams "charts," and use the term "filtration" to refer to the vertical component of an element in the resulting chart.

We illustrate with the determination of the chart $\mathcal{A}_4$ in grading ≤ 43. The first three $A(1)$-modules in forming $\mathcal{A}_4$ are $\Sigma^{32}\mathbb{Z}_2 \oplus \Sigma^{32}NU \oplus \Sigma^{40}\widetilde{\mathcal{M}}_4$, where NU and its Ext are given in Figure 12.1, and $\widetilde{\mathcal{M}}_4 = \langle x_1, \mathrm{Sq}^1 x_1\rangle = H^*(\Sigma M(2))$. In the left side of Figure 12.3, $\mathrm{Ext}_{A(1)}(\Sigma^{32}\mathbb{Z}_2 \oplus \Sigma^{32}NU, \mathbb{Z}_2)$ is shown, along with the d_5-differential between the two summands. There are exotic η-extensions on classes in 35 and 43 implied by (12.2) and an exotic $\cdot 2$ in 42 implied by (14.17). We prefer to elevate the chart for $\Sigma^{32}NU$ by 4 units so that the Adams differential looks like a d_1, and then the η and $\cdot 2$ actions appear nicely as in the chart on the right side of Figure 12.3.

A similar situation occurs when $\mathrm{Ext}_{A(1)}(\Sigma^{40}\widetilde{\mathcal{M}}_4, \mathbb{Z}_2)$ is incorporated, and is pictured in Figure 12.4. There is a d_6-differential into the previously-obtained chart, with implied η and $\cdot 2$ extensions. If we choose to elevate the $\mathrm{Ext}_{A(1)}(\Sigma^{40}\widetilde{\mathcal{M}}_4, \mathbb{Z}_2)$ so that the differential appears as a d_1, as in the middle portion of Figure 12.4, then the η and $\cdot 2$ line up better, resulting in the chart on the right side of Figure 12.4. The resulting chart agrees with the portion of $\mathcal{A}_4$ in grading ≤ 43 in Figure 3.2. Remaining $A(1)$-module summands in forming $\mathcal{A}_4$ account for subsequent changes. This should explain the rationale for our notion of charts, which are modifications of ordinary ASS diagrams.

At the beginning of Section 4, we introduce the term "edge" before it has been defined. The formal definition is in Theorem 4.10, based on the definition of pre-edge in Definition 4.8. Edges are central to our analysis

and descriptions. The list, immediately following Theorem 4.1, of the edges in $\widetilde{\mathcal{A}}_5$, displayed in Figure 3.3, should be useful in understanding edges.

3. Examples of $\mathcal{A}_k$

In this section, we display charts of $\mathcal{A}_k$ for $1 \leq k \leq 6$. We will make much use of these charts in later sections, as models for the general statements and proofs. These are ASS-type charts, but we frequently elevate filtrations of classes in order to better display the ko_*-module structure. In the transition from E_2 to E_∞, there have been many differentials, which are not displayed here. The short vertical lines are multiplication by 2, and short diagonal lines represent multiplication by $\eta \in ko_1$. In Figure 3.1, we depict $\mathcal{A}_1$, $\mathcal{A}_2$, and $\mathcal{A}_3$ on the same set of axes. The classes in grading 8–12 are $\mathcal{A}_2$, and $\mathcal{A}_1$ and $\mathcal{A}_3$ are on the left and right, respectively.

Figure 3.1. $\mathcal{A}_1$, $\mathcal{A}_2$, and $\mathcal{A}_3$

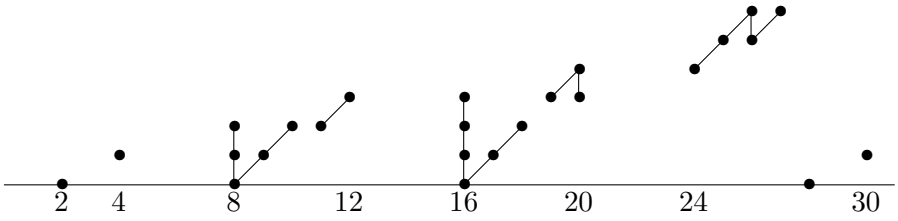

In Figure 3.2 and subsequently, the dashed lines are exotic extensions. These indicate multiplication by 2 on elements in different edges.

Figure 3.2. $\mathcal{A}_4$

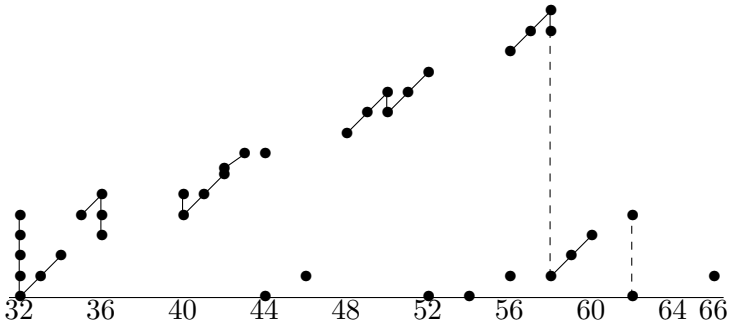

For $k \geq 2$, it will be convenient for us to work with $\Sigma^{-2^{k+1}}\mathcal{A}_k$, which we denote by $\widetilde{\mathcal{A}}_k$. The configuration of six classes which occurs in positive filtration in grading 48 to 52 in Figure 3.2 is often called a "lightning flash," terminology which we will use frequently.

In the top half of Figure 3.3 (resp. Figure 3.4) the upper edge should be 12 (resp. 28) units higher. This is to display the action of v_1^4, the Bott periodicity element in ko_8, which increases position by $(8, 4)$ in our charts. Although we are not particularly concerned about the action of the generator of ko_4 (see Figure 4.2), elements whose positions differ by $(4, 3)$ will generally be related by the action of this element.

Figure 3.3. $\widetilde{\mathcal{A}}_5$

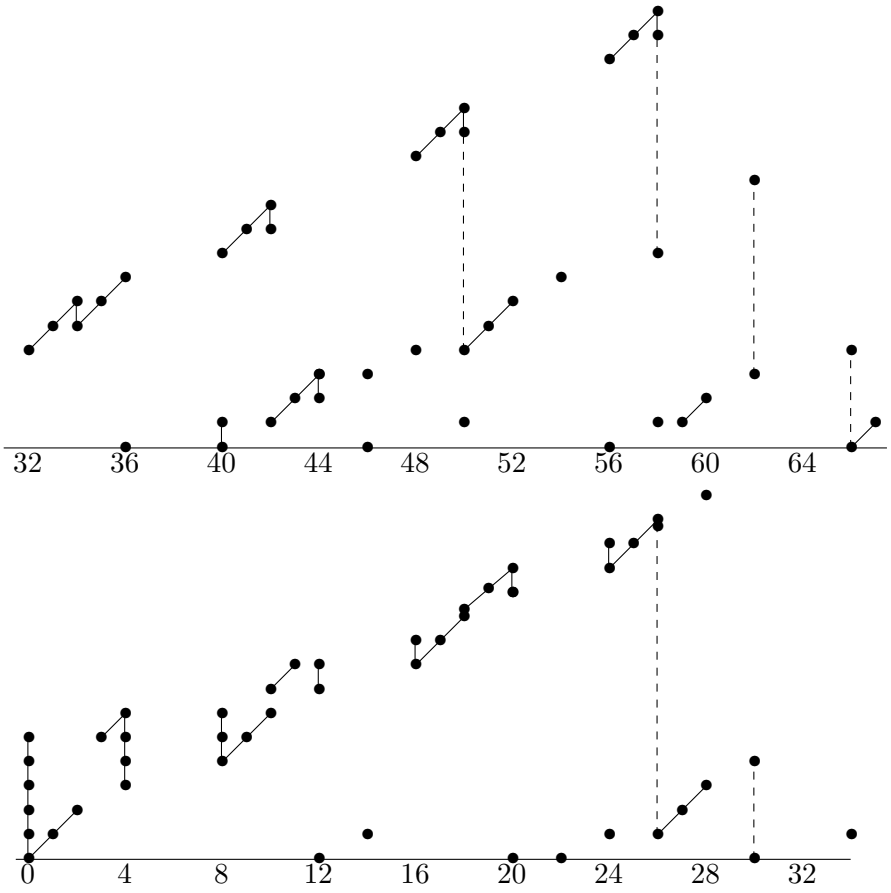

Figure 3.4. $\widetilde{\mathcal{A}}_6$

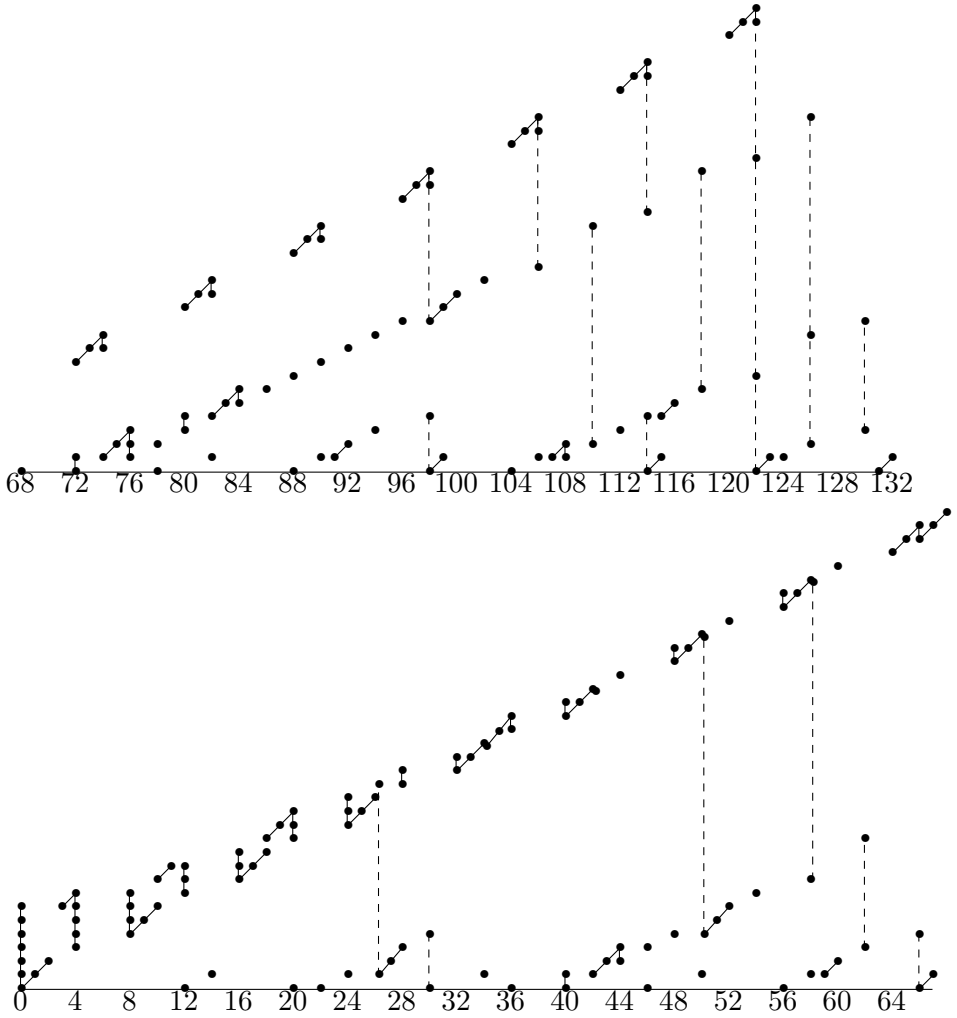

4. One description of $\mathcal{A}_k$

Each $\mathcal{A}_k$ is structured in terms of edges and subedges. In this section, we describe the subedge structure, and give an explicit description of all edges. The proof will be given in Section 14, the culmination of several preliminary sections. A more formulaic description of $\mathcal{A}_k$ is given in Section 7.

An edge $\mathcal{E}_{e,\ell}$ will always be suspended by some multiple of 8. It occurs for the first time in $\widetilde{\mathcal{A}}_\ell$, but, if $e > 1$, it will occur again as a subedge of $\widetilde{\mathcal{A}}_k$ for all $k > \ell$, often more than once for the same $\widetilde{\mathcal{A}}_k$. If $e = 4a + b > 1$ with $b = (0, 1, 2, 3)$, the bottom class of $\mathcal{E}_{e,\ell}$ is in grading $8a + (2, 3, 4, 8)$ for any ℓ, unless $e \equiv 3 \bmod 4$ and $\ell - e = 1$.

The following key theorem will be proved at the end of Section 13.

Theorem 4.1. *The ko_*-module $\widetilde{\mathcal{A}}_k$ is built up recursively, beginning with $\mathcal{E}_{1,k}$, which begins in grading 0. Then, for $1 \le e \le k-2$, each occurrence of $\Sigma^D \mathcal{E}_{e,\ell}$ contains subedges $\Sigma^{D+2^{d+1}} \mathcal{E}_{e+1,e+d}$ for $2 \le d \le \ell - e$.*

For example, $\widetilde{\mathcal{A}}_5$ has $\mathcal{E}_{1,5}$, then $\Sigma^8\mathcal{E}_{2,3}$, $\Sigma^{16}\mathcal{E}_{2,4}$, and $\Sigma^{32}\mathcal{E}_{2,5}$ under it. Then under $\Sigma^{16}\mathcal{E}_{2,4}$ is $\Sigma^{16+8}\mathcal{E}_{3,4}$, under $\Sigma^{32}\mathcal{E}_{2,5}$ are $\Sigma^{32+8}\mathcal{E}_{3,4}$ and $\Sigma^{32+16}\mathcal{E}_{3,5}$, and under $\Sigma^{48}\mathcal{E}_{3,5}$ is $\Sigma^{48+8}\mathcal{E}_{4,5}$. The reader should refer to Figure 3.3 for the following description of the edges of $\widetilde{\mathcal{A}}_5$.

$\mathcal{E}_{1,5}$	Everything above a line of slope 1/2 in the top and bottom halves of Figure 3.3.
$\Sigma^8\mathcal{E}_{2,3}$	Classes in $(12,0)$ and $(14,1)$.
$\Sigma^{16}\mathcal{E}_{2,4}$	Succession from $(20,0)$ to $(30,4)$.
$\Sigma^{24}\mathcal{E}_{3,4}$	Classes in $(30,0)$ and $(34,1)$.
$\Sigma^{32}\mathcal{E}_{2,5}$	Succession from $(36,0)$ to $(62,11)$.
$\Sigma^{40}\mathcal{E}_{3,4}$	Classes in $(46,0)$ and $(50,1)$.
$\Sigma^{48}\mathcal{E}_{3,5}$	Succession from $(56,0)$ to $(66,4)$.
$\Sigma^{56}\mathcal{E}_{4,5}$	Classes in $(66,0)$ and $(67,1)$.

We are interested in the ko_*-module structure of $ko_*(K_2)$, especially the action of η and v_1^4. By v_1^4, we mean Adams or Bott periodicity, of bigrading $(8,4)$. We include in Figure 4.2 the well-known chart of ko_*, periodic with period $(8,4)$. The elements η and v_1^4 are indicated with large dots.

Figure 4.2. ko_*

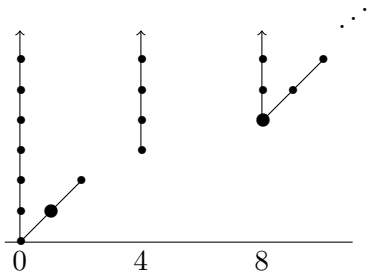

We now work toward a description of $\mathcal{E}_{e,k}$ for $e \geq 2$. We introduce some charts M_k^i that will appear repeatedly throughout the paper. The derivation and significance of these charts will be discussed in Section 11, when we begin our proof. By "charts," we mean ASS diagrams, often involving filtration shifts of some elements.

We begin with charts M_k^0 for $k \geq 4$, which are building blocks for our calculations. They are similar to familiar charts of $ko_*(RP^{2n})$ (e.g., [6]). In fact, there are isomorphisms $M_{4\ell+4}^0 \approx ko_*(RP^{8\ell+2})$ and $M_{4\ell+5}^0 \approx ko_*(RP^{8\ell+4})$. The charts M_k^0 were derived in [13]; their derivation will be explained in Section 11. For all k, all classes in M_k^0 are v_1^4-periodic. All the charts M_k^0 have the same upper edge. The lower edge drops by 1 for each increase in k, with classes of negative filtration removed. The chart M_4^0 is a sequence of lightning flashes starting in position $(8i+1, 4i)$ for $i \geq 0$. In Figure 4.3 we show the beginning of the charts for $5 \leq k \leq 7$.

Figure 4.3. M_k^0

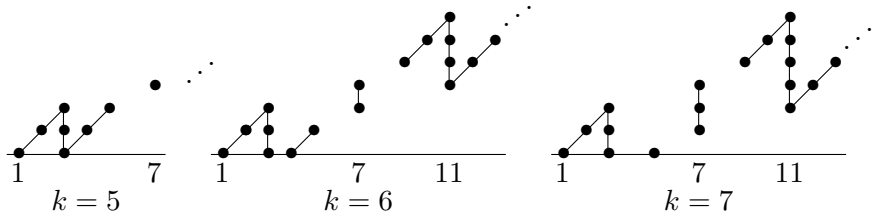

Explicitly, M_k^0 has, for $i \geq 0$,

- 0 in grading 0 and 6 mod 8,
- $\mathbb{Z}_2$ in grading $8i+1$ and $8i+2$ of filtration $4i$ and $4i+1$, respectively.
- $\mathbb{Z}_2$ in grading $8i+4$ and $8i+5$ of filtration $4i-k+6$ and $4i-k+7$, respectively, if the filtration is ≥ 0, else 0,
- $\mathbb{Z}/2^{k-4}$ in grading $8i+7$ with generator of filtration $4i-k+8$ if $4i-k+8 \geq 0$, else $\mathbb{Z}/2^{4i+4}$ with generator of filtration 0, and
- $\mathbb{Z}/2^{k-2}$ in grading $8i+3$ with generator of filtration $4i-k+5$ if $4i-k+5 \geq 0$, else $\mathbb{Z}/2^{4i+3}$ with generator of filtration 0.

Next we define M_k^i for $k \geq 4$ and $i \geq 0$ to be M_k^0 with classes of filtration less than i removed, and filtrations of other classes decreased by i. In Figure 4.4, we depict $\mathcal{M}_6^i$ for $1 \leq i \leq 3$. All elements are acted on freely by v_1^4. It follows that $M_k^{i+4} = \Sigma^8 M_k^i$.

Figure 4.4. M_6^i

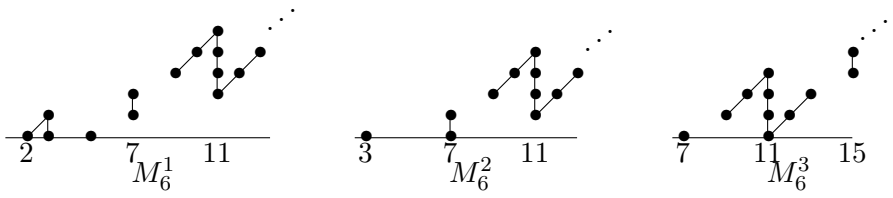

A variant of M_4^s that will be useful is given in the following definition.

Definition 4.5. *For $0 \leq s \leq 3$ and $s \geq 0$, the chart $\widehat{M}_4^s$ is formed from M_4^0 by removing classes of grading $\leq s$. If $s \geq 4$, $\widehat{M}_4^s = \Sigma^8 \widehat{M}_4^{s-4}$.*

As $\widehat{M}_4^s$ will always be combined into other charts, its filtration as an individual entity is irrelevant and undefined. Note that $\widehat{M}_4^s = M_4^s$ if $s \equiv 0, 1$ mod 4, while if $s \equiv 2, 3$ mod 4, $\widehat{M}_4^s$ is formed from M_4^s by adjoining one class. In Figure 4.6, we picture $\widehat{M}_4^s$ for $s \equiv 2, 3$ mod 4.

Figure 4.6. $\widehat{M}_4^s$ **for** $s \equiv 2, 3$ **mod 4**

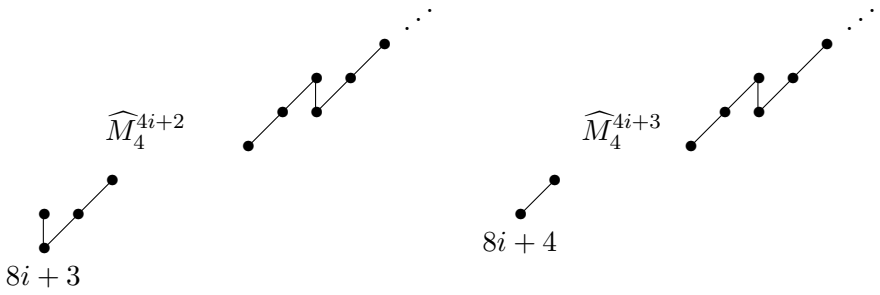

The following definition will be useful.

Definition 4.7. *A chart is* stably $\Sigma^i M_k$ *if it agrees with* $\Sigma^i M_k^0$ *in sufficiently large grading, without regard for filtration.*

Now we define what we call pre-edges $\mathcal{E}'_{e,\ell}$. This formulation will be derived in Section 13.

Definition 4.8. *For* $2 \le e < \ell$, $\mathcal{E}'_{e,\ell}$ *is formed from the following sequence of charts.*

$$\Sigma M^e_{\ell-e+3} \leftarrow \Sigma^8 M_4^{e-1} \leftarrow \cdots \leftarrow \Sigma^{2^i} M_4^{e-1} \leftarrow \cdots \leftarrow \Sigma^{2^{\ell-e+1}} M_4^{e-1} \leftarrow \Sigma^{2^{\ell-e+2}+2} \widehat{M}_4^{e-2}$$

Working from left to right, the filtration of each $\Sigma^{2^i} M_4^{e-1}$ *is increased so that it appears that there is a* d_1 *differential from its generators in grading* 1, 3, 4, *and* 5 *mod* 8 *to the upper edge of the chart resulting from the preceding steps, and there are* η *extensions on its remaining classes in grading* 3 *mod* 8. *The chart resulting after incorporating* $\Sigma^{2^i} M_4^{e-1}$ *is stably* $\Sigma M_{\ell-e+5-i}$. *The* $\Sigma^{2^{\ell-e+2}+2} \widehat{M}_4^{e-2}$ *is placed so that all its classes support* d_1 *differentials. The pre-edge* $\mathcal{E}'_{e,\ell}$ *is the chart remaining after all these* d_1*'s. It vanishes in the range of* $\Sigma^{2^{\ell-e+2}+2} \widehat{M}_4^{e-2}$.

We illustrate in Figure 4.9 the forming of $\mathcal{E}'_{4,7}$, which is derived from

$$\Sigma M_6^4 \leftarrow \Sigma^8 M_4^3 \leftarrow \Sigma^{16} M_4^3 \leftarrow \Sigma^{34} \widehat{M}_4^2.$$

At each step, the chart being adjoined is indicated in red, while the black part is the result of the preceding step. For example, the chart $\Sigma^8 M_4^3$ has been moved up by one unit, so that what were d_2-differentials in the ASS look like d_1-differentials. The effect is to improve the appearance of the chart and make it easier to use subsequently. Then $\mathcal{E}'_{4,7}$ consists of the classes remaining in the lower chart in Figure 4.9 after the indicated differentials.

Figure 4.9. Forming $\mathcal{E}'_{4,7}$

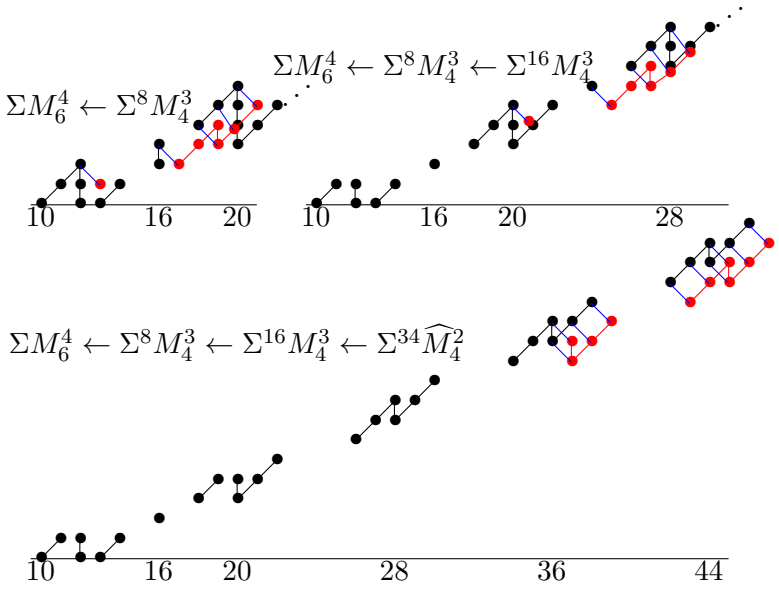

Since $M_k^{e+4} = \Sigma^8 M_k^e$ and $\widehat{M}_4^{e+4} = \Sigma^8 \widehat{M}_4^e$ for $e \geq 0$, it follows that $\mathcal{E}'_{e+4,\ell+4} = \Sigma^8 \mathcal{E}'_{e,\ell}$ for $e \geq 2$. So it suffices to study $\mathcal{E}'_{e,\ell}$ for $e \leq 5$.

Recall from Theorem 4.1 that beneath any edge $\Sigma^D \mathcal{E}_{e,\ell}$ in $\widetilde{\mathcal{A}}_k$ there occur subedges $\Sigma^{D+2^{d+1}} \mathcal{E}_{e+1,e+d}$ for $e+2 \leq e+d \leq \ell$. The same is true for $\mathcal{E}'_{e,\ell}$. The following theorem will be proved in Section 14.

Theorem 4.10. *For $e \geq 1$, there are differentials from $\Sigma^{2^{d+1}} \mathcal{E}'_{e+1,e+d}$ to elements of order 2 in $\mathcal{E}'_{e,\ell}$ from all classes in grading 4 or 5 mod 8, except filtration-0 classes x in grading 4 mod 8 with $\eta x = 0$. For $e \geq 2$, $\mathcal{E}_{e,\ell}$ is formed from $\mathcal{E}'_{e,\ell}$ by removing all classes either supporting or hit by these differentials. This is true, after appropriate suspension, of all occurrences of $\mathcal{E}_{e,\ell}$ as edges or subedges.*

In Figures 4.11, 4.12, 4.13, 4.14, and 4.15, we display $\mathcal{E}'_{e,e+d}$ for $2 \leq e \leq 5$ and $1 \leq d \leq 4$. We circle classes supporting differentials, and use a larger dot for classes hit by differentials. Then $\mathcal{E}_{e,e+d}$ consists of uncircled small dots.

For example, $\Sigma^{16} \mathcal{E}'_{3,5}$ appears beneath $\mathcal{E}'_{2,6}$, as indicated in Figure 4.12. The two circled dots in $\mathcal{E}'_{3,5}$ in Figure 4.11, after applying Σ^{16}, support differentials hitting the two big black dots in Figure 4.12 in grading 27 and 28. These are differentials in the ASS converging to $ko_*(K_2)$.

Figure 4.11. $\mathcal{E}'_{e,\ell}$ **and differentials**

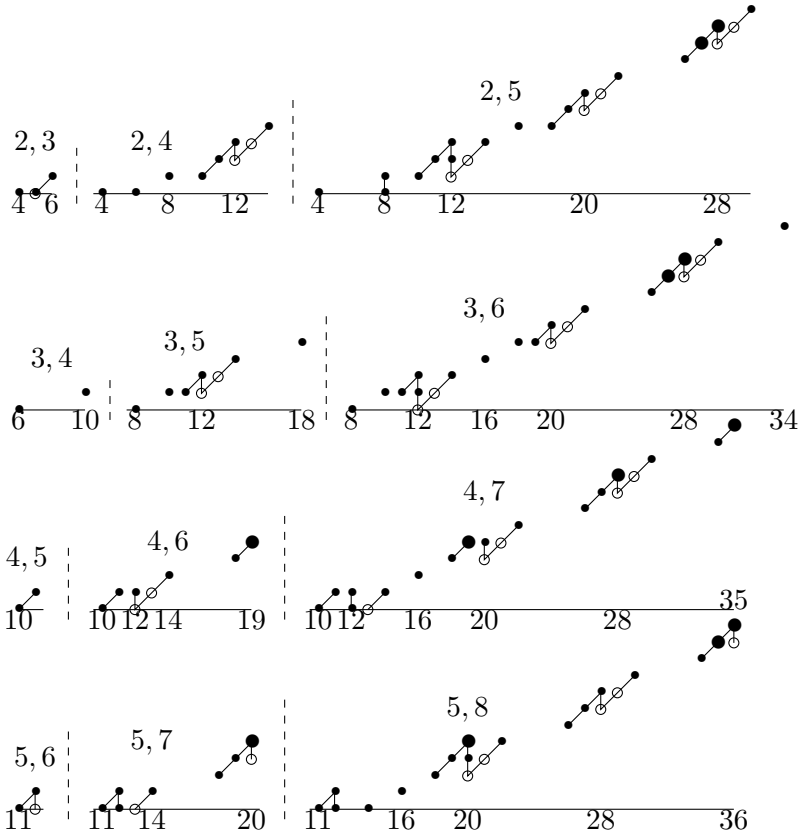

One added feature in Figures 4.12, 4.13, 4.14, and 4.15 is that for the classes hit by differentials, we include below them the name of the subedge that supported the differential. The classes supporting those differentials can be seen in Figure 4.11, where they appear with circles. Note that these are complete figures; they are finite charts.

Figure 4.12. $\mathcal{E}'_{2,6}$ **and differentials**

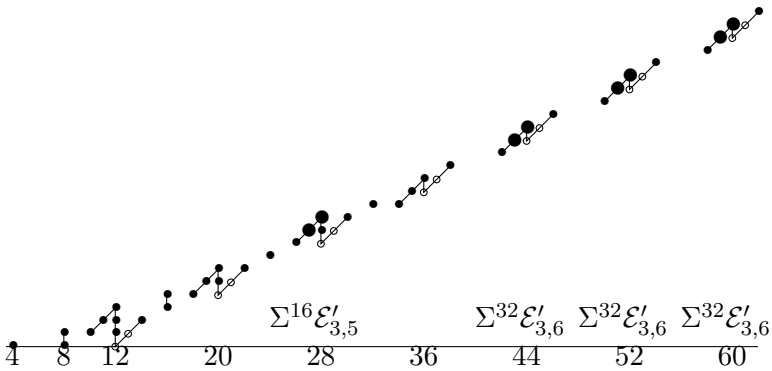

It is instructive to compare Figure 4.12 with Figure 3.4, in which $\Sigma^{64}\mathcal{E}_{2,6}$ appears prominently.

Figure 4.13. $\mathcal{E}'_{3,7}$ **and differentials**

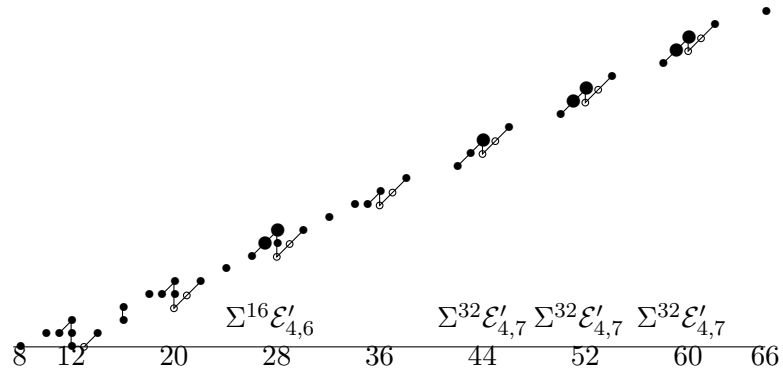

Figure 4.14. $\mathcal{E}'_{4,8}$ **and differentials**

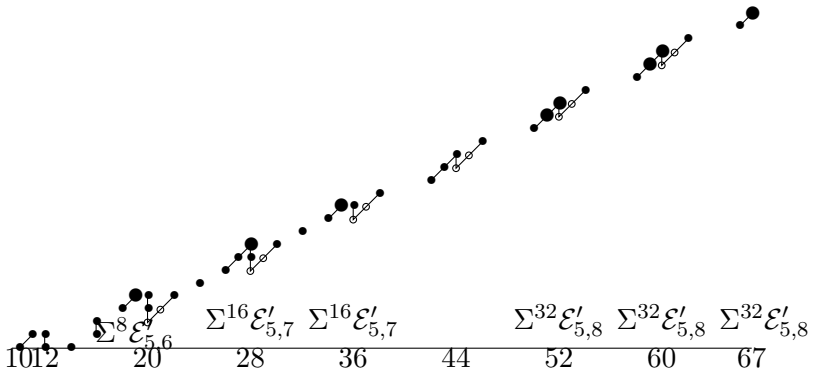

Figure 4.15. $\mathcal{E}'_{5,9}$ **and differentials**

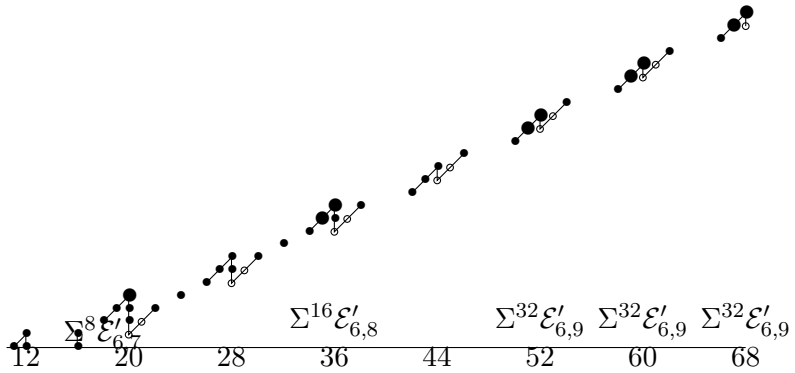

The sources of the differentials are very regular. There are differentials from $\Sigma^{2^{d+2}}\mathcal{E}'_{e,e+d}$ into $\mathcal{E}'_{e-1,\ell}$ for each $\ell \geq e+d$ on all classes in grading 4 and 5 mod 8 in $\Sigma^{2^{d+2}+1}M^e_{d+3}$ (except for a class x in filtration 0 and grading 4 mod 8 satisfying $\eta x = 0$) until the $\mathcal{E}'_{e,e+d}$ is ended by the differentials from $\Sigma^{2^{d+2}+2}\widehat{M}_4^{e-2}$.

Careful study of the above charts $\mathcal{E}'_{e,e+d}$ for $d = 1$, 2, 3, and 4 can give great insight into the form of $\mathcal{E}'_{e,e+d}$ for arbitrary d. As d increases, the upper edge of the chart stays fixed while the lower edge drops by 1 each time. Only $e = 2$, 3, 4, and 5 need be considered, since $\mathcal{E}_{e+4,k+4} = \Sigma^8\mathcal{E}_{e,k}$.

The slightly differing forms of the upper edge of $\mathcal{E}'_{e,e+d}$ depending on the mod 4 value of e are caused by the differing ways that M_4^{e-1} begins. In Figure 4.16, we show the formation of $\mathcal{E}'_{3,5}$. Comparison with Figure 4.9 is instructive.

Figure 4.16. Formation of $\mathcal{E}'_{3,5}$

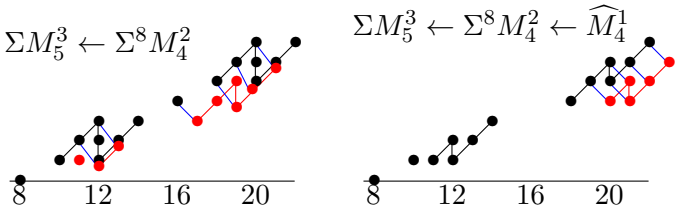

It is interesting to see how the ending of each $\mathcal{E}'_{e,e+d}$ occurs. Prior to the $\Sigma^{2^{d+2}+2}\widehat{M}_4^{e-2}$ at the end of the sequence in Definition 4.8, the sequence will have stabilized to a sequence of lightning flashes with initial classes in grading 2 mod 8. In Figure 4.17, we show how the lightning flash beginning in grading $2^{d+2}+2$ is hit by $\Sigma^{2^{d+2}+2}\widehat{M}_4^{e-2}$ for $2 \le e \le 5$. Increasing e by 4 would push this behavior out by 8 gradings. In Figure 4.17, the remaining classes are indicated with bigger dots. Compare with the endings in Figures 4.11, 4.12, 4.13, 4.14, and 4.15.

Figure 4.17. Termination of $\mathcal{E}'_{e,e+d}$

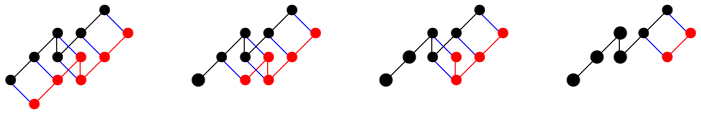

The upper edge $\mathcal{E}_{1,k}$ has a different form. The following definition will be illustrated in Figure 4.20 and justified at the end of Section 13.

Definition 4.18. *For $k \ge 2$, V_k is a chart with, for $i \ge 0$, classes g_{8i} in position $(8i, 4i)$, and g_{8i+4} in position $(8i+4, 4i+3)$, of order 2^{k-1} except that the order of g_0 is 2^{k+1}. There are also elements ηg_{8i} and $\eta^2 g_{8i}$, x_3 such that $\eta x_3 = 2^{k-2} g_4$, and, for $i > 0$, elements x_{8i+2} and ηx_{8i+2} such that $\eta^2 x_{8i+2} = g_{8i+4}$. If $k = 2$ and $i > 0$, then $2x_{8i+2} = \eta^2 g_{8i}$. In grading ≥ 8, V_k agrees with $ko_*(M(2^{k-1}))$, where $M(n)$ is the mod n Moore spectrum. (Note that both V_k and $ko_*(M(2^{k-1}))$ have generators in positions $(8i, 4i)$ for $i \ge 1$.)*

The chart $\mathcal{E}'_{1,k}$ is formed from the sequence

$$V_k \leftarrow \Sigma^8 M_4^0 \leftarrow \cdots \leftarrow \Sigma^{2^i} M_4^0 \leftarrow \cdots \leftarrow \Sigma^{2^{k+1}} M_4^0. \tag{4.19}$$

Working from left to right, each $\Sigma^{2^i} M_4^0$ is placed so that there are d_1 differentials from its generators in grading 1, 3, 4, and 5 mod 8 into the upper edge of the chart resulting from the preceding steps. For $2 \le i \le k-1$, $\mathcal{E}'_{1,k}$ agrees with $ko_*(M(2^{k-i}))$ in grading 2^{i+1} through $2^{i+2}-1$.

The edge $\mathcal{E}_{1,k}$ is obtained from $\mathcal{E}'_{1,k}$ by removing the classes in grading 3 or 4 mod 8 which are hit by the differentials from $\Sigma^{2^i}\mathcal{E}'_{2,i}$ for $3 \le i \le k$ described in Theorem 4.10.

In Figure 4.20, we show the formation of $\mathcal{E}'_{1,4}$ and $\mathcal{E}_{1,4}$. At each step, the chart being adjoined is shown in red. Then $\mathcal{E}'_{1,4}$ consists of all classes in the bottom chart of grading ≤ 28. The classes with the big dots are hit by differentials, and so do not appear in $\mathcal{E}_{1,4}$. The chart hitting them is indicated below them. The classes supporting those differentials can be seen in Figure 4.11. The result of Figure 4.20 can be seen in Figure 3.2.

Figure 4.20. Formation of $\mathcal{E}'_{1,4}$ and $\mathcal{E}_{1,4}$

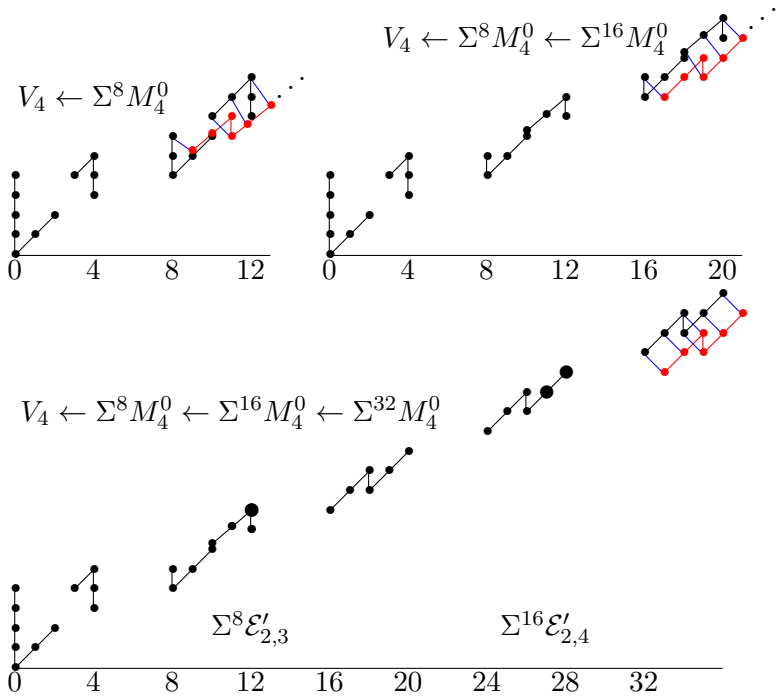

Now that we have described (in Definitions 4.8 and 4.18) all pre-edges and (in Theorem 4.10) the differentials that reduce them to edges, the description of $\widetilde{\mathcal{A}}_k$ follows from Theorem 4.1 once we describe the exotic extensions. This is done in the following theorem, which will be proved in Section 14.

Theorem 4.21. *The only exotic extensions in $\widetilde{\mathcal{A}}_k$ are as follows:*

1. *Into $\mathcal{E}_{1,k}$ from $\Sigma^{2^\ell}\mathcal{E}_{2,\ell}$ for $4 \le \ell \le k$ in grading $8i+2$ for $3 \cdot 2^{\ell-4} \le i \le 2^{\ell-2}-1$. The target is the class which is not in $\mathrm{im}(\eta)$.*
2. *For $e \ge 2$ and $e+1 < \ell \le k$, into $\Sigma^D \mathcal{E}_{e,\ell}$ from $\Sigma^{2^{\ell+1-e}+D}\mathcal{E}_{e+1,\ell}$ in grading 6 mod 8 throughout the entire extent of $\Sigma^{2^{\ell+1-e}+D}\mathcal{E}_{e+1,\ell}$.*
3. *For $e \ge 2$, $\ell \le k$, and $e+1 < m \le \ell$, into $\Sigma^D \mathcal{E}_{e,\ell}$ from $\Sigma^{2^{m+1-e}+D}\mathcal{E}_{e+1,m}$ in grading 2 mod 8 throughout the second half of $\mathcal{E}_{e+1,m}$ (the range of the lightning flashes in $\mathcal{E}'_{e+1,m}$, including the final element in 2 mod 8 if $e \equiv 0$ or 3 mod 4, but not if $e \equiv 2$ mod 4).*

Since $\mathcal{E}_{e,\ell}$ has order ≤ 2 in grading 2 mod 4, we don't have to specify which element is involved in the extension in parts (2) and (3) of the theorem. In Figure 3.4, the extensions into the upper edge are easily checked to agree with part (1). In (4.22), we list the other extensions in $\widetilde{\mathcal{A}}_6$, with those of type (2) in the left column and those of type (3) in the right column. We list the grading followed by the edges involved, with dashes indicating the extension.

$$\begin{aligned}
30:\ &\Sigma^{16}(\Sigma^{8}\mathcal{E}_{3,4}-\mathcal{E}_{2,4}) & 66:\ &\Sigma^{48}(\Sigma^{8}\mathcal{E}_{4,5}-\mathcal{E}_{3,5})\\
62:\ &\Sigma^{32}(\Sigma^{16}\mathcal{E}_{3,5}-\mathcal{E}_{2,5}) & 98:\ &\Sigma^{80}(\Sigma^{8}\mathcal{E}_{4,5}-\mathcal{E}_{3,5})\\
110:\ &\Sigma^{64}(\Sigma^{32}\mathcal{E}_{3,6}-\mathcal{E}_{2,6}) & 114:\ &\Sigma^{96}(\Sigma^{8}\mathcal{E}_{4,5}-\mathcal{E}_{3,6})\\
118:\ &\Sigma^{64}(\Sigma^{32}\mathcal{E}_{3,6}-\mathcal{E}_{2,6}) & 122:\ &\Sigma^{64}(\Sigma^{32}\mathcal{E}_{3,6}-\mathcal{E}_{2,6})\\
126:\ &\Sigma^{96}(\Sigma^{16}\mathcal{E}_{4,6}-\mathcal{E}_{3,6}) & 122:\ &\Sigma^{96}(\Sigma^{16}\mathcal{E}_{4,6}-\mathcal{E}_{3,6})\\
126:\ &\Sigma^{64}(\Sigma^{32}\mathcal{E}_{3,6}-\mathcal{E}_{2,6}) & 130:\ &\Sigma^{96}(\Sigma^{16}\mathcal{E}_{4,6}-\mathcal{E}_{3,6})
\end{aligned} \tag{4.22}$$

5. $z^i\mathcal{B}_{k,\ell}$

In this section, we describe the summands $z^i\mathcal{B}_{k,\ell}$, which appeared in Theorem 1.3. The proof will be in Section 15.

The description of $ku^*(K_2)$ in [11] was in terms of summands A_k, B_k, and $S_{k,\ell}$. It was stated in [11, Section 7] that $S_{k,\ell}$ and two specific copies of B_k combine together nicely, in the sense that differentials in the ASS that form them involve just the three[1], and that the contribution to $ku^*(K_2)$ of the three is isomorphic to the corresponding contribution to $ku_*(K_2)$ after dualizing the gradings, implying self-duality of $B_{k,\ell}$. The example there yielded the chart for $B_{3,4} \subset ku_*(K_2)$ in Figure 5.1.

Figure 5.1. $B_{3,4} \subset ku_*(K_2)$

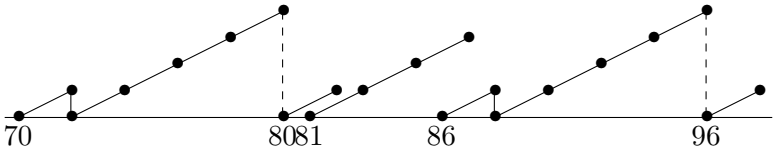

In Section 15, we explain how the ko analogues of $B_{k,\ell}$ are defined and explain how the ASS of this part is computed. We denote by $\mathcal{B}_{k,\ell}$ the resulting chart for this summand of $ko_*(K_2)$. The result for $\mathcal{B}_{3,4}$ is shown in Figure 5.2.

[1]This will be proved in Theorem 10.4.

Figure 5.2. $\mathcal{B}_{3,4}$

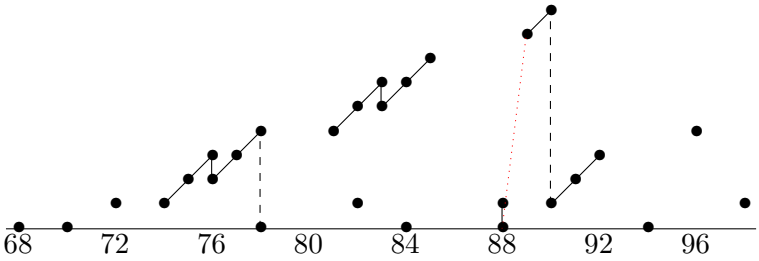

The lightning flash in the middle is the analogue of the $S_{3,4}$ part, which was the short v-tower in grading 81 to 87 in Figure 5.1. We choose to raise the filtration of this for two reasons. (a) When we look at the differentials in the ASS it is convenient to increase some filtrations to make the extensions clearer and the pictures nicer. (b) The classes in 84 and 85 are v_1^4 times the classes in 76 and 77, and we like to have our chart depict this.

In the ku version, the copies of B_k on either side of the $S_{k,\ell}$ are isomorphic, as is clear in Figure 5.1. This is not the case in the ko version, as can be observed in Figure 5.2. There is an exotic η extension from 88 to 89, accompanying the exotic $\cdot 2$ in 90. One might prefer to lower the filtrations of the high classes in 89 and 90, but they are v_1^4 times the classes in 81 and 82. Also, when we show how these charts are obtained, it will be clear that the high filtrations are warranted.

Let $\mathcal{E}'_{e,\infty} = \operatorname*{dirlim}_{\ell\to\infty} \mathcal{E}'_{e,\ell}$ and $M^e_\infty = \operatorname*{dirlim}_{\ell\to\infty} M^e_\ell$. Then $\mathcal{E}'_{e,\infty}$ can also be defined as the chart obtained from the sequence of d_1 differentials, situated as in Definition 4.8,

$$\Sigma M^e_\infty \leftarrow \Sigma^8 M_4^{e-1} \leftarrow \Sigma^{16} M_4^{e-1} \leftarrow \Sigma^{32} M_4^{e-1} \leftarrow \cdots .$$

Definition 5.3. *For $k \geq 2$, define functions h_k by*

$$h_k(8a+b) = 4a - k + \begin{cases} 0 & b = 2 \\ 1 & b = 3 \\ 2 & b = 4 \\ 3 & 5 \leq b \leq 9. \end{cases}$$

Let $C_{i,k}$ denote the subchart of $\mathcal{E}'_{2+i,\infty}$ consisting of elements in position (x, y) satisfying $y \geq h_{k+i}(x)$.

In Figure 5.4, we depict a portion of $\mathcal{E}'_{2,\infty}$ with all of $C_{0,4}$ indicated by big dots. The dashed line is the graph of h_4.

Figure 5.4. $C_{0,4}$

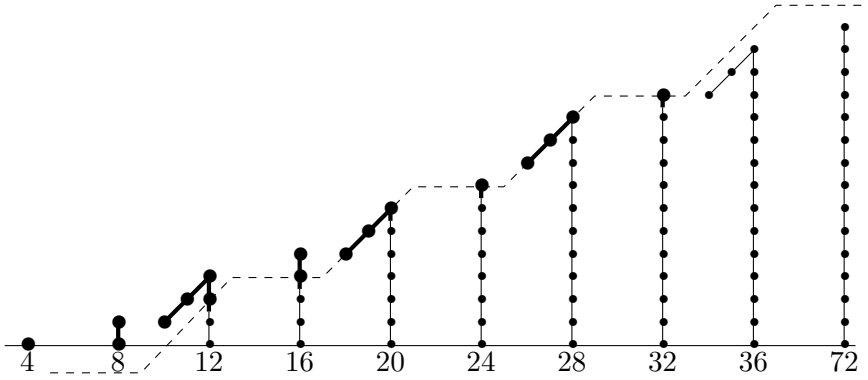

Theorem 1.3 involved summands $z^i\mathcal{B}_{k,\ell}$. These charts are described in Theorem 5.5, which will be proved in Section 15. Of course, $z^0\mathcal{B}_{k,\ell} = \mathcal{B}_{k,\ell}$. Just as we did with letting $\widetilde{\mathcal{A}}_k = \Sigma^{-2^{k+1}}\mathcal{A}_k$, it will be convenient to let $\widetilde{\mathcal{B}}_{k,\ell} = \Sigma^{-2^{\ell+2}}\mathcal{B}_{k,\ell}$.

Theorem 5.5. *For $i \geq 0$ and $1 \leq k < \ell$, the chart $z^i\widetilde{\mathcal{B}}_{k,\ell}$ consists of the following four parts:*

1. *The portion of $\Sigma^{2^{k+1}}M^i_{\ell-k+3}$ in filtration 0 through k, with filtrations increased by 2^k-k-1. If $M^i_{\ell-k+3}$ has a filtration-k element in grading 1 mod 8, that element is omitted, since it appears in part (4).*
2. *A modification of $\mathcal{E}_{\ell-k+i+1,\ell+i}$ and all edges under it, as enumerated in Theorem 4.1, including extensions among these edges. The modification is that the elements of $\mathcal{E}'_{\ell-k+i+1,\ell+i}$ in grading 4 and 5 mod 8, which supported differentials in forming $\mathcal{E}_{\ell-k+i+1,\ell+i}$, do not support differentials in this case.*
3. *A chart formed from $\Sigma^{2^{k+1}}C_{i,k}$ together with all the edges strictly under $\Sigma^{2^{k+1}}\mathcal{E}_{2+i,k+1+i}$, incorporating all the differentials and extensions among these lower edges, and from them into $\Sigma^{2^{k+1}}\mathcal{E}'_{2+i,k+i+1}$. The target elements in $\Sigma^{2^{k+1}}\mathcal{E}'_{2+i,k+i+1}$ are part of $\Sigma^{2^{k+1}}C_{i,k}$.*
4. *For $\left[\frac{k+3+i}{4}\right] \leq j \leq 2^{k-2} + \left[\frac{i+3}{4}\right] - 1$, elements x_j in $(2^{k+1}+1+8j, 2^k-k-1+4j-i)$ and ηx_j. If $i = 4t+1$ for some t, and $j = 2^{k-2}+t$, then ηx_j is not present. If $j \geq 2^{k-3} + \left[\frac{i+3}{4}\right]$, there is an exotic extension from the element in $(2^{k+1}+8j+2, 4j-k-i)$ to ηx_j.*

Remark 5.6. If $\ell-k+i \equiv 0 \bmod 4$, there is an η-extension from the last element of $\mathcal{E}_{\ell-k+i+1,\ell+i}$ in $z^i\widetilde{\mathcal{B}}_{k,\ell}$ to a $\mathbb{Z}_2$ in the lowest filtration of $\Sigma^{2^{k+1}}M^i_{\ell-k+3}$. The first element is like the circled element at the end of the $e = 5$ part of Figure 4.11 (which does not support a differential in $z^i\widetilde{\mathcal{B}}_{k,\ell}$) and the second element is like the element in grading 5 in the M^1_6 chart in Figure 4.4.

Remark 5.7. There are exotic η extensions in $z^i\widetilde{\mathcal{B}}_{k,\ell}$ wherever the exotic $\cdot 2$ extensions occur in part (4) of the theorem. If $2\alpha = \eta\beta$ and $v_1\gamma = \alpha$, then $\eta\gamma = \beta$. In Figure 5.11, the classes α are the two classes supporting

the exotic extensions, and if α is in position (x, y), then γ is in position $(x-2, y-1)$.

The middle lightning flash in Figure 5.2 furnishes one example of part (1) of the theorem, which corresponds to the $S_{k,\ell}$ portion in $ku^*(K_2)$. In Figure 5.8, we provide three more examples, without indicating the filtration.

Figure 5.8. Examples of Theorem 5.5(1)

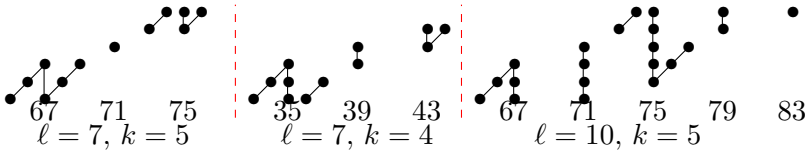

In Figure 5.9, we provide another example, $\widetilde{\mathcal{B}}_{4,7}$. The portion from part (2) of Theorem 5.5 is in black, and parts (1), (3), and (4) are in red. The black part corresponds to the modified version of $\mathcal{E}_{4,7}$ and the edges under it. Compare with $\mathcal{E}'_{4,7}$ in Figure 4.11.

The low red part is $\Sigma^{32}C_{0,4}$ together with the edges under $\Sigma^{32}\mathcal{E}_{2,5}$, which are $\Sigma^{40}\mathcal{E}_{3,4}$, $\Sigma^{48}\mathcal{E}_{3,5}$, and $\Sigma^{56}\mathcal{E}_{4,5}$. Compare with Figure 5.4 and Figure 4.11. Note that elements in $\Sigma^{48}\mathcal{E}'_{3,5}$ support differentials killing elements in $\Sigma^{32}C_{0,4}$ in grading 59 and 60.

The top red part has part (1), which is the middle chart in Figure 5.8, and the three η pairs, which are part (4).

Figure 5.9. $\widetilde{\mathcal{B}}_{4,7}$

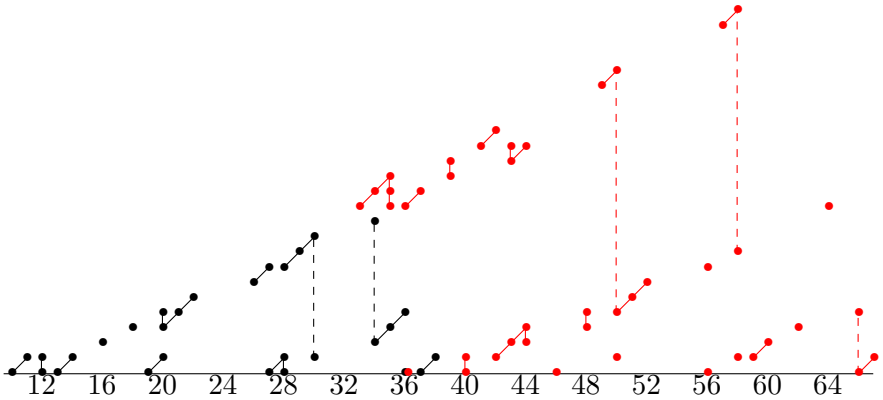

Although $z^i\widetilde{\mathcal{B}}_{k,\ell}$ is built from various $z^iM^a_b$ $(= M^{a+i}_b)$, and multiplying M^a_b by z^i just lowers all filtrations by i, the effect of z^i on $\widetilde{\mathcal{B}}_{k,\ell}$ is more complicated, due to differentials. In Figure 5.10, we display $z^i\widetilde{\mathcal{B}}_{3,4}$ for $1 \leq i \leq 3$, for comparison with the case $i = 0$ in Figure 5.2 (which is $\Sigma^{64}\widetilde{\mathcal{B}}_{3,4}$).

Figure 5.10. $z^i\widetilde{\mathcal{B}}_{3,4}$

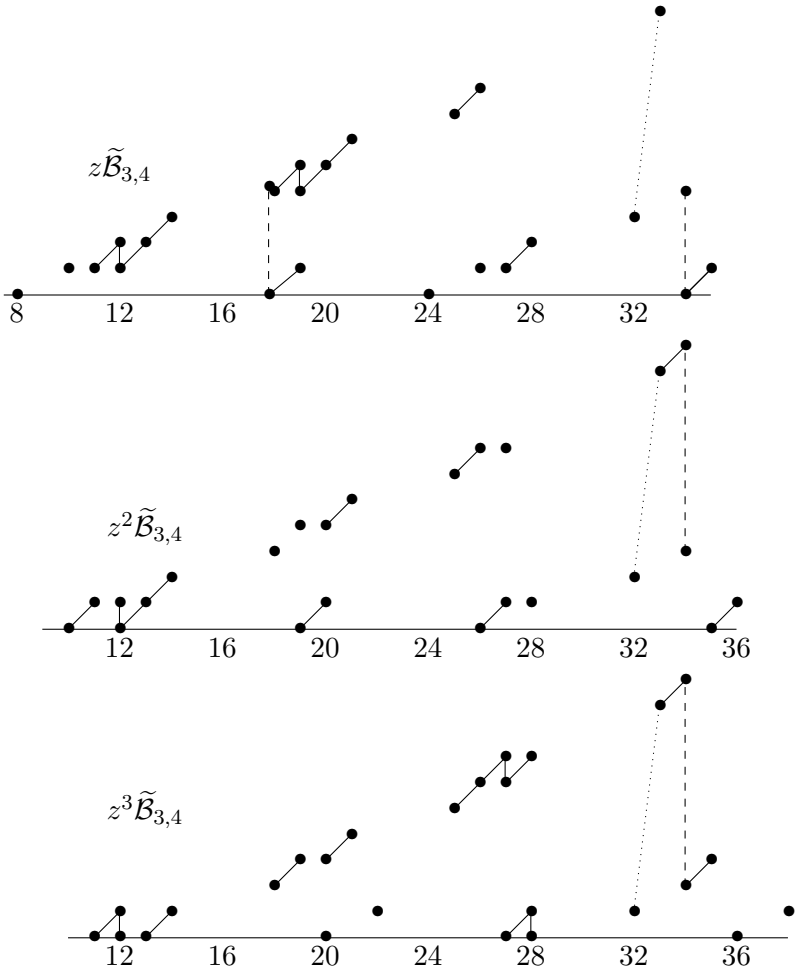

We close this descriptive section by describing a way of visualizing how parts (1), (3), and (4) of Theorem 5.5 come about. For simplicity, we restrict to $i = 0$. In Section 15, we will explain why this description is valid.

For this part of $\widetilde{\mathcal{B}}_{k,\ell}$, we combine two charts. One chart has the resultant of

$$\Sigma^{2^{k+1}}(\Sigma M^2_{\ell+2} \leftarrow \Sigma^8 M^1_4 \leftarrow \cdots \leftarrow \Sigma^{2^i} M^1_4 \leftarrow \cdots \leftarrow \Sigma^{2^{k+1}} M^1_4)$$

with the usual placement for d_1 differentials. The other chart has $\Sigma^{2^{k+1}} M^0_{\ell-k+3}$, with filtrations increased by $2^k - k - 1$. See Figure 5.11 for $\widetilde{\mathcal{B}}_{4,9}$.

Beginning in grading slightly greater than 2^{k+2}, the two charts will have isomorphic forms, stably $M_{\ell-k+3}$, displaced by 1 horizontal unit. There must be a differential annihilating these; it will be d_{2^k}. We apply (v_1^{-4}) periodicity to these differentials whenever it applies. In Figure 5.11, we indicate by small red dots the elements that are related by these differentials. For example, applying v_1^{-4} to the $\mathbb{Z}/16$ in 72 and 71 shows that the bottom four elements in 64 support differentials, but the top one survives. The elements which survive are indicated by large black dots. Three η-pairs at the top are part (4) of Theorem 5.5. The other black elements in the top half in filtration 0 to

4 (before the filtration shift) are type (1). The black elements in the bottom half are of type (3). They lie on or above the dashed line in Figure 5.4. This description does not incorporate the type-(3) elements on subedges under $\Sigma^{2^{k+1}}\mathcal{E}_{2,k+1}$.

Figure 5.11. Some differentials (in red) in $\widetilde{\mathcal{B}}_{4,9}$

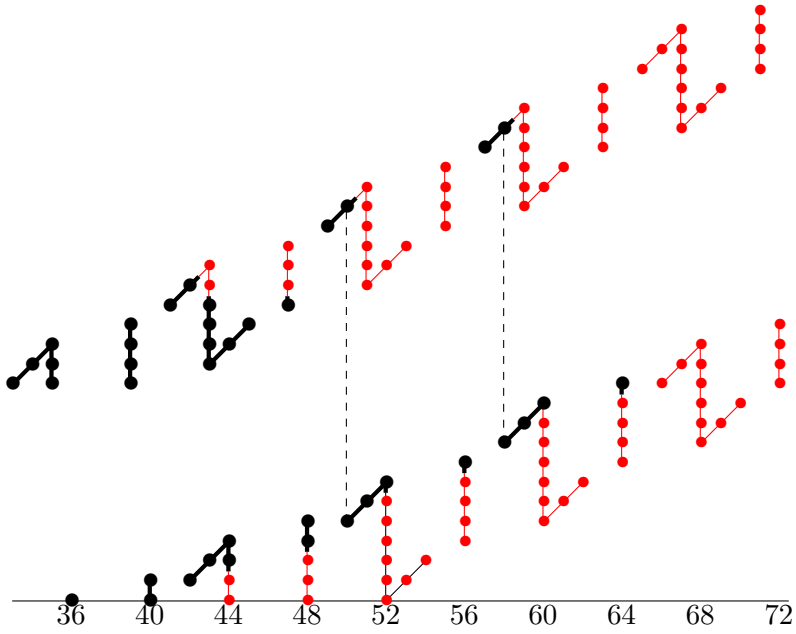

6. Complete description through grading 42

We can easily depict $ko_*(K_2)$ for $* < 42$, and much farther. In Figure 6.1 we present it in three labeled rows, to avoid congestion. It is the sum of the three. We omit the trivial ko_*-submodule, which is enumerated through grading 24 at the end of Section 11.

Figure 6.1. $ko_*(K_2)$**,** $* < 42$

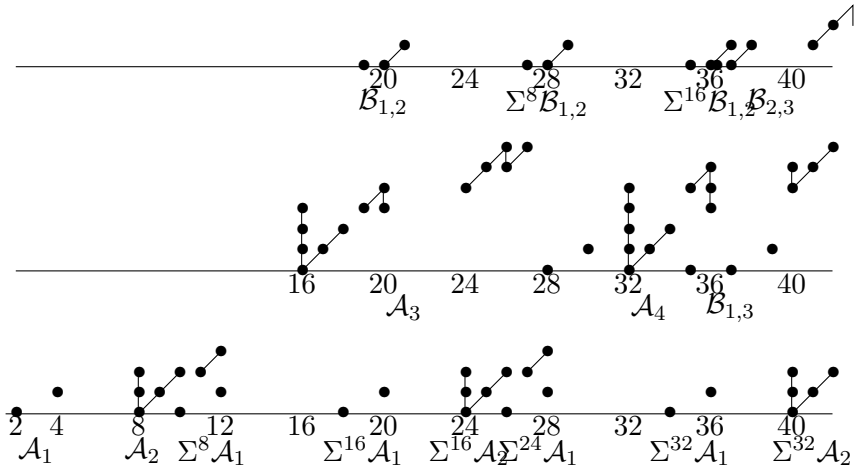

7. A formulaic description of edges

In this section, we give a more formulaic description of edges.
Let $R = \mathbb{Z}_{(2)}[\eta]/(2\eta, \eta^3)$.
The upper edge $\mathcal{E}_{1,k}$ has a different form than the other edges.

Definition 7.1. *For $t \geq 1$ and $0 \leq \varepsilon \leq 2$, we define R-modules $L_{t,\varepsilon}(x,y)$ to have generators g, g', and g'' in positions (x,y), $(x+2, y+t)$, and $(x+4, y+3)$, respectively, with relations $2^t g$, $\eta^2 g' = 2^{t-1} g''$, $\eta^{3-\varepsilon} g'$, $\eta g''$, and*

$$2g' = \begin{cases} \eta^2 g & t = 1 \\ 0 & t > 1. \end{cases}$$

Let I_k denote the R-module with generators G, G', and G'' in positions $(0,0)$, $(3,k)$, and $(4,3)$, respectively, with relations $2^{k+1}G$, $\eta G' = 2^{k-2} G''$, $2G'$, and $\eta G''$.

For example, I_4 is the portion of Figure 4.20 in grading ≤ 7. The second subscript in $L_{t,\varepsilon}$ indicates the number of elements killed in forming $L_{t,\varepsilon}$ from $L_{t,0}$. In Figure 7.2 we show $L_{t,\varepsilon}$ for $t \leq 4$, omitting (x,y), which is the position of the lower-left element.

Figure 7.2. $L_{t,\varepsilon}$

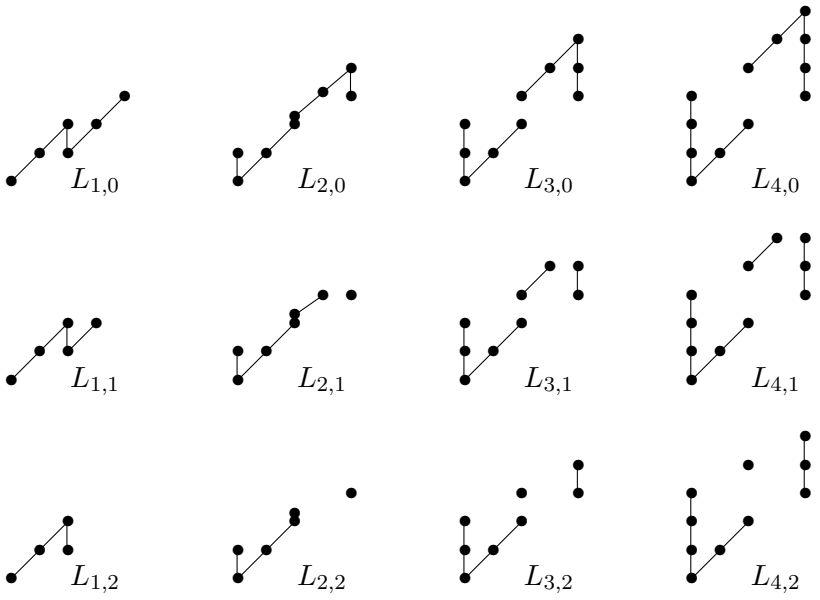

Theorem 7.3. *Let $\lg(i) = [\log_2(i)]$. The upper edge, $\mathcal{E}_{1,k}$, of $\Sigma^{-2^{k+1}}\mathcal{A}_k$, as an R-module is*

$$I_k \oplus \bigoplus_{i=1}^{2^{k-2}-1} L_{k-\lg(i)-2, f_1(i)}(8i, 4i),$$

where

$$f_1(i) = \begin{cases} 0 & 2^j \leq i \leq 2^j + [(j-1)/4] \\ 1 & i = 2^j + \frac{j}{4}, j \equiv 0 \ (4) \\ 2 & 2^j + 1 + [j/4] \leq i \leq 2^{j+1} - 1 \end{cases}$$

for some j.

Many values of f_1 are presented in Table 1. For example, the upper edge in Figure 3.3 satisfies

$$\mathcal{E}_{1,5} = I_5 \oplus L_{3,1} \oplus L_{2,0} \oplus L_{2,2} \oplus L_{1,0} \oplus L_{1,2} \oplus L_{1,2} \oplus L_{1,2},$$

where the ith L is in position $(8i, 4i)$, $1 \le i \le 7$.

The other edges are formed from R-modules $K_{t,\varepsilon}$, which we now define.

Definition 7.4. *For $t \ge 1$ and $0 \le \varepsilon \le 2$, the R-module $K_{t,\varepsilon}(x,y)$ has generators g, g', g'', and g''' in positions (x,y), $(x-2,y+t-3)$, $(x+2,y+1)$, and $(x+4,y+2)$, respectively, with relations*

$$2^{t-1}g = \eta^2 g',\ 2g',\ \eta g,\ 2g'',\ \eta g'',\ 2^{t-1}g''',\ \eta g''',\ \eta^{3-\varepsilon} g'.$$

In Figure 7.5, we depict $K_{t,\varepsilon}$ for $t \le 4$. Position (x,y) is circled. Note that $K_{1,2}$ has its only nonzero elements in $(x-2,y-2)$ and $(x+2,y+1)$. Again, the second subscript is the number of elements killed in forming $K_{t,\varepsilon}$ from $K_{t,0}$.

Figure 7.5. $K_{t,\varepsilon}$

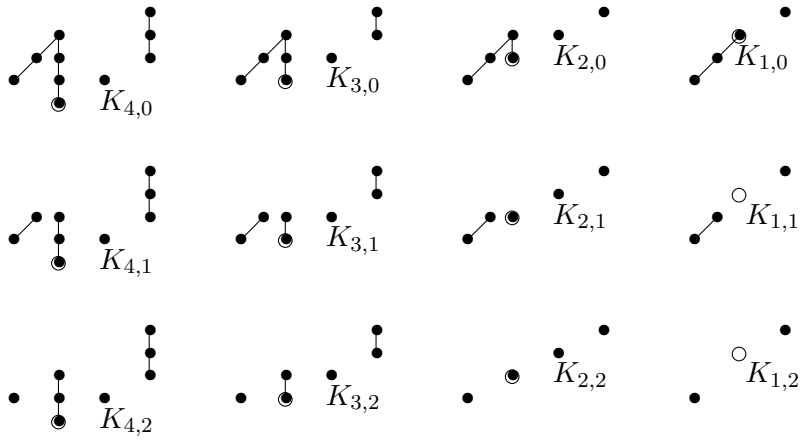

Now we describe the remaining edges.

Theorem 7.6. *For $0 \le b \le 3$ define f_b by*

$$f_b(0) = \begin{cases} 1 & b = 0 \\ 0 & b = 1,2,3, \end{cases}$$

and for $i \ge 1$ and any j,

$$f_b(i) = \begin{cases} 0 & 2^j \le i \le 2^j + [(b+j-2)/4] \\ 1 & i = 2^j + (b+j-1)/4,\ b+j \equiv 1\ (4) \\ 2 & 2^j + [(b+j-1)/4] + 1 \le i \le 2^{j+1} - 1. \end{cases}$$

For $2 \le e \le k-1$, let $e = 4a+b$ with $0 \le b \le 3$. Then

$$\mathcal{E}_{e,k} = \bigoplus_{i=0}^{2^{k-1-e}-1} K_{k-\lg(i)-1-e, f_b(i)}(8(i+a)+4, 3-k+4(i+a)),$$

with $\lg(0) = -1$ and the following modifications:

(1) *If $b = 3$ and $K_{t,\varepsilon}(x,y)$ is the summand for i a 2-power, then the element g' in $(x-2, y+t-3)$ is replaced by an element in $(x-2, y+t-2)$;*
(2) *If $b = 0$ or 1 and $K_{t,\varepsilon}(x,y)$ is the summand for $i+1$ a 2-power, and $t > 1$, then the top element in grading $x+4$ is killed; i.e., $2^{t-2}g''' = 0$;*
(3) *If $b = 0$ or 1 and $i = 2^{k-1-e} - 1$, the element in grading $x+2$ in this $K_{1,\varepsilon}(x,y)$ is killed.*
(4) *If $b = 3$, there is an additional element in $(2^{k+2-e} + 8a + 2, 2^{k+1-e} - k + 4a + 1)$, which would be the first element if the string of $K_{1,2}$'s at the end was extended one farther.*

In Table 1, we list a sample of values of $f_b(i)$. If $i < 256$ is not included in the table, then $f_b(i) = 2$ for all b.

i	0	1	2	4	5	8	9	16	17	32	33	64	65	66	128	129	130
$f_0(i)$	1	2	1	0	2	0	2	0	2	0	1	0	0	2	0	0	2
$f_1(i)$	0	1	0	0	2	0	2	0	1	0	0	0	0	2	0	0	2
$f_2(i)$	0	0	0	0	2	0	1	0	0	0	0	0	0	2	0	0	1
$f_3(i)$	0	0	0	0	1	0	0	0	0	0	0	0	0	1	0	0	0

Table 1: Values of $f_b(i)$

For example, in Figure 3.4, you can see $\Sigma^{32}\mathcal{E}_{2,5}$ with

$$\mathcal{E}_{2,5} = K_{3,0}(4,-2) \oplus K_{2,0}(12,2) \oplus K_{1,0}(20,6) \oplus K_{1,2}(28,10), \tag{7.7}$$

and $\Sigma^{48}\mathcal{E}_{3,5}$ and $\Sigma^{80}\mathcal{E}_{3,5}$ with

$$\mathcal{E}_{3,5} = K_{2,0}(4,-2) \oplus K'_{1,0}(12,2) \oplus \mathbb{Z}_2(18,3),$$

where K' incorporates modification (1), and $\mathbb{Z}_2(18,3)$ is modification (3).

8. Outline of proof

In this section, we outline the proof, which occupies the seven sections which follow.

In [11], we obtained the E_2 page of the ASS converging to $ku^*(K_2)$ and used a comparison with results about $k(1)^*(K_2)$ obtained in [10] to obtain formulas for differentials in this ASS. In Section 10 here, we show that the result of [11] *could have been grouped* into summands A_k and $B_{k,\ell}$, multiplied by various coefficients, rather than the A_k, B_k, and $S_{k,\ell}$ used there. By this, we mean that the cohomology classes underlying these summands fill out $H^*(K_2)$ (Theorem 10.3) and (Theorem 10.4) they are closed under the differentials in the ASS obtained in [11, Theorem 3.1].

These summands A_k and $B_{k,\ell}$ have analogues for the ASS converging to $ku_*(K_2)$, and in Section 9, we show how the duality between $ku_*(K_2)$ and $ku^*(K_2)$ obtained in [8] can be used to obtain differentials in the ASS converging to $ku_*(K_2)$. These will be used in Section 14.

In [13], we obtained the ko analogues, $\mathcal{M}_k$, of the basic summands M_k used in the ku work in [11]. A complication for the ko work is that whereas coefficients z_j for the M_k's in ku just resulted in suspensions, the ko analogue causes a change in form, resulting in charts M_k^i if there are i z_j's. In Section

11, we describe the way in which the ko_* analogues $\mathcal{A}_k$ of A_k, and $z^i\mathcal{B}_{k,\ell}$ of $B_{k,\ell}$ (if there are i z_j's) are built from a sequence of charts M_b^a with differentials between them. The results of Section 10 imply that these are closed under differentials and fill out $ko_*(K_2)$.

In Section 12, we use a small example, $\mathcal{A}_4$, to illustrate how the differentials combine to yield a nice picture for this summand of $ko_*(K_2)$. We also explain how the initial part of $\mathcal{A}_k$, which differs from everything else, is handled.

Our favored description of $\mathcal{A}_k$ in Section 4 is in terms of pre-edges and subedges. There is a nice pattern of differentials from the subedges to the pre-edges, turning pre-edges into edges. In Section 13 we show how the 2^{k-1} charts M_b^a which form $\mathcal{A}_k$ work together to form the pre-edges and subedges. The upper edge, which involves the initial part considered in Section 12, is slightly different than the others, and is discussed at the end of Section 13.

In Subsection 14.1, we describe how the summands that build $\widetilde{\mathcal{A}}_k$ work together in the spectral sequence. The proof that the differentials are as claimed is given in Subsection 14.2, by comparison with the ku_* differentials obtained in Sections 9 and 10. In Subsection 14.3, we explain how the nice pattern of exotic extensions in the ko_* ASS is established, using comparison with ku_* extensions, Toda brackets, and Adams periodicity.

In Section 15, we discuss modifications required in the formation of $z^i\mathcal{B}_{k,\ell}$.

9. Using the ku^* differentials

In this section, we make our first, very preliminary, step toward a proof. Our input is formulas ([11, Theorem 3.1]) for differentials in the ASS converging to $ku^*(K_2)$, which were derived in [11] by complicated ad hoc methods. In the final section of [11], almost as an afterthought, we sketched an approach to $ku^*(K_2)$ and $ku_*(K_2)$ which involved summands in a splitting of $H^*(K_2)$[2] as a module over a subalgebra of the mod-2 Steenrod algebra. This summand approach will be the way that we compute $ko_*(K_2)$.

In this section, we focus on the summand A_4 of $ku^*(K_2)$ and show specifically how the formulas for the differentials in the ASS of $ku^*(K_2)$ can be applied to the summand approach to $ku^*(K_2)$ and then to $ku_*(K_2)$. There is an exterior subalgebra E_1 of the mod 2 Steenrod algebra with generators Q_0 and Q_1 of grading 1 and 3, respectively, such that the E_2 page of the ASS converging to $ku^*(K_2)$ is $\mathrm{Ext}_{E_1}(\mathbb{Z}_2, H^*(K_2))$. We depict the spectral sequence using ku^* gradings increasing from right to left, as was done in [11]. We draw E_1-modules using straight lines for the action of Q_0 and curved lines for the action of Q_1.

In [11], we introduced classes $z_i \in H^{2^{i+2}+2}(K_2)$, $y_1 \in H^4(K_2)$, and $q \in H^9(K_2)$, and E_1-submodules M_k for $k \geq 4$, which we picture in Figure 9.1 for $4 \leq k \leq 6$, indicating the grading of the classes.

Figure 9.1. E_1-modules M_k.

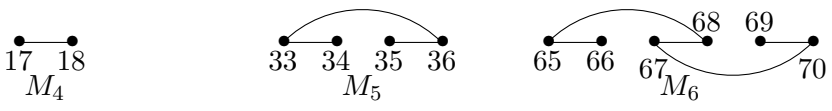

[2]Coefficients of cohomology groups are $\mathbb{Z}_2$ unless noted to the contrary.

The classes in Figure 9.1 with grading 18, 34, 36, 66, 68, and 70 are

$$z_2,\ z_3,\ z_2^2,\ z_4,\ z_3^2,\ \text{and } z_2^2 z_3, \tag{9.2}$$

respectively. Pictures of $\mathrm{Ext}_{E_1}(\mathbb{Z}_2, M_k)$ are given in Figure 9.3, where vertical lines indicate multiplication by h_0, and diagonal lines multiplication by $v \in ku^{-2}$.

Figure 9.3. $\mathrm{Ext}_{E_1}(\mathbb{Z}_2, M_k)$**.**

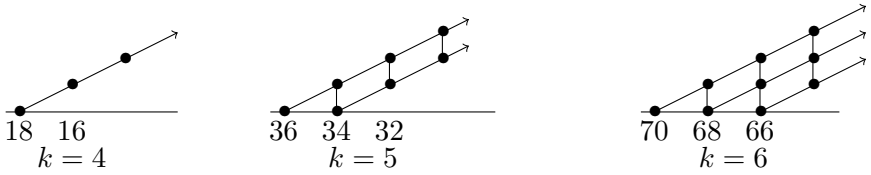

We call the diagonal lines v-towers. Their generators are the classes listed in (9.2).

Analogous to [11, Figure 17] is the list in Figure 9.4 of E_1-submodules which combine to form $A_4 \subset ku^*(K_2)$. We list them in order of decreasing grading to correspond to the order in the $ku^*(K_2)$ chart.

Figure 9.4. E_1**-modules building** A_4**.**

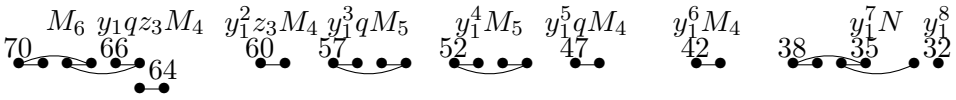

Here N is an E_1-module pictured in Figure 9.5; $\mathrm{Ext}_{E_1}(\mathbb{Z}_2, N)$ is also in Figure 9.5. The cohomology class in grading 9 is q, and, as shown in [11, Figures 8 and 9], the generator of the first infinite tower in Ext corresponds to v^2q.

Figure 9.5. N **and** $\mathrm{Ext}_{E_1}(\mathbb{Z}_2, N)$**.**

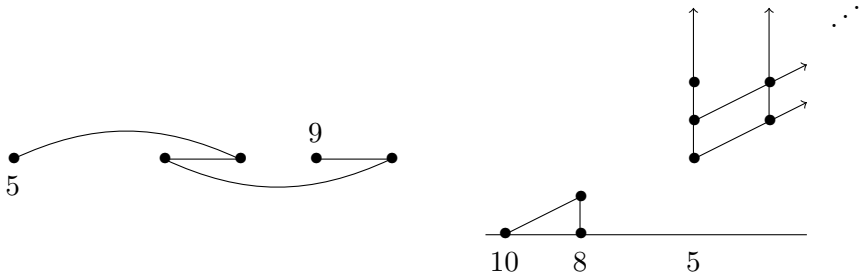

We extract from [11, Theorem 3.1] the formulas for differentials in the ASS converging to $ku^*(K_2)$ relevant to this approach to A_4. Here Λ_{j+1} is an exterior algebra on classes z_i with $i \geq j+1$, and $\otimes\Lambda_{j+1}$ means that the

formula can be multiplied by any monomial in Λ_{j+1}.

$$\begin{aligned}
d^5(y_1^8) &= h_0^3 v^2 q y_1^7 \\
d^2(q y_1^{2a+1} z_j) &= v^2 y_1^{2a} z_2 z_j \qquad \otimes \Lambda_{j+1},\ j \geq 2 \\
d^5(q y_1^{4a+3} z_{j-1}^2) &= v^5 y_1^{4a} z_3 z_j \qquad \otimes \Lambda_{j+1},\ j \geq 3 \\
d^{12}(q y_1^{8a+7} z_{j-2}^2 z_{j-1}) &= v^{12} y_1^{8a} z_4 z_j \qquad \otimes \Lambda_{j+1},\ j \geq 4 \\
d^2(v^2 q y_1^{2a+1}) &= v^4 y_1^{2a} z_2 \\
d^5(h_0 v^2 q y_1^{4a+3}) &= v^8 y_1^{4a} z_3 \\
d^{12}(h_0^2 v^2 q y_1^{8a+7}) &= v^{16} y_1^{8a} z_4.
\end{aligned}$$

After the first formula is applied to $y_1^7 N \oplus \langle y_1^8 \rangle$, the surviving v-towers are $h_0^t v^2 q y_1^7$ for $0 \leq t \leq 2$. The other formulas apply to these v-towers and all those in the other summands in Figure 9.4. We show these in Figure 9.6.

Figure 9.6. Differentials leading to A_4.

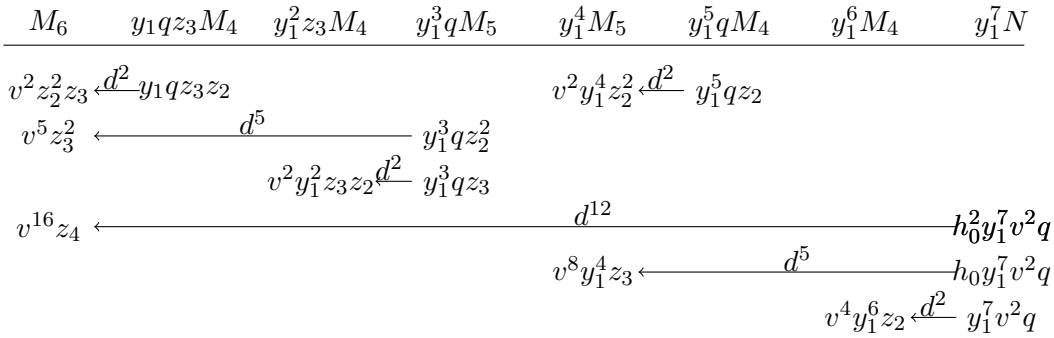

After these differentials, what remains in A_4 are truncated v-towers of the targets of the differentials in Figure 9.6. We depict this in Figure 9.7. The classes in the lower right corner come from Figure 9.5 after multiplying by y_1^7. This chart agrees with the A_4 part of [11, Figure 1] except that we do not address the exotic extensions here.

Figure 9.7. v-towers in A_4.

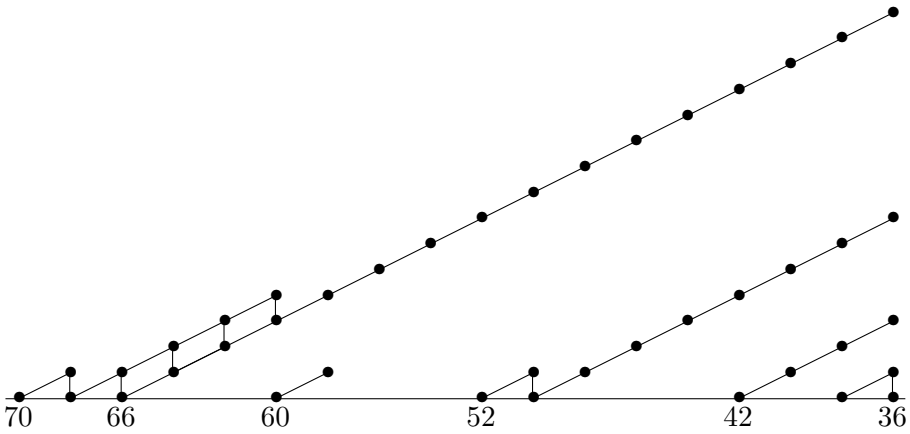

For $ku_*(K_2)$, the E_2-page is $\mathrm{Ext}_{E_1}^{*,*}(H^*K_2, \mathbb{Z}_2)$. For its A_4, called $\mathscr{A}_4$, we use the summands of Figure 9.4 but arrange them in the opposite order. The

Ext groups corresponding to Figures 9.3 and 9.5 are presented in Figure 9.8. See [12, Figure 4.2] for N.

Figure 9.8. $\mathrm{Ext}_{E_1}(M_k, \mathbb{Z}_2)$ **and** $\mathrm{Ext}_{E_1}(N, \mathbb{Z}_2)$**.**

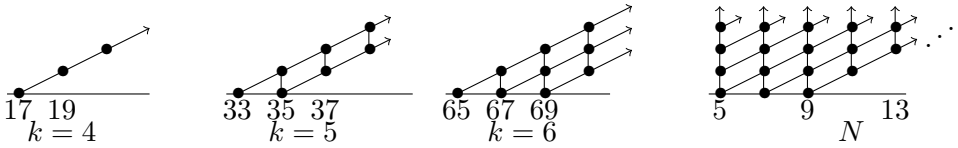

We dualize the ku^* differentials, similarly to [10]. In Figure 9.9, we show the dualization of a d^2 and d^5 differential from 9.6.

Figure 9.9. Dualizing d^2 **and** d^5 **differentials.**

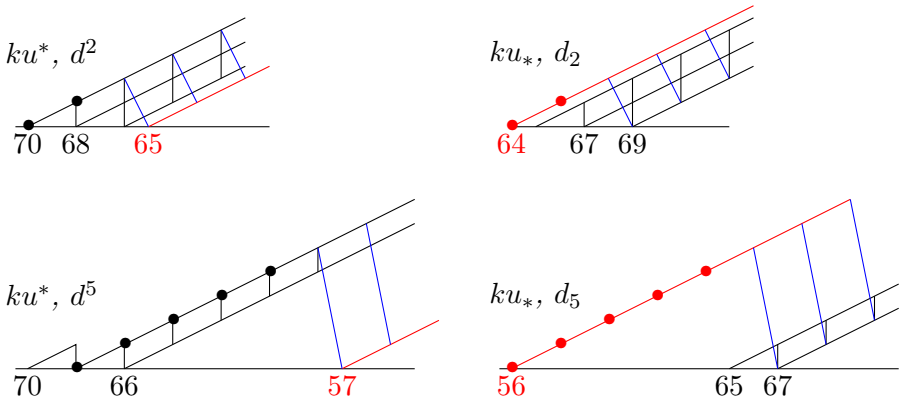

The justification for this duality of differentials is the duality of ku_*-modules,

$$ku_*(K_2) \approx (ku^{*+4}(K_2))^\vee, \tag{9.10}$$

which was proved in [8, Example 3.4] and restated in [11, Theorem 1.20]. Here $M^\vee$ is the Pontryagin dual of M. The Pontryagin dual of the two ku^* charts in Figure 9.9 have v-towers of height 2 and 5 on classes of grading 68 and 60, respectively, corresponding to v-towers on classes of grading 64 and 56, respectively, in the ku_* charts. Note that in the Pontryagin dual, the action of $\cdot 2$ and v appears backwards from its usual appearance.

There is a d_5-differential from $\mathrm{Ext}_{E_1}(y_1^7 N, \mathbb{Z}_2)$ to $\mathrm{Ext}_{E_1}(\langle y_1^8 \rangle, \mathbb{Z}_2)$ pictured in Figure 9.11. This and the first differential in the above list of seven differential formulas in $ku^*(K_2)$ are derived from [4] as discussed in [12, Section 4] and [11, Section 3]. This truncates all the infinite vertical towers, leaving the classes indicated by dots.

Figure 9.11. Differential killing infinite towers in $\mathscr{A}_4$.

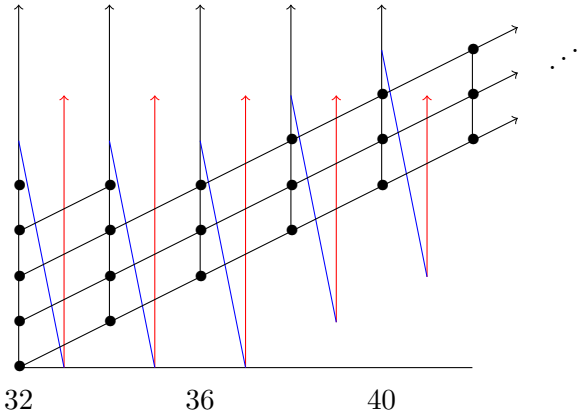

This leaves three infinite v-towers from the $\langle y_1^8\rangle \oplus y_1^7 N$ summand in the summand approach to determining $\mathscr{A}_4$. In Figure 9.13 we dualize Figure 9.6. We write the summands in the opposite order. The direction of the differentials is reversed. For example, the duals of the d^2 and d^5 differentials in the upper left part of Figure 9.6 are shown in Figure 9.9 and appear in the upper right corner of Figure 9.13. The classes now have different names. What will be useful for us in passing to ko_* is the type of differential between the summands. One difference is that the d^2, d^5, and d^{12} differentials in the lower right part of Figure 9.6 become d_6, d_9, and d_{16}. We show this for the d^2 in Figure 9.12. This is caused by the triangle of classes of height 4 in the ku_* diagram.

Figure 9.12. Duality of a d^2 and d_6 differential.

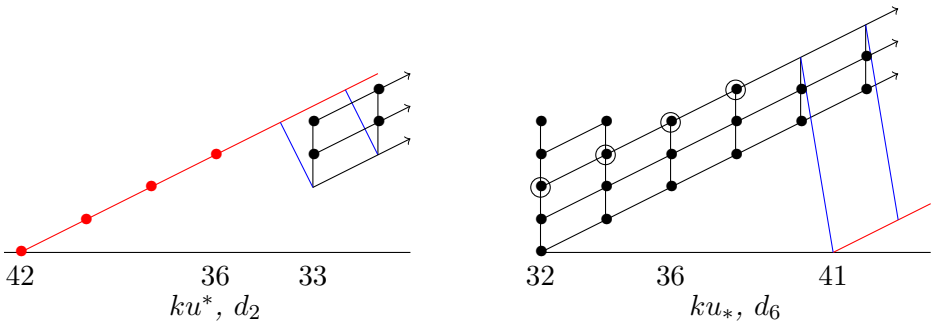

The v-tower of height 4 in $ku^*(K_2)^\vee$ on a class of grading 36 corresponds to a v-tower of height 4 on a class of grading 32 in $ku_*(K_2)$, consistent with (9.10).

In Figure 9.13, we list the differentials for the summand approach to $\mathscr{A}_4$. We write the gradings of the generators of the v towers involved in the differentials. For example, the ku_* differentials in Figure 9.9 are in the upper right corner of Figure 9.13, while the ku_* differential in Figure 9.12 is in the lower left.

Figure 9.13. Summand approach to $\mathscr{A}_4$.

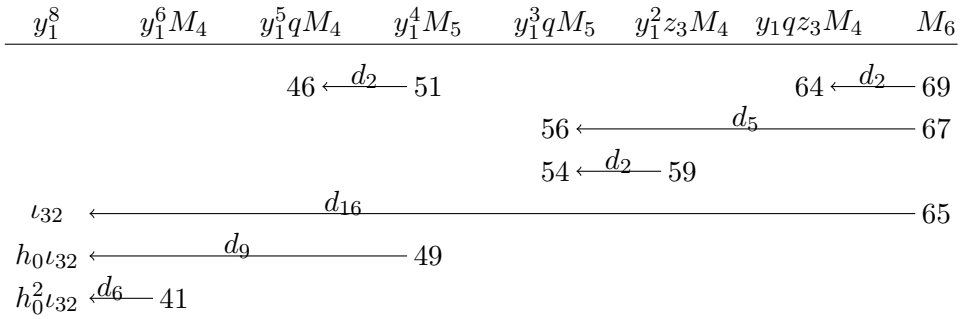

We close this section by displaying in Figure 9.14 the result of these differentials, the A_4 analogue of Figure 1.2 without the exotic extensions. For example, the d_6 differential to $h_0^2\iota_{32}$ hits $v^4h_0^2\iota_{32}$.

Figure 9.14. $\mathscr{A}_4$ without exotic extensions.

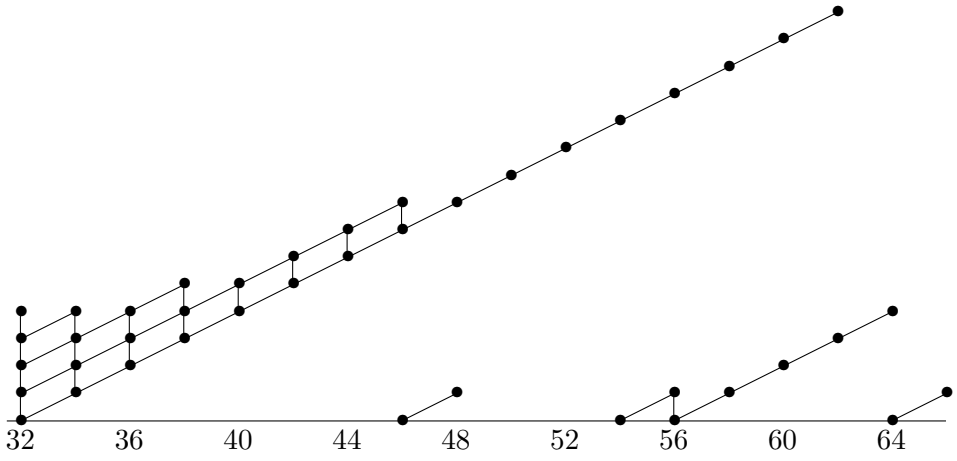

10. Summand approach to $ku^*(K_2)$

In this section, we provide more details to the summand approach to $ku^*(K_2)$ initiated briefly in [11, Section 7] and introduced here in Section 9. In subsequent sections, we will use it to determine $ko_*(K_2)$. We use the notation of [11] as recalled early in Section 9.

First we define some E_1-submodules of $H^*(K_2)$ which generalize Figure 9.4. Here and elsewhere $\nu(m)$ is the 2-exponent of an integer m.

Definition 10.1. *For $k \geq 1$, let*

$$C_k = (y_1q \oplus y_1^2) \cdot \bigoplus_{i=1}^{2^{k-2}-1} y_1^{2i-2} z(J(k,i)) M_{\nu(i)+4},$$

where $J(k,i) = 2^k - 4(2^{\nu(i)} + i)$ and $z(\sum 2^{j_t}) = \prod z_{j_t}$ if j_t are distinct integers.

For example, C_4 is the sum of the modules in Figure 9.4, omitting M_6 and the last two. Note that $C_1 = C_2 = 0$. Also $M_3 = 0$. We recall notation from [11], $Z_k^\ell = z_k \cdots z_{\ell-1}$.

Definition 10.2. *For $k \geq 1$,*

$$\widehat{A}_k = M_{k+2} \oplus C_k \oplus y_1^{2^{k-1}-1} N \oplus \langle y_1^{2^{k-1}} \rangle.$$

For $1 \leq k < \ell$,

$$\widehat{B}_{k,\ell} = z_\ell M_{k+2} \oplus z_\ell C_k \oplus y_1^{2^{k-1}-1} q M_{\ell+2} \oplus y_1^{2^{k-1}} M_{\ell+2} \\ \oplus y_1^{2^{k-1}} Z_k^\ell C_k \oplus y_1^{2^{k-1}-1} q Z_{k+1}^\ell M_{k+2}.$$

For example, $\widehat{A}_4$ is in Figure 9.4. Since we are thinking here of the spectral sequence converging to $ku^*(K_2)$, and we depict that spectral sequence with gradings decreasing from left to right, we prefer to list our modules in that order, too.

In this section, we prove the following two key theorems. As in [11], Λ_j denotes the exterior algebra generated by all z_i with $i \geq j$, thought of as a set of monomials used as coefficients. We often use juxtaposition for tensor products.

Theorem 10.3. *There is an isomorphism of E_1-modules,*

$$H^*(K_2) = \bigoplus_{i \geq 0,\, k \geq 1} y_1^{2^k i} \widehat{A}_k \oplus \bigoplus_{\substack{1 \leq k < \ell \\ i \geq 0}} y_1^{2^k i} \Lambda_{\ell+1} \widehat{B}_{k,\ell} \oplus F,$$

where F is a free E_1-module.

As in [11], F is computable but not of interest. It gives rise to a trivial ku^*-submodule of $ku^*(K_2)$.

Theorem 10.4. *Each $y_1^{2^k i} \widehat{A}_k$ and $y_1^{2^k i} \Lambda_{\ell+1} \widehat{B}_{k,\ell}$ is closed under the differentials in the ASS converging to $ku^*(K_2)$, as listed in* [11, Theorem 3.1].

The ideas in the following proofs will not be needed elsewhere.

Proof of Theorem 10.3. By [11, Proposition 2.11, (2.16)], ignoring the free part, the E_1-summands of $H^*(K_2)$ are

$$\{\langle y_1^i \rangle : i \geq 1\} \cup \{y_1^i N : i \geq 0\} \cup \{y_1^i M_j \Lambda_{j-1},\, q y_1^i M_j \Lambda_{j-1} : i \geq 0,\, j \geq 4\}. \tag{10.5}$$

From the last two summands of the $\widehat{A}_k$'s, with their coefficients, we get

$$\{y_1^{2^{k-1}-1} N \cdot y_1^{2^k i} : k \geq 1, i \geq 0\} = \{y_1^i N : i \geq 0\}$$

and

$$\{\langle y_1^{2^{k-1}} \rangle y_1^{2^k i} : k \geq 1, i \geq 0\} = \{\langle y_1^i \rangle : i \geq 1\}.$$

Since $C_1 = 0$ and $M_3 = 0$, all $\widehat{B}_{1,\ell}$ with their coefficients give all $y_1^{2i+1} M_j \Lambda_{j-1}$ and all $y_1^{2i} q M_j \Lambda_{j-1}$.

For the rest, we consider the part without the q factor. We will show that we obtain exactly all $y_1^{2i} M_j \Lambda_{j-1}$ with $j \geq 4$. The part with q follows similarly.

As in [11], let $y_k = y_1^{2^{k-1}}$. We let $\Gamma_k = \{y_1^{2^{k-1}i} : i \geq 0\}$, which we think of additively as an exterior algebra on $\{y_i : i \geq k\}$, analogous to Λ_k for the z's.

We consider the coefficient of M_k. When we talk about $\widehat{A}$'s and $\widehat{B}$'s, we always include their coefficients as given in Theorem 10.3. We consider first just the non-C part in Definition 10.2. Then $\widehat{A}_{k-2}$ gives Γ_{k-1} as coefficient of M_k. Next, $\bigcup_{\ell\geq k-1} \widehat{B}_{k-2,\ell}$ gives $\Gamma_{k-1}\cdot\bigcup_{\ell\geq k-1} z_\ell\Lambda_{\ell+1} = \Gamma_{k-1}\overline{\Lambda}_{k-1}$, where the bar denotes the augmentation ideal. Combining with the part obtained from $\widehat{A}_{k-2}$ yields $\Gamma_{k-1}\Lambda_{k-1}$.

The $y_1^{2^{i-1}}M_k$ part of $\widehat{B}_{i,k-2}$ for $2 \leq i \leq k-3$ gives $\Lambda_{k-1}\cdot\{y_1^t : 1 \leq \nu(t) \leq k-4\}$ as coefficient of M_k. The $\Gamma_{k-1}\Lambda_{k-1}$ obtained in the preceding paragraph gave the portion with $\nu(t) \geq k-2$. So the combination of the non-C parts gave everything that we want except $y_{k-2}\Gamma_{k-1}\Lambda_{k-1}$.

One can show that, for $p \geq k-1$, the coefficient of M_k in C_p is

$$y_{k-2}\prod_{i=k-1}^{p-1}\{z_i, y_i\}, \tag{10.6}$$

where, as in [11, (1.7)], the product-of-sets notation means the set of all products containing one choice of the two elements in each factor. For example, if $p = k+1$, this product is $\{z_{k-1}y_{k-1}, z_ky_{k-1}, z_{k-1}y_k, z_ky_k\}$. An empty product equals 1. We verify the claim when $p = k+1$. The relevant values of i in Definition 10.1 are $2^{k-4}u$ for $u = 1, 3, 5, 7$. For these, the $z(J(k+1,i))$ equal, respectively, $z_{k-1}z_k$, z_k, z_{k-1}, and 1, while y_1^{2i} are y_{k-2}, $y_{k-2}y_{k-1}$, $y_{k-2}y_k$, and $y_{k-2}y_{k-1}y_k$. The case of arbitrary p is similar.

Now we complete the proof by showing that the coefficient of M_k coming from the occurrences of various C_p's in $\widehat{A}_p$'s and $\widehat{B}_{p,\ell}$'s is $y_{k-2}\Gamma_{k-1}\Lambda_{k-1}$. Since y_{k-2} is always a factor in (10.6), we shall omit writing it in what follows. When we write "From $\widehat{A}_p$" or "from $\widehat{B}_{p,\ell}$," we always mean to include their coefficients as stated in the theorem.

From $\widehat{A}_{k-1}$, we get Γ_k (as coefficient of M_k), since the product in (10.6) is empty. From $\bigcup_{\ell\geq k}\widehat{B}_{k-1,\ell}$, we get

$$\begin{aligned} &\Gamma_k\cdot\bigcup_{\ell\geq k} z_\ell\Lambda_{\ell+1} \cup y_{k-1}\Gamma_k\bigcup_{\ell\geq k} Z_{k-1}^\ell\Lambda_{\ell+1} \\ = \;& \Gamma_k\overline{\Lambda}_k \cup y_{k-1}\Gamma_k z_{k-1}\Lambda_k. \end{aligned}$$

We combine with the part from $\widehat{A}_{k-1}$ to remove the bar, yielding

$$\Gamma_k\Lambda_k\{1, y_{k-1}z_{k-1}\}. \tag{10.7}$$

From $\widehat{A}_k$, using (10.6), we get $\Gamma_{k+1}\cdot\{z_{k-1}, y_{k-1}\}$. From $\bigcup_{\ell\geq k+1}\widehat{B}_{k,\ell}$, we get

$$\begin{aligned} &\{z_{k-1}, y_{k-1}\}\Gamma_{k+1}\bigcup_{\ell\geq k+1}\{z_\ell\Lambda_{\ell+1}, y_kZ_k^\ell\Lambda_{\ell+1}\} \\ = \;& \{z_{k-1}, y_{k-1}\}\Gamma_{k+1}\big(\overline{\Lambda}_{k+1}\cup y_kz_k\Lambda_{k+1}\big). \end{aligned}$$

The part from $\widehat{A}_k$ removes the bar, yielding

$$\Gamma_{k+1}\Lambda_{k+1}\{z_{k-1}, y_{k-1}\}\cdot\{1, y_kz_k\}. \tag{10.8}$$

The part in (10.7) is everything in $\Gamma_{k-1}\Lambda_{k-1}$ with an even number of factors with subscript $k-1$. The part in (10.8) is everything with an odd (resp. even) number of factors with subscript $k-1$ (resp. k). Using $\widehat{A}_{k+1}$ and $\widehat{B}_{k+1,\ell}$, we will get those with odd (resp. odd, even) number with subscript $k-1$ (resp. k, $k+1$). This will continue, yielding all of $\Gamma_{k-1}\Lambda_{k-1}$, as desired. ■

Proof of Theorem 10.4. We begin by considering the differentials within C_k. In Table 2, we list C_5 as a guide.

$y_1qz_3z_4M_4$	$y_1^2z_3z_4M_4$	$y_1^3qz_4M_5$	$y_1^4z_4M_5$	$y_1^5qz_4M_4$	$y_1^6z_4M_4$	$y_1^7qM_6$
$y_1^8M_6$	$y_1^9qz_3M_4$	$y_1^{10}z_3M_4$	$y_1^{11}qM_5$	$y_1^{12}M_5$	$y_1^{13}qM_4$	$y_1^{14}M_4$

Table 2: C_5

Let $Y_{j,k}$ denote the term in C_k containing y_1^j as a factor. For example, $Y_{3,5} = y_1^3qz_4M_5$. We conflate M_j with its chart, $\mathrm{Ext}_{E_1}(\mathbb{Z}_2, M_j)$, as pictured in Figure 9.3. Note that M_j has $j-3$ v-towers. For example, the v-towers of M_7 are generated by $z_2^2z_3z_4$, $z_3^2z_4$, z_4^2, and z_5, in order of decreasing grading. We let $b_i(M_r)$ denote the ith generator from the bottom of M_r, and $\tau_i(M_r)$ the ith generator from the top. For example, $b_1(M_7) = z_5$ and $\tau_2(M_7) = z_3^2z_4$.

We recall the notation of [11, 1.12)]:

$$z_{i,j} = \begin{cases} z_i(z_i \cdots z_{j-1}) & i < j \\ z_i & i = j \end{cases}$$

Then $b_i(M_r) = z_{r-1-i,r-2}$ and $\tau_i(M_r) = z_{i+1,r-2}$. If $Y_{r,k} = c\,M_j$, we let $b_i(Y_{r,k}) = c\,b_i(M_j)$ and $\tau_i(Y_{r,k}) = c\,\tau_i(M_j)$. Our claim is that the differentials of [11, Theorem 3.1] are exactly

$$d^{2^{t+1}-(t+1)}(b_t(Y_{2^t(a+1)-1,k})) = v^{2^{t+1}-(t+1)}\tau_t(Y_{2^ta,k}) \tag{10.9}$$

for $1 \le a \le 2^{k-t-1} - 2$ with $1 \le t \le k-3$. This will remove or truncate all v-towers except $\tau_1(Y_{2^r-1,k})$ and $b_1(Y_{2^{k-1}-2^r,k})$ for $1 \le r \le k-2$. To justify this, we use C_5 as our example and consider $Y_{r,k}$ with r even. The image of d^2 is all $\tau_1(Y_{2a,5})$ for $1 \le a \le 6$, while $\mathrm{im}(d^5)$ is $\{\tau_2(Y_{4,5}), \tau_2(Y_{8,5})\}$. Since $Y_{r,k}$ has $\nu(r)$ classes when r is even, the elements not in $\mathrm{im}(d)$ are $\tau_3(Y_{8,5})$, $\tau_2(Y_{12,5})$, and $\tau_1(Y_{14,5})$, each of which is b_1.

Now we work toward proving (10.9). The formula in [11, Theorem 3.1] is

$$d^{2^{t+1}-(t+1)}(y_1^{2^t(a+1)-1}qz_{j-t+1,j}) = v^{2^{t+1}-(t+1)}y_1^{2^t\,a}z_{t+1}z_j \tag{10.10}$$

for $j \ge t+1$. This can be multiplied by Λ_{j+1}. Our formula (10.9) says

$$\begin{aligned} & d^{2^{t+1}-(t+1)}(y_1^{2^t(a+1)-1}qz(J(k,2^{t-1}(a+1)))b_t(M_{t+3+\nu(a+1)})) \\ = \;& v^{2^{t+1}-(t+1)}y_1^{2^ta}z(J(k,2^{t-1}a))\tau_t(M_{t+3+\nu(a)}). \end{aligned} \tag{10.11}$$

We have

$$z(J(k,2^{t-1}(a+1))) = 2^k - 2^{t+1}(2^{\nu(a+1)} + a + 1)$$

and

$$z(J(k,2^{t-1}a)) = 2^k - 2^{t+1}(2^{\nu(a)}+a).$$

If a is odd, then

$$z(J(k,2^{t-1}a)) = z(J(k,2^{t-1}(a+1))) + 2^{t+1+\nu(a+1)}$$

with $\nu(z(J(k,2^{t-1}(a+1)))) > t+1+\nu(a+1)$. If a is even, then

$$z(J(k,2^{t-1}(a+1))) = z(J(k,2^{t-1}a)) + 2^{t+1}(2^{\nu(a)}-2)$$

with $\nu(z(J(k,2^{t-1}a))) > t+1+\nu(a)$.

If a is odd, then, with $\nu = \nu(a+1)$,

$$b_t(M_{t+3+\nu}) = z_{2+\nu,t+1+\nu}$$

and $\tau_t(M_{t+3}) = z_{t+1}$. In this case, our formula (10.11) becomes

$$d^{2^{t+1}-(t+1)}(y_1^{2^t(a+1)-1}qPz_{2+\nu,t+1+\nu}) = v^{2^{t+1}-(t+1)}y_1^{2^t a}z_{t+1+\nu}Pz_{t+1}$$

with $P \in \Lambda_{t+2+\nu}$. This agrees with (10.10) with $j = t+1+\nu$.

If a is even, then, with $\nu = \nu(j)$, $b_t(M_{t+3}) = z_{2,t+1}$ and $\tau_t(M_{t+3+\nu}) = z_{t+1,t+1+\nu}$. In this case, our formula (10.11) becomes

$$d^{2^{t+1}-(t+1)}(y_1^{2^t(a+1)-1}qz_{t+2}\cdots z_{t+\nu}Pz_{2,t+1}) = y^{2^{t+1}-(t+1)}y_1^{2^t a}Pz_{t+1,t+1+\nu}$$

with $P \in \Lambda_{t+2+\nu}$. Since $z_{t+1,t+1+\nu} = z_{t+1}^2 \cdot z_{t+2}\cdots z_{t+\nu}$, this agrees with (10.10) with $j = t+1$. This completes the proof regarding differentials within C_k.

Next we handle the differentials in $\widehat{A}_k$ from C_k to M_{k+2}. We claim that

$$d^{2^{t+1}-(t+1)}(\tau_1(Y_{2^t-1,k})) = v^{2^{t+1}-(t+1)}\tau_t(M_{k+2})$$

for $1 \le t \le k-2$ follows from (10.10). These can be seen in Figure 9.6 when $k=4$. We have

$$\begin{aligned}\tau_1(Y_{2^t-1,k}) &= y_1^{2^t-1}qz(J(k,2^{t-1}))\cdot\tau_1(M_{t+3}) \\ &= y_1^{2^t-1}qz_{t+2}\cdots z_{k-1}\cdot z_{2,t+1}.\end{aligned}$$

By (10.10), $d^{2^{t+1}-(t+1)}$ applied to this equals

$$v^{2^{t+1}-(t+1)}z_{t+1}^2\cdot z_{t+2}\cdots z_{k-1} = v^{2^{t+1}-(t+1)}z_{t+1,k} = v^{2^{t+1}-(t+1)}\tau_t(M_{k+2}),$$

as claimed. The same argument applies to differentials in $\widehat{B}_{k,\ell}$ from $z_\ell C_k$ to $z_\ell M_{k+2}$.

Next we explain the differentials in $\widehat{A}_k$ from the $y_1^{2^{k-1}-1}N$ part. See Figure 9.6 for a depiction of the case $k=4$. Using the Ext calculation pictured in Figure 9.5 and the differential

$$d^{\nu(i)+2}(y_1^i) = h_0^{\nu(i)}v^2qy_1^{i-1}$$

from [11, Theorem 3.1], the v-towers remaining in $y_1^{2^{k-1}-1}N$ are

$$h_0^s v^2 q y_1^{2^{k-1}-1} \text{ for } 0 \le s \le k-2.$$

These satisfy

$$d^{2^{t+1}-(t+1)}(h_0^{t-1}v^2qy_1^{(a+1)2^t-1}) = v^{2^{t+1}}y_1^{2^t a}z_{t+1}$$

by [11, Theorem 3.1]. Here $1 \le t \le k-1$. With $(a+1)2^t = 2^{k-1}$, so $2^t a = 2^{k-1} - 2^t$, the target classes are the remaining classes $b_1(Y_{2^{k-1}-2^t,k})$ (see after (10.9)), including also $b_1(M_{k+2})$.

Next we discuss the differentials in $\widehat{B}_{k,\ell}$ from the $y_1^{2^k-1} q Z_{k+1}^\ell M_{k+2}$ part. We factor out the Z_{k+1}^ℓ, so are hitting into $y_1^{2^{k-1}} z_k C_k$. We have, using [11, Theorem 3.1], if $1 \le t \le k-2$,

$$\begin{aligned} d^{2^{t+1}-(t+1)}(y_1^{2^k-1} q b_t(M_{k+2})) &= d^{2^{t+1}-(t+1)}(y_1^{2^k-1} q z_{k+1-t,k}) \\ &= v^{2^{t+1}-(t+1)} y_1^{2^k-2^t} z_{t+1} z_k \\ &= v^{2^{t+1}-(t+1)} y_1^{2^{k-1}} y_1^{2^{k-1}-2^t} z_{t+1} z_k \\ &= v^{2^{t+1}-(t+1)} y_1^{2^{k-1}} b_1(Y_{2^{k-1}-2^t,k}) z_k, \end{aligned}$$

which were the remaining v-towers in $y_1^{2^{k-1}} z_k C_k$. If $t = k-1$, then

$$\begin{aligned} & d^{2^{t+1}-(t+1)}(y_1^{2^k-1} q\, Z_{k+1}^\ell b_t(M_{k+2})) \\ = \;& v^{2^{t+1}-(t+1)} y_1^{2^{k-1}} Z_{k+1}^\ell z_k^2 \\ = \;& v^{2^{t+1}-(t+1)} y_1^{2^{k-1}} z_{k,\ell} \\ = \;& v^{2^{t+1}-(t+1)} y_1^{2^{k-1}} \tau_{k-1}(M_{\ell+2}) \end{aligned}$$

in $y_1^{2^{k-1}} M_{\ell+2}$.

The argument for differentials in $\widehat{B}_{k,\ell}$ from $y_1^{2^{k-1}-1} q M_{\ell+2}$ to $z_\ell C_k$ is almost identical.

$$\begin{aligned} d^{2^{t+1}-(t+1)}(y_1^{2^{k-1}-1} q b_t(M_{\ell+2})) &= d^{2^{t+1}-(t+1)}(y_1^{2^{k-1}-1} q z_{\ell+1-t,\ell}) \\ &= v^{2^{t+1}-(t+1)} y_1^{2^{k-1}-2^t} z_{t+1} z_\ell \\ &= v^{2^{t+1}-(t+1)} b_1(Y_{2^{k-1}-2^t,k}) z_\ell, \end{aligned}$$

for $1 \le t \le k-2$. If $t = k-1$, this is hitting $v^{2^{t+1}-(t+1)} z_\ell \tau_1(M_{k+2})$ in the $z_\ell M_{k+2}$ part of $\widehat{B}_{k,\ell}$. Note that v-towers on $y_1^{2^{k-1}-1} q b_t(M_{\ell+2})$ for $k \le t \le \ell - 1$ are not yet accounted for by these differentials.

Next we show that (10.10) implies that the differentials from $y_1^{2^{k-1}} Z_k^\ell C_k$ into $y_1^{2^{k-1}} M_{\ell+2}$ hit $v^{2^{t+1}-(t+1)} y_1^{2^{k-1}} \tau_t(M_{\ell+2})$ for $1 \le t \le k-2$. (The case $t = k-1$ was also hit, two paragraphs earlier.) We may ignore the $y_1^{2^{k-1}}$ factor. The v-towers in C_k remaining to support differentials are

$$\tau_1(Y_{2^t-1,k}) = y_1^{2^t-1} q\, z(J(k, 2^{t-1}))\tau_1(M_{t+3}) = y_1^{2^t-1} q\, Z_{t+2}^k\, z_{2,t+1}$$

for $1 \le t \le k-2$. By (10.10)

$$\begin{aligned} & d^{2^{t+1}-(t+1)}(Z_k^\ell\, \tau_1(Y_{2^t-1,k})) = Z_k^\ell\, Z_{t+2}^k v^{2^{t+1}-(t+1)} z_{t+1}^2 \\ = \;& v^{2^{t+1}-(t+1)} z_{t+1,\ell} = v^{2^{t+1}-(t+1)} \tau_t(M_{\ell+2}). \end{aligned}$$

What remains to consider in $\widehat{B}_{k,\ell}$ are the v-towers on $y_1^{2^{k-1}} b_i(M_{\ell+2})$ and $y_1^{2^{k-1}-1} q\, b_{k-1+i}(M_{\ell+2})$ for $1 \le i \le \ell - k$. (Here we have used $b_i(M_{\ell+2}) = \tau_{\ell-i}(M_{\ell+2})$.) A different formula from [11, Theorem 3.1] says

$$d^{k+1}(y_1^{2^{k-1}} z_\ell) = v^{k+1} y_1^{2^{k-1}-1} q\, z_{\ell-(k-1),\ell}$$

for $\ell \geq k+1$. This says

$$d^{k+1}(y_1^{2^{k-1}} b_1(M_{\ell+2})) = v^{k+1} y_1^{2^{k-1}-1} q\, b_k(M_{\ell+2}).$$

This differential is taking place in the sum of two charts of the form illustrated in Figure 9.3. The charts are displaced by 1 unit. For $i \leq \ell - k$, we have

$$\begin{aligned} v^{i-1} d^{k+1}(y_1^{2^{k-1}} b_i(M_{\ell+2})) &= d^{k+1}(y_1^{2^{k-1}} v^{i-1} b_i(M_{\ell+2})) \\ &= d^{k+1}(y_1^{2^{k-1}} h_0^{i-1} b_1(M_{\ell+2})) \\ &= v^{k+1} y_1^{2^{k-1}-1} q\, h_0^{i-1} b_k(M_{\ell+2}) \\ &= v^{k+1} y_1^{2^{k-1}-1} q\, v^{i-1} b_{k+i-1}(M_{\ell+2}). \end{aligned}$$

Hence for $i \leq \ell - k$, we have

$$d^{k+1}(y_1^{2^{k-1}} b_i(M_{\ell+2})) = v^{k+1} y_1^{2^{k-1}-1} q\, b_{k+i-1}(M_{\ell+2}).$$

■

11. The summands for $\mathcal{A}_k$ and $\mathcal{B}_{k,\ell}$

As we illustrated for A_4 in Section 9, if we apply $\mathrm{Ext}_{E_1}(-, \mathbb{Z}_2)$ to the summands of $\widehat{A}_k$ or $\widehat{B}_{k,\ell}$, we obtain the E_2 page of the ASS converging to summands of $ku_*(K_2)$, and the differentials are dual to those in the ASS converging to $ku^*(K_2)$.

The ASS converging to $ko_*(K_2)$ has $E_2 = \mathrm{Ext}_{A(1)}(H^*K_2, \mathbb{Z}_2)$, where $A(1)$ is the subalgebra of the mod-2 Steenrod algebra generated by Sq^1 and Sq^2. In [13], we found $A(1)$-submodules of H^*K_2 corresponding to the E_1-submodules in the splitting (10.5). We also found $\mathrm{Ext}_{A(1)}(-, \mathbb{Z}_2)$ for each of these summands. We review this now.

Multiplying by y_1^2 just suspends by Σ^8. Corresponding to y_1 is an $A(1)$-module U. There is an $A(1)$-module N, corresponding to the E_1-element q, which restricts to the E_1-module N. Corresponding to $y_1 N$ is an $A(1)$-module NU, which satisfies $N \otimes U = NU \oplus F$, with F free. We defer discussion of the charts for these modules themselves until the next section.

We denote by $\mathcal{M}_k$ the $A(1)$-submodule of H^*K_2 found in [13, Theorem 2,2] whose E_1-module structure equals that of the E_1-module M_k in (10.5) plus possibly a free E_1-module of rank 1, and let $\widetilde{\mathcal{M}}_k = \Sigma^{-2^k}\mathcal{M}_k$. The chart for $\widetilde{\mathcal{M}}_k$ is M_k^0, where M_k^0 is described in Figure 4.3 and subsequent discussion. If $z_J = z_{j_1} \cdots z_{j_r}$ with j_i distinct integers satisfying $j_i \geq k-1$, then $z_J \widetilde{\mathcal{M}}_k$ is an $A(1)$-submodule of H^*K_2 with chart $\Sigma^{4D} M_k^r$, where $D = \sum 2^{j_i}$ and M_k^r is as defined just before Figure 4.4. It is formed from M_k^0 by decreasing filtrations by r. This follows from [13, Proposition 3.4].

Corresponding to multiplication by q in (10.5) is just 9-fold suspension. Corresponding to $y_1 z_J M_k$ in (10.5), with J as above, is an $A(1)$-module $U z_J \mathcal{M}_k$ described in [13, after Proposition 3.6], where its chart is shown to be $\Sigma^{2^k}\Sigma^{4D} M_k^{r+2}$, with D as above. That is, multiplying $z_J \mathcal{M}_k$ by U reduces filtrations by 2 without changing the number of suspensions.

We have now described the $A(1)$-submodules corresponding to all the E_1-submodules in (10.5), and [13, Theorem 3.8] says that a sum of them

gives an $A(1)$-module splitting of H^*K_2. We define $\widehat{A}^{\rm o}_k$ and $z_J\widehat{B}^{\rm o}_{k,\ell}$ to be $A(1)$-modules formed from the $A(1)$-module analogues of the E_1-modules that formed $\widehat{A}_k$ and $z_J\widehat{B}_{k,\ell}$ in Definition 10.2. The proof of Theorem 10.3 applies to $A(1)$-modules just as well as to E_1-modules, and so we have the $A(1)$ analogue of Theorem 10.3.

Theorem 11.1. *There is an isomorphism of $A(1)$-modules,*

$$H^*(K_2) = \bigoplus_{i\geq 0,\, k\geq 1} y_1^{2^k\, i}\widehat{A}^o_k \oplus \bigoplus_{\substack{1\leq k<\ell \\ i\geq 0}} y_1^{2^k\, i}\Lambda_{\ell+1}\widehat{B}^o_{k,\ell} \oplus F,$$

where F is a free $A(1)$-module.

We will see in subsequent sections how the differentials among the summands of $\widehat{A}_k$ or $z_J\widehat{B}_{k,\ell}$ imply differentials among the corresponding summands of $\widehat{A}^{\rm o}_k$ or $z^i\widehat{B}^{\rm o}_{k,\ell}$, and these are closed under differentials by comparison with the ku result, Theorem 10.4.

Incorporating this observation, we can prove Theorem 1.3.

Proof of Theorem 1.3. Since $y_1^2 = \Sigma^8$ and $\mathcal{A}_k$ is the resultant of differentials and extensions in the ASS of $\widehat{A}^o_k$, the first half follows immediately from the first half of Theorem 11.1. There is a 1-1 correspondence between integers $2^{\ell+1}i$ and monomials in $\Lambda_{\ell+1}$, given by $2^{\ell+1}i = \sum 2^{j_i} \leftrightarrow \prod z_{j_i} = z_J$ with $j_i \geq \ell+1$ distinct. Since $\alpha(i)$ equals the number of 2^j's, we have $z_J\mathcal{B}_{k,\ell} = \Sigma^{4\cdot 2^{\ell+1}i}z^{\alpha(i)}\mathcal{B}_{k,\ell}$, and the second half of the theorem follows from this and the second half of Theorem 11.1. ■

We will be working with charts rather than their associated $A(1)$-modules, and so we wish to take advantage of the M^r_k notation. Recall from Sections 3 and 5 that $\widetilde{\mathcal{A}}_k = \Sigma^{-2^{k+1}}\mathcal{A}_k$ and $\widetilde{\mathcal{B}}_{k,\ell} = \Sigma^{-2^{\ell+2}}\mathcal{B}_{k,\ell}$. We define a tableau for $\widetilde{\mathcal{A}}_k$ or $\widetilde{\mathcal{B}}_{k,\ell}$ to be a list or direct sum of the charts which combine to give their E_2 page, but also usually include arrows for the d_2-differentials. These are listed in order of increasing grading. The first two summands of the tableau of $\widetilde{\mathcal{A}}_k$ are different and will be discussed in the next section; they involve higher differentials. The first summand, called V_k, was defined already in Definition 4.18.

In either the ku^* or ku_* or ko_* context, we associate to M_k or $\mathcal{M}_k$ the grading 2^k (even though it starts in grading 2^k+1.) Then M^r_k will have associated grading 0, even though it starts in some positive grading. A summand $y_1^{2i}z(J(k,i))\mathcal{M}_{\nu(i)+4}$ appearing in C_k in Definition 10.1 has associated grading

$$8i + 4(2^k - 4(2^{\nu(i)} + i)) + 2^{\nu(i)+4} = 2^{k+2} - 8i.$$

For $\widetilde{\mathcal{A}}_k$, we subtract 2^{k+1} from the grading, and so, listing them in order of increasing grading, opposite to the order in Section 9, associated to grading $8t$ in $\widetilde{\mathcal{A}}_k$ is $y_1^{2^{k-1}-2t}z(J(k,2^{k-2}-t))\mathcal{M}_{\nu(t)+4}$. For $1 \leq t < 2^{k-2}$, $J(k,2^{k-2}-t) = 4(t-\nu(t))$, so there are $\alpha(t)-1$ z's in $z(J(k,2^{k-2}-t))$. Hence the chart will be $\Sigma^{8t}M^{\alpha(t)-1}_{\nu(t)+4}$. The next term in the list will be the one with the

same i value in Definition 10.1 but with y_1^2 replaced by y_1q, so Σ^8 replaced by Σ^9U, and U adds 2 to the superscript of M. Thus the tableau for $\widetilde{\mathcal{A}}_k$ is

$$(V_k \leftarrow \Sigma^8 M_4^0) \oplus \bigoplus_{i=1}^{2^{k-2}-1} (\Sigma^{8i+1} M_{4+\nu(i)}^{\alpha(i)+1} \leftarrow \Sigma^{8i+8} M_{4+\nu(i+1)}^{\alpha(i+1)-1}). \tag{11.2}$$

For example, the tableaux for $\widetilde{\mathcal{A}}_4$ and $\widetilde{\mathcal{A}}_5$ are in (11.3) and (11.4).

$$V_4 \leftarrow \Sigma^8 M_4^0 \quad \Sigma^9 M_4^2 \leftarrow \Sigma^{16} M_5^0 \quad \Sigma^{17} M_5^2 \leftarrow \Sigma^{24} M_4^1 \quad \Sigma^{25} M_4^3 \leftarrow \Sigma^{32} M_6^0 \tag{11.3}$$

$$\begin{aligned} V_5 \leftarrow \Sigma^8 M_4^0 \quad \Sigma^9 M_4^2 \leftarrow \Sigma^{16} M_5^0 \quad \Sigma^{17} M_5^2 \leftarrow \Sigma^{24} M_4^1 \quad \Sigma^{25} M_4^3 \leftarrow \Sigma^{32} M_6^0 \\ \Sigma^{33} M_6^2 \leftarrow \Sigma^{40} M_4^1 \quad \Sigma^{41} M_4^3 \leftarrow \Sigma^{48} M_5^1 \quad \Sigma^{49} M_5^3 \leftarrow \Sigma^{56} M_4^2 \quad \Sigma^{57} M_4^4 \leftarrow \Sigma^{64} M_7^0. \end{aligned} \tag{11.4}$$

If the reader wishes to compare with Table 2, note that the order of terms is reversed. For example the entry $\Sigma^{33} M_6^2$ at the beginning of the second row of (11.4) corresponds to the $y_1^7 q M_6$ at the end of the first row of Table 2. The grading associated to the latter term in $\widetilde{\mathcal{A}}_5$ is $24 + 9 + 64 - 64$. Recall that multiplying by a single y_1 doesn't change the number of suspensions; it lowers filtrations by 2 since its $A(1)$ analogue is U.

We elaborate on the tableau (11.3) for $\widetilde{\mathcal{A}}_4$. The $A(1)$-modules underlying $\mathcal{A}_4$ are the $A(1)$-analogues of the E_1-modules in Figure 9.4, which was for ku-cohomology, so the order of the summands is reversed for ko-homology. The $A(1)$-modules corresponding to the eight charts in the tableau (11.3) are

$$\begin{aligned} (\Sigma^{32}\mathbb{Z}_2 \oplus \Sigma^{32} NU) \quad \Sigma^{40}\widetilde{\mathcal{M}}_4 \quad \Sigma^{40} NU\widetilde{\mathcal{M}}_4 \quad \Sigma^{48}\widetilde{\mathcal{M}}_5 \\ \Sigma^{48} NU\widetilde{\mathcal{M}}_5 \quad \Sigma^{24} z_3\widetilde{\mathcal{M}}_4 \quad \Sigma^{24} NU z_3\widetilde{\mathcal{M}}_4 \quad \Sigma^{64}\widetilde{\mathcal{M}}_6. \end{aligned}$$

Since (11.3) is for $\widetilde{\mathcal{A}}_4$, while these are for $\mathcal{A}_4$, Σ^{32} should be applied to (11.3) to make the correspondence precise. Then $\mathrm{Ext}_{A(1)}(-, \mathbb{Z}_2)$ for these $A(1)$-modules are Σ^{32} applied to the charts in the tableau (11.3), except that V_4 is formed from $\mathrm{Ext}_{A(1)}(\mathbb{Z}_2 \oplus NU, \mathbb{Z}_2)$ after incorporating a d_5-differential and filtration shift. For example,

$$\mathrm{Ext}_{A(1)}(\Sigma^{40} NU\widetilde{\mathcal{M}}_4, \mathbb{Z}_2) \approx \Sigma^{41} M_4^2,$$

as was shown in [13, Proposition 3.6,(3.7)].

The crux of our work is to see how the charts in a tableau combine. That is where the filtration shifts come into play.

The tableau for $\widetilde{\mathcal{B}}_{k,\ell}$ when $k \geq 3$ is in (11.5). For $k \leq 2$, they are in (11.6). These are seen by comparison with Definition 10.2.

$$(\Sigma M_{k+2}^{\ell-k+1} \leftarrow \Sigma^8 M_4^{\ell-k}) \oplus \bigoplus_{i=1}^{2^{k-2}-2} (\Sigma^{8i+1} M_{4+\nu(i)}^{\ell-k+\alpha(i)+1} \leftarrow \Sigma^{8i+8} M_{4+\nu(i+1)}^{\ell-k+\alpha(i+1)-1})$$
$$\oplus(\Sigma^{2^{k+1}-7} M_4^{\ell-1} \leftarrow \Sigma^{2^{k+1}} M_{\ell+2}^0) \oplus (\Sigma^{2^{k+1}+1} M_{\ell+2}^2 \leftarrow \Sigma^{2^{k+1}+8} M_4^1)$$
$$\oplus \bigoplus_{i=2^{k-2}+1}^{2^{k-1}-2} (\Sigma^{8i+1} M_{4+\nu(i)}^{\alpha(i)+1} \leftarrow \Sigma^{8i+8} M_{4+\nu(i+1)}^{\alpha(i+1)-1}) \oplus (\Sigma^{2^{k+2}-7} M_4^k \leftarrow \Sigma^{2^{k+2}} M_{k+2}^1). \tag{11.5}$$

$$\widetilde{\mathcal{B}}_{1,\ell} : M_{\ell+2}^2 \leftarrow \Sigma^9 M_{\ell+2}^0 \tag{11.6}$$
$$\widetilde{\mathcal{B}}_{2,\ell} : \Sigma M_4^{\ell-1} \leftarrow \Sigma^8 M_{\ell+2}^0 \quad \Sigma^9 M_{\ell+2}^2 \leftarrow \Sigma^{16} M_4^1.$$

The surprising change in position of superscripts when $k = 1$ is due to the 2^{k-1} in Definition 10.2.

We will compare these tableaux with their ku-homology analogues. In the ku context, the role of the superscript is Σ^2. This is because the role of z_j in ku-homology or ku-cohomology charts is $\Sigma^{2^{j+2}+2}$. Recalling that reducing filtration in M charts by 4 is equivalent to an 8-fold suspension lends credence to the correspondence between reducing filtration by 1 (for ko) and suspending twice (for ku).

The tableau for $z^i \widetilde{\mathcal{B}}_{k,\ell}$ is obtained from (11.5) by increasing all superscripts by i. As mentioned in the introduction, z^i refers to any product of i distinct $\Sigma^{-2^{j+2}} z_j$'s.

We close this section by discussing briefly the trivial ko_*-submodule of $ko_*(K_2)$. The $A(1)$-module $\tilde{H}^*(K_2)$ can be decomposed as $I \oplus F$, where I has no free summands, and F is free. The trivial ko_*-submodule corresponds to a basis of F. By [13, Theorem 3.9], I can be written as

$$P[y_1^2] \otimes (U \oplus \langle y_1^2 \rangle \oplus N \oplus NU \oplus (\mathbb{Z}_2 \oplus \Sigma^9) \bigoplus_{k \geq 4} (\mathcal{M}_k \Lambda_{k-1} \oplus \mathcal{M}_k \Lambda_{k-1} U)).$$

Using results of [13], one can write a Poincaré series for I. For summands such as $z_J \mathcal{M}_k$, we know the Ext chart, and can determine from that the $A(1)$-module structure. Since things become quite complicated, here we just present through grading 24. In this range, I is just $P[y_1^2] \otimes (U \oplus \langle y_1^2 \rangle \oplus N \oplus NU \oplus \mathcal{M}_4 \oplus \mathcal{M}_4 U)$, and the Poincaré series P_I is

$$x^2 + x^3 + x^4 + 2x^5 + x^6 + x^7 + 2x^8 + 2x^9 + 2x^{10} + 3x^{11} + 3x^{12} + 3x^{13} + 3x^{14} \tag{11.7}$$
$$+2x^{15} + 2x^{16} + 3x^{17} + 3x^{18} + 4x^{19} + 5x^{20} + 5x^{21} + 5x^{22} + 4x^{23} + 3x^{24}. \tag{11.8}$$

Unreduced $H^*(K_2)$ is a polynomial algebra on classes of grading $2^j + 1$, $j \geq 0$, from which its Poincaré series P_H is easily written. The Poincaré series for $A(1)$ is $P_{A(1)} = 1 + x + x^2 + 2x^3 + x^4 + x^5 + x^6$. The Poincaré series P_F for F must satisfy

$$P_H - 1 = P_I + (P_{A(1)} \cdot P_F).$$

We compute P_F to begin

$$P_F = x^6+x^{10}+x^{12}+3x^{14}+x^{15}+x^{16}+3x^{18}+x^{19}+3x^{20}+x^{21}+5x^{22}+3x^{23}+5x^{24},$$

the start of the Poincaré series for the trivial ko_*-submodule of $ko_*(K_2)$ through grading 24.

12. Computation of $\mathcal{A}_4$ and $\mathcal{A}_1$

In this section, we present a detailed argument for the ko-homology chart $\mathcal{A}_4$ given in Figure 3.2, setting the stage for more general arguments to follow. At the end of the section, we also do $\mathcal{A}_1$, which does not follow some formulas for larger k.

The first part of $\widehat{A}_4^o$ is the $A(1)$-module $\langle y_1^8\rangle \oplus y_1^6 NU$, where NU is an $A(1)$-module discussed in [13]. Its $A(1)$-module structure and the chart $\mathrm{Ext}_{A(1)}(NU, \mathbb{Z}_2)$ appear in Figure 12.1.

Figure 12.1. *NU* **and its chart.**

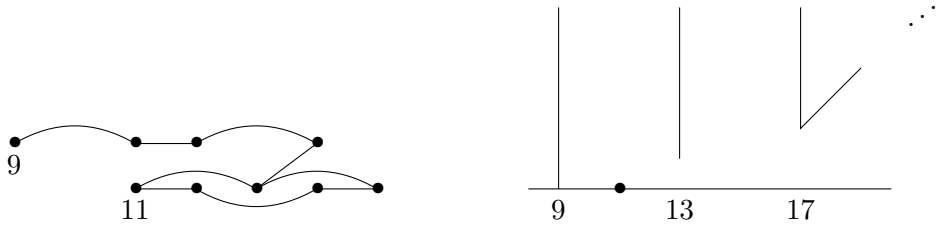

The chart for $\langle y_1^8\rangle \oplus y_1^6 NU$ appears in Figure 12.3. There is a d_5-differential from grading 33 to 32 implied by comparison with Browder's result ([4, Theorem 5.5]) (see also [5, Theorem 1.3.2].) that $H_{32}(K_2) \approx \mathbb{Z}/32$. See [15, p.124], [12, near Figure 4.2], or [11, Figure 11] for similar discussions. The d_5-differential is promulgated by the action of ko_* on the spectral sequence.

There is an exotic η extension from $(35, 0)$ to $(36, 5)$, and this is promulgated by v_1^4-periodicity. This follows from a result in [9, p.228], which says that

$$\text{if } d_r(\langle \alpha, \eta, 2\rangle) = 2\beta, \text{ then } \alpha\eta = \beta. \tag{12.2}$$

Here $\langle \alpha, \eta, 2\rangle$ is a Toda bracket which gives $v_1\alpha$. The bracket relation can be deduced from Figure 12.1, since the class in $(13, 1)$ comes from the relation $\mathrm{Sq}^3 g_{11} = \mathrm{Sq}^2 \mathrm{Sq}^3 g_9$. That v_1 times the class in $(43, 4)$ in Figure 12.3 equals the class in $(45, 5)$ can be deduced from the morphism $ku_* \xrightarrow{r} ko_*$. We prefer to elevate filtrations of classes to make η extensions easier to see. In effect, whenever we have a d_r-differential, we elevate the classes supporting the differential, and most of those already related to them via h_0 or h_1 or v_1^4, so that the differential looks like a d_1. When this is done to the chart on the left side of Figure 12.3, the chart on the right hand side is obtained.

Figure 12.3. $\langle y_1^8\rangle \oplus y_1^6 NU$ **with differentials, and redrawing.**

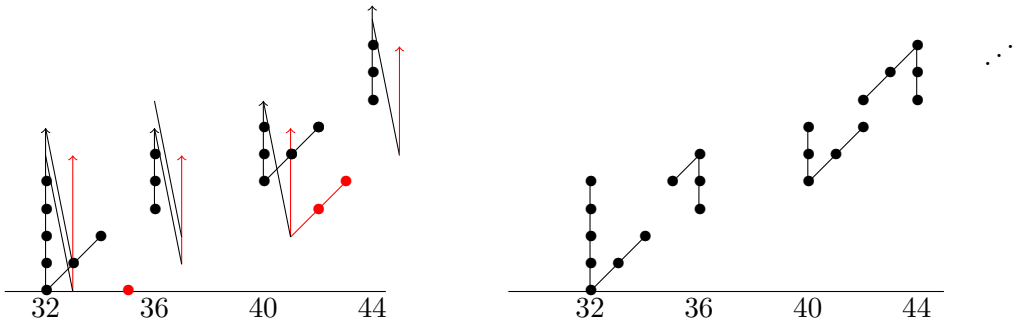

The right side of Figure 12.3 is what we called $\Sigma^{32}V_4$ in (11.2). It was useful to incorporate the Σ^{32} at the outset because it affected the differential in V_4. But now we wish to switch to $\widetilde{\mathcal{A}}_4$, by applying Σ^{-32}. Now we consider $(V_4 \leftarrow \Sigma^8 M_4^0)$ in (11.2). The chart is on the left hand side of Figure 12.4. The differential follows by comparison with the ku case, which is pictured in the right side of Figure 9.12. The differential agrees with the first morphism in the exact sequence

$$ko_*(M(2)) \to ko_*(M(8)) \to ko_*(M(4)) \to ko_*(\Sigma M(2)),$$

where $M(n)$ is the mod-n Moore spectrum. So the resultant must be $ko_*(M(4))$. In the middle part of Figure 12.4, we show the differential interpreted as a d_1, and in the right hand side we show the result, with the η extension incorporated. The middle and right parts omit the portion in grading less than 8. It should be included, and several of its classes are promulgated by v_1^4-periodicity. The η extension from 11 to 12 in the right hand chart can also be deduced from (12.2).

Figure 12.4. $V_4 \leftarrow \Sigma^8 M_4^0$

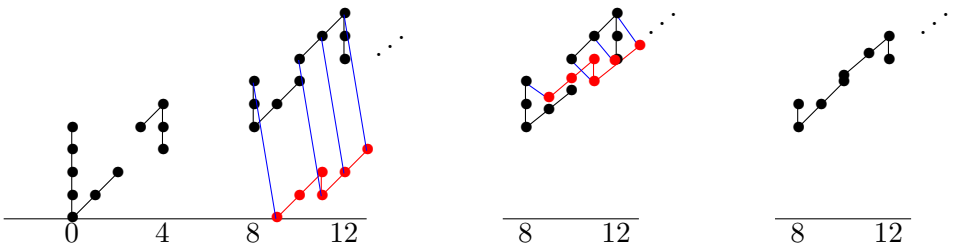

In Figure 12.5, we show how the next d_2 differential in the tableau (11.3), $\Sigma^9 M_4^2 \leftarrow \Sigma^{16} M_5^0$, is deduced by naturality from the d_2 in the ku spectral sequence. The ku differential can be seen as the $46 \leftarrow 51$ arrow in Figure 9.13. In Figure 12.5, we are using gradings for $\widetilde{\mathcal{A}}_4$, which are 32 less than the A_4 gradings in Figure 9.13. The first ko differential is implied by naturality, and the next two are implied by the action of η. The fourth one can be thought of as being implied by the action of v_1, or can be deduced from the map $ku_{*+2}(-) \to ko_*(-)$. In the figure, we use big dots for the ones that map across under c.

Figure 12.5. Deducing a ko differential from ku

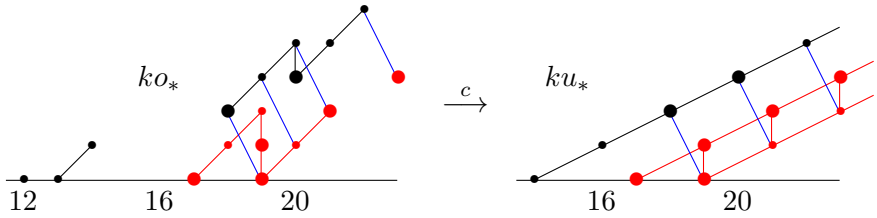

In the next three figures, we show the three d_2-differentials involved in forming $\widetilde{\mathcal{A}}_4$. (See (11.3).) In each case, the domain chart has its filtrations increased by 1, so that the d_2 looks like a d_1. In the right side of each chart, we show the resultant. Of the early classes in the target chart, some are v_1^4-periodic in the resultant charts, while others are not. The ones that are not are indicated with open circles in the resultant chart. They will "stay behind" when subsequent differentials are considered, and will form the subedges.

Figure 12.6. $\Sigma^9 M_4^2 \leftarrow \Sigma^{16} M_5^0$

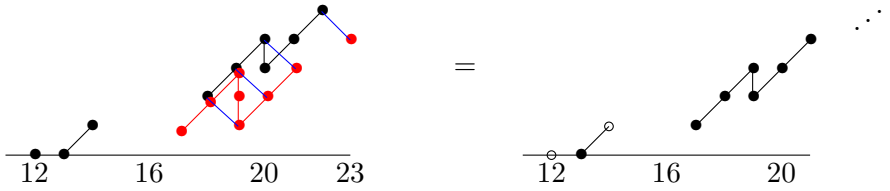

Figure 12.7. $\Sigma^{17} M_5^2 \leftarrow \Sigma^{24} M_4^1$

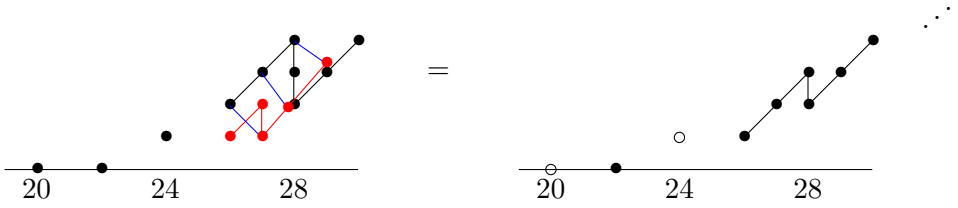

Figure 12.8. $\Sigma^{25} M_4^3 \leftarrow \Sigma^{32} M_6^0$

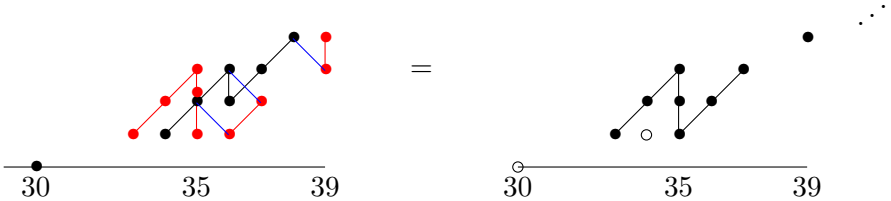

In Figure 12.9, we combine Figures 12.4, 12.6, 12.7, and 12.8. There is a d_8 from the periodic part of Figure 12.6 to 12.4, and a d_4 from the periodic part of Figure 12.8 to 12.7. These are deduced by naturality from the d_5 and d_9 in Figure 9.13. The indices of the differentials are decreased by 1

because of the filtration shift incorporated in the d_2's above. In Figure 12.9, we increase filtrations of periodic classes so that the differentials look like d_1's. This allows for nicer pictures showing $\cdot 2$'s and η's more clearly, which is useful in consideration of subsequent differentials.

We use double circles for the previously-circled classes, and use single circles for classes in Figure 12.7 which survive but do not lead to periodic classes, since v_1^{4i} times them are hit by differentials. These circled classes form another edge. Note the significance of the periodic class in grading 13 in Figure 12.6; it supports a differential in Figure 12.9 because v_1^4 times it does.

Figure 12.9. Forming $\widetilde{\mathcal{A}}_4$

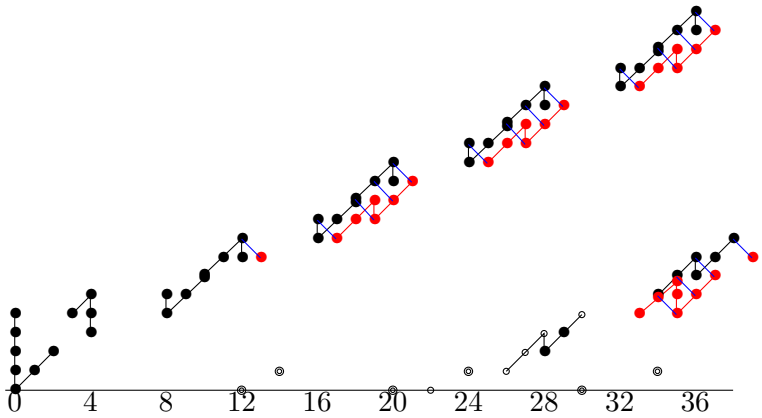

The result of each of the three sets of differentials pictured along the upper edge of Figure 12.9 is a lightning flash, starting in grading 16, 24, and 32, continuing indefinitely. The result of the group of differentials in the lower edge is a lightning flash, beginning in 33, promulgated by v_1^4-periodicity. There is a d_{12}-differential from this lightning flash in 33 to the one in 32, deduced from the morphism of ASS's for $ko_*(K_2) \to ku_*(K_2)$. The differential in the ku_* spectral sequence is the d_{16} in Figure 9.13. (This would have been a d_{12} if we had employed similar filtration shifts in the ku_* spectral sequence. Note also that gradings in Figure 12.9 differ by 32 from those in Figures 9.13, 3.2, and 9.14 because those are for A_4, while here we have been considering $\widetilde{\mathcal{A}}_4$.) The d_{12} totally annihilates both lightning flashes and all subsequent ones, turning what had been an infinite picture into a finite one.

Note that v_1^4 times the classes in $(28, 2)$ and $(29, 3)$ in Figure 12.9 are in the lightning flash supporting differentials, and so they support d_{12} differentials into the end of the lightning flash that started in 24. The result of this is Figure 3.2.

The relationship of the above analysis with the approach to edges given in Section 4 will be explained in the next section. As a preview, the circled classes in Figure 12.9 are $\Sigma^8\mathcal{E}_{2,3}$ (grading 12 and 14), $\Sigma^{16}\mathcal{E}_{2,4}$ (gradings 20 to 30 (top class)), and $\Sigma^{24}\mathcal{E}_{3,4}$ (30 and 34). (See Figure 4.11.)

The exact sequence

$$ko_{*-1}(K_2) \xrightarrow{\eta} ko_*(K_2) \xrightarrow{c} ku_*(K_2) \to ko_{*-2}(K_2) \xrightarrow{\eta} ko_{*-1}(K_2) \quad (12.10)$$

can be used to deduce extensions. In [11], we established that there are nontrivial extensions in Figure 9.14 in grading 58, 60, 62, and 64. The classes in $ko_{58}(K_2)$ which are not in $\mathrm{im}(\eta)$ must map to $ku_{58}(K_2)$; the extension in the latter implies one in the former. The two classes in $ko_{62}(K_2)$ in Figure 3.2 must be in the image from $ku_{64}(K_2)$, where the extension is present, implying the extension in $ko_{62}(K_2)$.

We conclude this section by deriving the chart for $\mathcal{A}_1$, since it is slightly special. Its chart is formed from the $A(1)$-module $U \oplus N$. These modules are defined in [13, Section 3] and their charts are in [13, Figure 3.10]. We reproduce them here in Figure 12.11 with N in red.

Figure 12.11. Forming $\mathcal{A}_1$

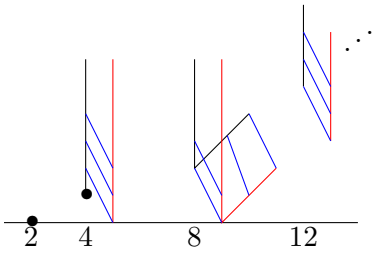

The d_2-differential was first noted in [15, p.124] and was shown in [12, Figure 3.1]. It follows from [4]. The only nonzero classes in $\mathcal{A}_1$ are the $\mathbb{Z}_2$'s in grading 2 and 4.

13. Derivation of edge description

The derivation of Definition 4.8 requires a careful study of the tableau (11.2) for $\widetilde{\mathcal{A}}_k$ and the ways that pre-edges are associated to arrows in the tableau. For every arrow with target $\Sigma^{8i+1}M_\ell^s$, there is a corresponding pre-edge $\Sigma^{8i}\mathcal{E}'_{s,s+\ell-3}$, which involves $2^{\ell-4}$ arrows beginning with the specified one. We have found it very useful to list, as an example, the tableau for $\widetilde{\mathcal{A}}_7$ with arrows labeled by their corresponding pre-edge. This is done in (13.1). The labeled tableau for $\widetilde{\mathcal{A}}_k$ for $k = 4$, 5, and 6 can be read off from this by taking the first 1, 2, or 4 rows, respectively, with V_7 replaced by V_k.

$$
\begin{array}{cccc}
V_7 \overset{1,7}{\leftarrow} \Sigma^8 M_4^0 & \Sigma^9 M_4^2 \overset{2,3}{\leftarrow} \Sigma^{16} M_5^0 & \Sigma^{17} M_5^2 \overset{2,4}{\leftarrow} \Sigma^{24} M_4^1 & \Sigma^{25} M_4^3 \overset{3,4}{\leftarrow} \Sigma^{32} M_6^0 \\
\Sigma^{33} M_6^2 \overset{2,5}{\leftarrow} \Sigma^{40} M_4^1 & \Sigma^{41} M_4^3 \overset{3,4}{\leftarrow} \Sigma^{48} M_5^1 & \Sigma^{49} M_5^3 \overset{3,5}{\leftarrow} \Sigma^{56} M_4^2 & \Sigma^{57} M_4^4 \overset{4,5}{\leftarrow} \Sigma^{64} M_7^0 \\
\Sigma^{65} M_7^2 \overset{2,6}{\leftarrow} \Sigma^{72} M_4^1 & \Sigma^{73} M_4^3 \overset{3,4}{\leftarrow} \Sigma^{80} M_5^1 & \Sigma^{81} M_5^3 \overset{3,5}{\leftarrow} \Sigma^{88} M_4^2 & \Sigma^{89} M_4^4 \overset{4,5}{\leftarrow} \Sigma^{96} M_6^1 \\
\Sigma^{97} M_6^3 \overset{3,6}{\leftarrow} \Sigma^{104} M_4^2 & \Sigma^{105} M_4^4 \overset{4,5}{\leftarrow} \Sigma^{112} M_5^2 & \Sigma^{113} M_5^4 \overset{4,6}{\leftarrow} \Sigma^{120} M_4^3 & \Sigma^{121} M_4^5 \overset{5,6}{\leftarrow} \Sigma^{128} M_8^0 \\
\Sigma^{129} M_8^2 \overset{2,7}{\leftarrow} \Sigma^{136} M_4^1 & \Sigma^{137} M_4^3 \overset{3,4}{\leftarrow} \Sigma^{144} M_5^1 & \Sigma^{145} M_5^3 \overset{3,5}{\leftarrow} \Sigma^{152} M_4^2 & \Sigma^{153} M_4^4 \overset{4,5}{\leftarrow} \Sigma^{160} M_6^1 \\
\Sigma^{161} M_6^3 \overset{3,6}{\leftarrow} \Sigma^{168} M_4^2 & \Sigma^{169} M_4^4 \overset{4,5}{\leftarrow} \Sigma^{176} M_5^2 & \Sigma^{177} M_5^4 \overset{4,6}{\leftarrow} \Sigma^{184} M_4^3 & \Sigma^{185} M_4^5 \overset{5,6}{\leftarrow} \Sigma^{192} M_7^1 \\
\Sigma^{193} M_7^3 \overset{3,7}{\leftarrow} \Sigma^{200} M_4^2 & \Sigma^{201} M_4^4 \overset{4,5}{\leftarrow} \Sigma^{208} M_5^2 & \Sigma^{209} M_5^4 \overset{4,6}{\leftarrow} \Sigma^{216} M_4^3 & \Sigma^{217} M_4^5 \overset{5,6}{\leftarrow} \Sigma^{224} M_6^2 \\
\Sigma^{225} M_6^4 \overset{4,7}{\leftarrow} \Sigma^{232} M_4^3 & \Sigma^{233} M_4^5 \overset{5,6}{\leftarrow} \Sigma^{240} M_5^3 & \Sigma^{241} M_5^5 \overset{5,7}{\leftarrow} \Sigma^{248} M_4^4 & \Sigma^{249} M_4^6 \overset{6,7}{\leftarrow} \Sigma^{256} M_9^0
\end{array}
\tag{13.1}
$$

We begin our derivation of Definition 4.8 by considering $\mathcal{E}'_{5,6}$. As can be seen in (13.1), it can come from any of $\Sigma M_4^5 \leftarrow \Sigma^8 M_t^{8-t}$ for $5 \le t \le 8$. In Figure 13.2 we consider the cases $t = 6$ and $t = 8$. The other two are similar.

The left side depicts the arrow as a d_1 differential, with ΣM_4^5 in red, while the right side shows the result, with $\mathcal{E}'_{5,6}$ in red, and $\Sigma^8 M_{t-1}^{8-t}$ in black.

Figure 13.2. Two ways of forming $\mathcal{E}'_{5,6}$

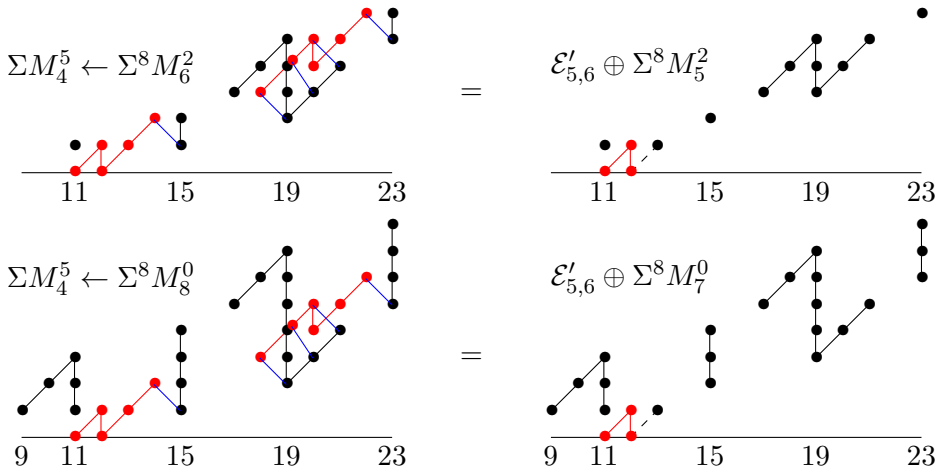

The job of this d_2 pair is to change $\Sigma^8 M_t^{8-t}$ to $\Sigma^8 M_{t-1}^{8-t}$. The $\mathcal{E}'_{5,6}$ is the extra part, and is not involved in subsequent arrows until we consider the differentials which change $\mathcal{E}'_{e,\ell}$ to $\mathcal{E}_{e,\ell}$. Its class in $(12,0)$ will support such a differential. In Figure 13.3, we show that the result of $\Sigma M_4^5 \leftarrow \Sigma^{10}\widehat{M}_4^3$ is exactly the $\mathcal{E}'_{5,6}$ just obtained, as claimed in Definition 4.8. Here $\Sigma^{10}\widehat{M}_4^3$ is in red.

Figure 13.3. $\Sigma M_4^5 \leftarrow \Sigma^{10}\widehat{M}_4^3$

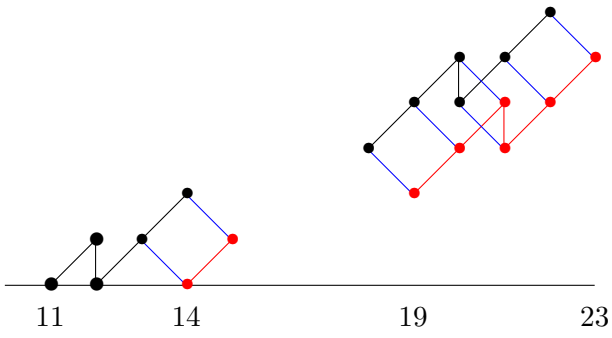

We now give a chart-theoretic explanation of why this occurs, which is useful in seeing how it generalizes. We illustrate with M_8^0. The cofiber of $M_7^0 \to M_8^0$ is $\Sigma^2\widehat{M}_4^3$. In Figure 13.4 we show that M_8^0 can be formed from $M_7^0 + \Sigma^2\widehat{M}_4^3$.

Figure 13.4. $M_7^0 + \Sigma^2 \widehat{M}_4^3 = M_8^0$

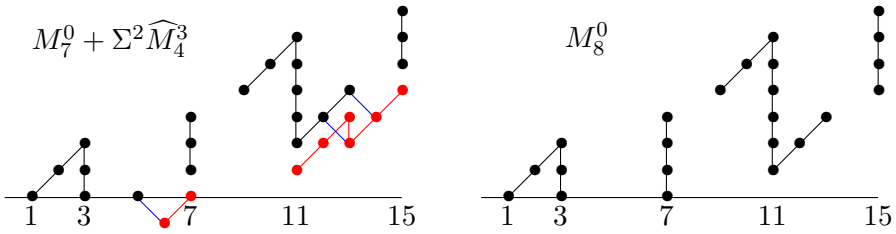

In Figure 13.5 we modify the lower left part of Figure 13.2 by replacing $\Sigma^8 M_8^0$ by $\Sigma^8 M_7^0 + \Sigma^{10} \widehat{M}_4^3$. The result is the desired $\mathcal{E}'_{5,6} \oplus \Sigma^8 M_7^0$. Indeed, the ΣM_4^5 and $\Sigma^{10} \widehat{M}_4^3$ combine to yield $\mathcal{E}'_{5,6}$ as in Figure 13.3, and the $\Sigma^8 M_7^0$ remains unchanged. In chart arithmetic, we have

$$(\Sigma M_4^5 \leftarrow M_7^0 \oplus \Sigma^2 \widehat{M}_4^3) = (\mathcal{E}'_{5,6} \oplus M_7^0),$$

then cancel the M_7^0 to obtain the $\mathcal{E}'_{5,6}$ case of Definition 4.8. This may seem roundabout, but will be useful.

Figure 13.5. Figure 13.2 after replacement

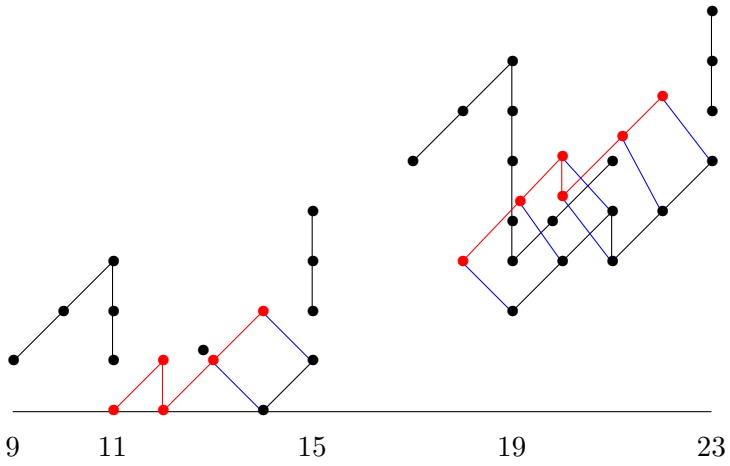

The following proposition is the generalization of the phenomenon observed in Figure 13.4.

Proposition 13.6. *For $k \geq 4$ and $i \geq 0$, we have*

$$M_k^i + \Sigma^2 \widehat{M}_4^{k+i-4} = M_{k+1}^i$$

in the sense that if $\Sigma^2 \widehat{M}_4^{k+i-4}$ is placed beneath M_k^i so that there are d_1 differentials as in Figure 13.8, then the result is M_{k+1}^i.

Proof. First note that all M_k^i with the same mod 4 value of $k+i$ have the same general form as indicated in Figure 13.7. This refers to the way in which they leave filtration 0.

Figure 13.7. M_k^i

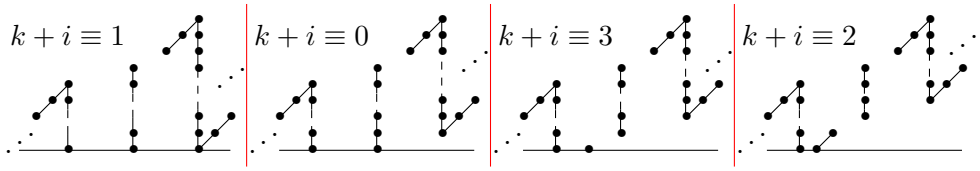

Then note that k and $k+i$ are increased by 1 by the additions in Figure 13.8, each of which illustrates $M_k^i + \Sigma^2 \widehat{M}_4^{k+i-4}$, so i is unchanged. Here we use that $\widehat{M}_4^{4t+i} = \Sigma^{8t}\widehat{M}_4^i$. ■

Figure 13.8. $M_k^i + \Sigma^2 \widehat{M}_4^{k+i-4}$

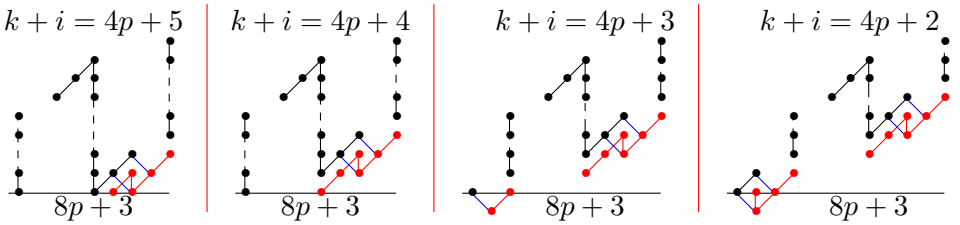

We saw in Figure 13.2 that $\mathcal{E}'_{5,6}$ is what was left over after $\Sigma M_4^5 \leftarrow \Sigma^8 M_t^{8-t}$ is used to change $\Sigma^8 M_t^{8-t}$ to $\Sigma^8 M_{t-1}^{8-t}$, and then since $\Sigma^8 M_t^{8-t}$ can be obtained from $\Sigma^8 M_{t-1}^{8-t} + \Sigma^{10}\widehat{M}_4^3$, we can obtain $\mathcal{E}'_{5,6}$ itself from $\Sigma M_4^5 \leftarrow \Sigma^{10}\widehat{M}_4^3$. The same argument, together with Proposition 13.6, yields that, for any $e > 1$, $\mathcal{E}'_{e,e+1}$, the part left over when $\Sigma M_4^e \leftarrow \Sigma^8 M_t^{e+3-t}$ is used to change $\Sigma^8 M_t^{e+3-t}$ to $\Sigma^8 M_{t-1}^{e+3-t}$, can be obtained from $\Sigma M_4^e \leftarrow \Sigma^2 \widehat{M}_4^{e-2}$, as claimed in Definition 4.8.

Next we consider $\mathcal{E}'_{4,6}$, which (13.1) shows to be related to

$$\Sigma M_5^4 \overset{4,6}{\leftarrow} \Sigma^8 M_4^3 \quad \Sigma^9 M_4^5 \overset{5,6}{\leftarrow} \Sigma^{16} M_t^{8-t}$$

for $t \in \{6,7,8\}$. We have already seen that the resultant of the second arrow is $\Sigma^8 \mathcal{E}'_{5,6} + \Sigma^{16} M_{t-1}^{8-t}$. The $\mathcal{E}'_{5,6}$ is not involved in finding $\mathcal{E}'_{4,6}$. (It may be involved in differentials which change $\mathcal{E}'$ to $\mathcal{E}$; this will be considered in Section 14.) We will show in the next paragraph that the resultant of $\Sigma M_5^4 \leftarrow \Sigma^8 M_4^3 \leftarrow \Sigma^{16} M_{t-1}^{8-t}$ is $\Sigma^{16} M_{t-2}^{8-t}$ plus a remainder term, which is defined to be $\mathcal{E}'_{4,6}$. Then we can use Proposition 13.6 to replace $\Sigma^{16} M_{t-1}^{8-t}$ by $\Sigma^{16} M_{t-2}^{8-t} + \Sigma^{18}\widehat{M}_4^2$, and deduce, similarly to what we did before, that $\mathcal{E}'_{4,6}$ itself can be obtained from

$$\Sigma M_5^4 \leftarrow \Sigma^8 M_4^3 \leftarrow \Sigma^{18}\widehat{M}_4^2.$$

In this paragraph, we use $t = 8$ in the above discussion, but $t = 6$ or 7 work similarly. In the left side of Figure 13.9, we show $\Sigma M_5^4 \leftarrow \Sigma^8 M_4^3$, with $\Sigma^8 M_4^3$ in red. On the right side, we place the resultant of the left side in black and $\Sigma^{16} M_7^0$ in red, placed so that the differential appears as a d_1. (The justification for the differentials will be given in Section 14.) The differential reduces the $\Sigma^{16} M_7^0$ to $\Sigma^{16} M_6^0$, as claimed in the preceding paragraph. The

classes in 20 and 21 are part of $\Sigma^{16}M_6^0$. The black classes in grading ≤ 19 form $\mathcal{E}'_{4,6}$. A similar thing happens in consideration of any $\mathcal{E}'_{e,e+2}$. It will come from

$$\Sigma M_5^e \leftarrow \Sigma^8 M_4^{e-1} \quad \Sigma^9 M_4^{e+1} \leftarrow \Sigma^{16} M_t^{e+4-t}.$$

The second arrow produces $\Sigma^8\mathcal{E}'_{e+1,e+2} \oplus \Sigma^{16}M_{t-1}^{e+4-t}$. After some initial deviation, the first arrow will produce pure lightning flashes in time to work with $\Sigma^{16}M_{t-1}^{e+4-t}$ to form $\Sigma^{16}M_{t-2}^{e+4-t}$.

Figure 13.9. Forming $\mathcal{E}'_{4,6} + \Sigma^{16}M_6^0$

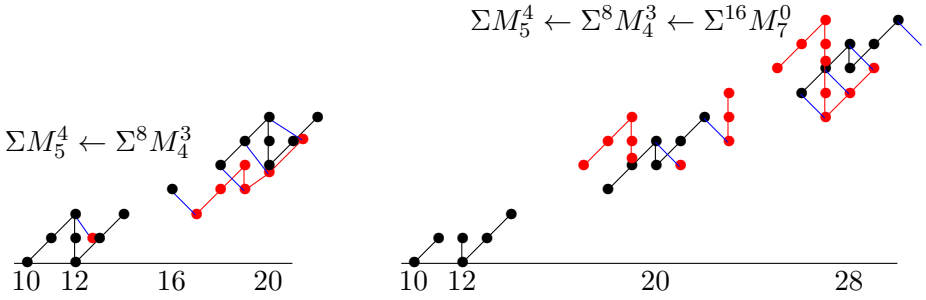

A similar argument works for any $\mathcal{E}'_{e,e+d}$. We are proving that the sequence of 2^{d-1} arrows including and following any $\overset{e,e+d}{\leftarrow}$ in the tableau (11.2) yields the chart described in Definition 4.8 plus the chart obtained from the last M_ℓ^s in the sequence with its subscript decreased by d. The tableau (13.1) is very helpful in getting started. For $e \ge 2$ and $d \ge 1$, there are $\binom{k-2-d}{e-2}$ arrows labeled $(e, e+d)$ in the tableau for $\widetilde{\mathcal{A}}_k$. Each gives rise to an occurrence of $\mathcal{E}'_{e,e+d}$. The structure of $\mathcal{E}'_{e,e+d}$ is determined by 2^{d-1} arrows beginning with one labeled $(e, e+d)$. The sequence of these arrow labels is the same for every occurrence of $(e, e+d)$, and the sequence of the 2^d M charts is also the same except for the very last one, which can be $\Sigma^{2^{d+2}}M_t^{e+d+2-t}$ for $t = e+d+2 \le k+2$ or $d+4 \le t \le e+d+1 \le k$.

We take a major step toward justifying Definition 4.8 by considering $\mathcal{E}'_{e,e+3}$. This is determined by the four arrows in (13.10),

$$\Sigma M_6^e \overset{e,e+3}{\leftarrow} \Sigma^8 M_4^{e-1} \quad \Sigma^9 M_4^{e+1} \overset{e+1,e+2}{\leftarrow} \Sigma^{16} M_5^{e-1}$$
$$\Sigma^{17} M_5^{e+1} \overset{e+1,e+3}{\leftarrow} \Sigma^{24} M_4^e \quad \Sigma^{25} M_4^{e+2} \overset{e+2,e+3}{\leftarrow} \Sigma^{32} M_t^{e+5-t} \tag{13.10}$$

where either $t = e+5 \le k+2$ or $7 \le t \le e+4 \le k$. This can be seen in (11.2), where it will be suspended by Σ^{64b+32} for some b. Then (13.10) corresponds to $i = 8b + (4,5,6,7)$ in (11.2). Also $e = \alpha(b)+2$ and $M_t^{e+5-t} = M_{7+\nu(b+1)}^{\alpha(b+1)-1}$.

Similarly to our analysis of $\mathcal{E}'_{5,6}$ and $\mathcal{E}'_{4,6}$, the resultant of the second arrow in (13.10) is $\Sigma^8\mathcal{E}'_{e+1,e+2} \oplus \Sigma^{16}M_4^{e-1}$, and the resultant of the last two arrows is $\Sigma^{16}\mathcal{E}'_{e+1,e+3} + \Sigma^{24}\mathcal{E}'_{e+2,e+3} \oplus \Sigma^{32}M_{t-2}^{e+5-t}$. We leave the $\Sigma^8\mathcal{E}'_{e+1,e+2}$, $\Sigma^{16}\mathcal{E}'_{e+1,e+3}$, and $\Sigma^{24}\mathcal{E}'_{e+2,e+3}$ behind, and are left with

$$\Sigma M_6^e \leftarrow \Sigma^8 M_4^{e-1} \leftarrow \Sigma^{16} M_4^{e-1} \leftarrow \Sigma^{32} M_{t-2}^{e+5-t}. \tag{13.11}$$

In Figure 13.12, which is the case $e = 4$, we show the result of the first two arrows.

Figure 13.12. First two arrows of (13.11)

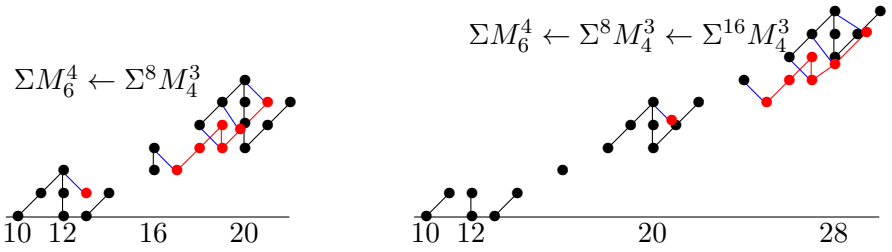

Then in Figure 13.13, which is the case $t = 9$, we place $\Sigma^{32} M_{t-2}^{e+5-t}$ so that it has a d_1 differential into the stable lightning flash beyond the end of Figure 13.12. This reduces it to $\Sigma^{32} M_{t-3}^{e+5-t}$, and the leftover part is defined to be $\mathcal{E}'_{e,e+3}$. Note that the classes in the lightning flash in grading 36 and 37 become part of $\Sigma^{32} M_6^0$, while the classes in 34 and 35 are the last two elements in $\mathcal{E}'_{4,7}$. So the result of (13.11) is $\Sigma^{32} M_{t-3}^{e+5-t} \oplus \mathcal{E}'_{e,e+3}$.

Figure 13.13. Forming $\Sigma^{32} M_{t-3}^{e+5-t} \oplus \mathcal{E}'_{e,e+3}$

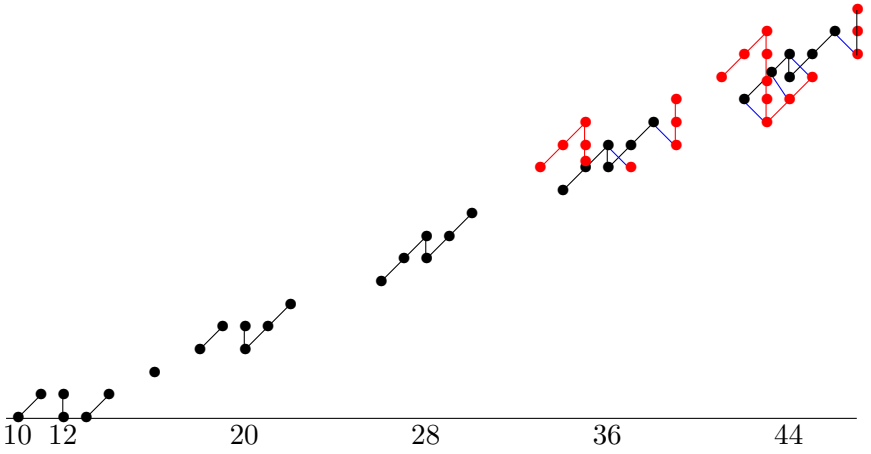

We use Proposition 13.6 to replace $\Sigma^{32} M_{t-2}^{e+5-t}$ in (13.11) by $\Sigma^{32} M_{t-3}^{e+5-t} + \Sigma^{34} \widehat{M}_4^{e-2}$, similarly to Figure 13.5. Since the result of

$$\Sigma M_6^e \leftarrow \Sigma^8 M_4^{e-1} \leftarrow \Sigma^{16} M_4^{e-1} \leftarrow (\Sigma^{32} M_{t-3}^{e+5-t} + \Sigma^{34} \widehat{M}_4^{e-2})$$

equals $\Sigma^{32} M_{t-3}^{e+5-t} \oplus \mathcal{E}'_{e,e+3}$, and, as in Figure 13.5, the two copies of $\Sigma^{32} M_{t-3}^{e+5-t}$ split off, we derive the $\ell = e + 3$ case of Definition 4.8.

The general case $\mathcal{E}'_{e,e+d}$ does not differ significantly from the case $d = 3$ just considered. The arrows involve $i = 2^d b + (2^{d-1}, \dots, 2^d - 1)$ in (11.2) with $e = \alpha(b) + 2$. Rather than constructing a full-blown induction argument, we will explain how the result for $d = 4$ follows from the argument for $d < 4$. The general case $\mathcal{E}'_{e,e+4}$ is embodied in the last two rows of (13.1), which are Σ^{192} times the case with $e = 3$. For arbitrary e, increase all superscripts of M by $e - 3$. We subtract 192 from all the suspension parameters and

discuss the eight arrows. By the work we have already performed, the result of the second arrow is $\Sigma^8\mathcal{E}'_{4,5} \oplus \Sigma^{16}M_4^2$, the result of the third and fourth arrows is $\Sigma^{16}\mathcal{E}'_{4,6} + \Sigma^{24}E'_{5,6} \oplus \Sigma^{32}M_4^2$, and that of the final four arrows is $\Sigma^{32}\mathcal{E}'_{4,7} + \Sigma^{40}\mathcal{E}'_{5,6} + \Sigma^{48}\mathcal{E}'_{5,7} + \Sigma^{56}\mathcal{E}'_{6,7} \oplus \Sigma^{64}M_6^0$. (We distinguish between $+$ and $\oplus$ because the $\mathcal{E}'$'s can have differentials into one another, but not into the M.) We split off all the $\mathcal{E}'$'s and are left with

$$\Sigma M_7^3 \leftarrow \Sigma^8 M_4^2 \leftarrow \Sigma^{16} M_4^2 \leftarrow \Sigma^{32} M_4^2 \leftarrow \Sigma^{64} M_6^0. \tag{13.14}$$

The resultant of the first three arrows will, after initial deviations, stabilize into a sequence of lightning flashes well before the $\Sigma^{64}M_6^0$ has started. We claim that the lightning flashes will change it to $\Sigma^{64}M_5^0$, and $\mathcal{E}'_{3,7}$ is defined to be everything left over.

Considering the slightly subtle phenomenon observed in Figure 13.13 regarding the classes in 34, 35, 36, and 37, scrutiny is warranted here. We claim that if M_k^i is placed into a sequence of lightning flashes so that its generators of (full) order 2^{k-2} hit generators of lightning flashes with a d_1, then the result is M_{k-1}^i plus the first $(k+i-1)$ mod 4 gradings of the last lightning flash before total incorporation. We illustrate this in Figure 13.15, in which bigger red dots are incorporated into the M.

Recall from Figure 13.7 that the way M_k^i leaves filtration 0 depends only on $(k+i)$ mod 4. In Figure 13.15, we see that these differentials decrease the $(k+i)$ mod 4 type by 1 and decrease k by 1, so they leave i unchanged.

Now we explain why the "$(k+i-1)$ mod 4 gradings" noted above are consistent with everything else. As discussed just before (13.10), the sequence of 2^d charts which define $\mathcal{E}'_{e,e+d}$ ends with $\Sigma^{2^{d+2}}M_t^{e+d+2-t}$. When this sequence is reduced to a sequence of the type illustrated by (13.11), the subscript of M will be reduced $d-1$ times, so that the sequence of type (13.11) will end with M_k^i satisfying $k+i = e+3$. Thus the first $(e+2)$ mod 4 gradings of the last lightning flash before total incorporation will be left behind for the end of $\mathcal{E}'_{e,e+d}$. This is consistent with the endings of Figures 4.11, 4.12, 4.13, 4.14, and 4.15.

Figure 13.15. Cutting off M_k^i with lightning flashes

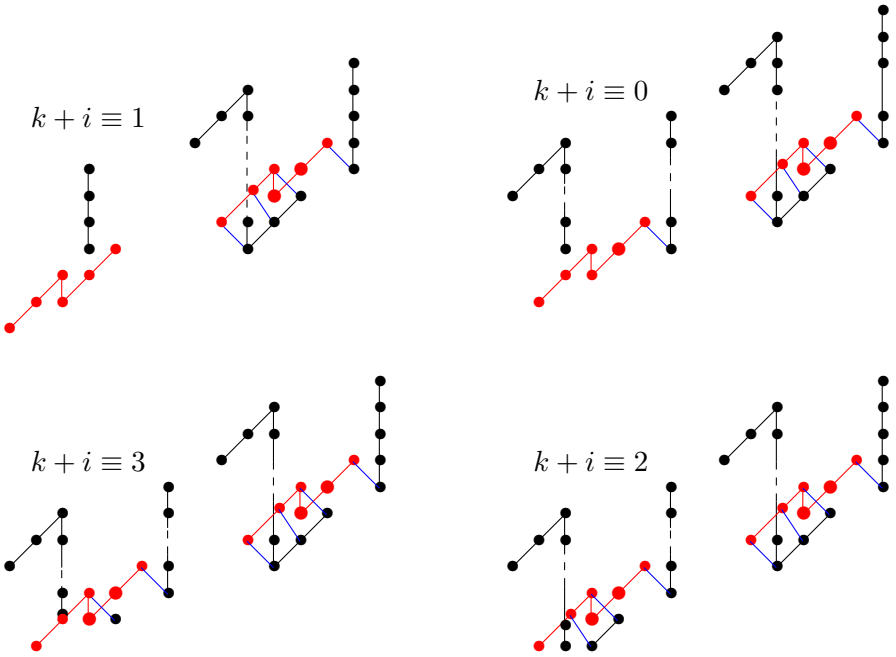

Returning to $\mathcal{E}'_{3,7}$, (13.14) results in $\Sigma^{64}M_5^0 \oplus \mathcal{E}'_{3,7}$. Replace $\Sigma^{64}M_6^0$ by $\Sigma^{64}M_5^0 \oplus \Sigma^{66}\widehat{M}_4^2$ in (13.14), using Proposition 13.6. The $\Sigma^{64}M_5^0$ splits off, similarly to Figure 13.5, and we deduce that the result of

$$\Sigma M_7^3 \leftarrow \Sigma^8 M_4^2 \leftarrow \Sigma^{16} M_4^2 \leftarrow \Sigma^{32} M_4^2 \leftarrow \Sigma^{66}\widehat{M}_4^2$$

is $\mathcal{E}'_{3,7}$. The same argument applies if the M_9^0 at the end of (13.1) is replaced by M_8^1, the other way that the sequence of arrows defining $\mathcal{E}'_{3,7}$ can end. Then the M_6^0 in (13.14) becomes M_5^1, with the same value of $k+i$. If e is changed, then all superscripts in (13.14) are changed by the same amount, and the replacement argument using Proposition 13.6 still applies.

This completes the induction step for the case $d = 4$. The same argument works for arbitrary d. The conclusion of this section is the following theorem.

Theorem 13.16. *A sequence*

$$\Sigma M_{\ell-e+3}^e \leftarrow \Sigma^8 M_4^{e-1} \leftarrow \Sigma^{16} M_4^{e-1} \leftarrow \cdots \leftarrow \Sigma^{2^{\ell-e+1}} M_4^{e-1} \leftarrow \Sigma^{2^{\ell-e+2}} M_{k+1}^i$$

with all arrows being d_1 on generators in grading 1, 3, 4, *and* 5 *mod* 8, *and η inserted, and satisfying $k+i = e+2$ equals $\mathcal{E}'_{e,\ell} \oplus \Sigma^{2^{\ell-e+2}} M_k^i$.*

The theorem also holds if the sequence and the conclusion are suspended by any amount.

Now we justify Definition 4.18. The description of V_k in Definition 4.18 is a straightforward generalization of Figure 12.3. For the sequence (4.19) in Definition 4.18, we refer to (13.1) for the case $k = 7$. We have seen in the analysis above that the $\overset{2,3}{\leftarrow}$ yields $\Sigma^8\mathcal{E}'_{2,3} \oplus \Sigma^{16}M_4^0$, and that the last two arrows in the first row of (13.1) yield $\Sigma^{16}\mathcal{E}'_{2,4} + \Sigma^{24}\mathcal{E}'_{3,4} \oplus \Sigma^{32}M_4^0$. The second row of (13.1) yields $\Sigma^{32}\mathcal{E}'_{2,5} + \Sigma^{40}\mathcal{E}'_{3,4} + \Sigma^{48}\mathcal{E}'_{3,5} + \Sigma^{56}\mathcal{E}'_{4,5} \oplus \Sigma^{64}M_4^0$, as the M_7^0 at the end will have its subscript decreased three times. A similar analysis

applies to the third and fourth rows of (13.1) together, yielding eight $\mathcal{E}'$'s $\oplus\Sigma^{128}M_4^0$, and to the last four rows of (13.1) combined, yielding sixteen $\mathcal{E}'$'s $\oplus\Sigma^{256}M_4^0$. We split off all the $\mathcal{E}'$'s, and the various $\Sigma^{2^i}M_4^0$'s combine to give the sequence in Definition 4.18. The placement of the $\Sigma^{2^i}M_4^0$'s in the sequence, i.e., the d_1-differentials, will be justified in the paragraph preceding Figure 14.14.

We can use (13.1) similarly to justify the subedge structure of $\widetilde{\mathcal{A}}_k$ described in Theorem 4.1. Under $\mathcal{E}'_{1,7}$, we have suitable suspensions of $\mathcal{E}'_{2,3}$ and $\mathcal{E}'_{2,4}$ in the first row of (13.1), $\mathcal{E}'_{2,5}$ in the second, $\mathcal{E}'_{2,6}$ in the third, and $\mathcal{E}'_{2,7}$ in the fifth. Then, under the $\mathcal{E}'_{2,4}$ is the $\mathcal{E}'_{3,4}$ just after it, and under the $\mathcal{E}'_{2,5}$ are the $\mathcal{E}'_{3,4}$ and $\mathcal{E}'_{3,5}$ in the second row. Also under that $\mathcal{E}'_{3,5}$ is the $\mathcal{E}'_{4,5}$ at the end of the second row. That exhausts the second row of (13.1).

Next we consider the third and fourth rows together. The $\mathcal{E}'_{3,4}$, $\mathcal{E}'_{3,5}$, and $\mathcal{E}'_{3,6}$ under $\mathcal{E}'_{2,6}$ are apparent. Then under the $\mathcal{E}'_{3,5}$ is the $\mathcal{E}'_{4,5}$ which follows it, and under the $\mathcal{E}'_{3,6}$ are the $\mathcal{E}'_{4,5}$ and $\mathcal{E}'_{4,6}$ in the fourth row. We also have $\mathcal{E}'_{5,6}$ under the $\mathcal{E}'_{4,6}$.

A similar analysis applies to the last four rows of (13.1) to give the subedge structure under $\mathcal{E}'_{2,7}$. This procedure generalizes to any $\widetilde{\mathcal{A}}_k$. The discussion following (13.10) suggests how the formulas in (11.2) enable one to see how the pattern of edges in (13.1) generalizes.

14. The spectral sequence for $\mathcal{A}_k$, with proofs

In this section, we show how the spectral sequence converging to $\widetilde{\mathcal{A}}_k$ works, and then justify that the differentials and extensions work as claimed, by comparing with the ku analysis. Referring to the tableau for $\widetilde{\mathcal{A}}_7$ in (13.1) is strongly recommended. We will use $\widetilde{\mathcal{A}}_7$ as a model for much of the proof.

14.1. Description of spectral sequence. The following definition contains several useful notations.

Definition 14.1. *We will use the following notations.*

- *If C is a chart, then $\Phi^i C$ is the chart obtained from C by increasing filtration of all elements by i.*
- *For $n > 0$ and $n \equiv 0$ or 7 mod 8, let W^n denote the Σ^n term in the tableau for $\widetilde{\mathcal{A}}_k$, which is independent of k except that n must be $\le 2^{k+1}$. If $W^n = \Sigma^n M_t^s$, let $W_i^n = \Sigma^n M_{t-i}^s$.*
- *If C is a chart and M is an M_t^s chart, positioned so that there are d_1 differentials from the stable lower edge of M_t^s into C, we denote by $C \cup_{d_1} M$ the resulting chart, including η extensions from 2α to $v_1\beta$ inserted whenever $d_1(\alpha) = \beta$, following (12.2).*
- *Let $L(8a)$ denote the label on the arrow $W^{8a-7} \leftarrow W^{8a}$.*

Now we describe the way the ASS for $\widetilde{\mathcal{A}}_k$ works. We make frequent use of Theorem 13.16 to see the increasing subscripts of W (corresponding to decreased subscripts of the associated M). All claims will be justified later in this section.

Step 1 says that for $a \ge 1$,

$$W^{16a-7} \cup_{d_1} \Phi^1 W^{16a} = \Phi^1 W_1^{16a} \oplus \Sigma^{16a-8}\mathcal{E}'_{L(16a)}. \tag{14.2}$$

Then **Step 2** says that for $a \geq 1$,

$$(W^{32a-15} \cup_{d_1} \Phi^1 W^{32a-8}) \cup_{d_1} \Phi^4 W_1^{32a} = \Phi^4 W_2^{32a} \oplus \Sigma^{32a-16} \mathcal{E}'_{L(32a-8)}. \quad (14.3)$$

At each step, we leave all $\mathcal{E}'$'s behind, until consideration of differentials among them at the very end.

After Steps 1 and 2, the second row of (13.1) is, for any $\widetilde{\mathcal{A}}_k$ with $k \geq 5$,

$$((\Sigma^{33} M_6^2 \cup_{d_1} \Phi^1 \Sigma^{40} M_4^1) \leftarrow \Phi^1 \Sigma^{48} M_4^1) \leftarrow \Phi^4 \Sigma^{64} M_5^0, \quad (14.4)$$

where filtrations of $\Phi^1 \Sigma^{48} M_4^1$ and then $\Phi^4 \Sigma^{64} M_5^0$ will have to be increased (to Φ^4 and Φ^{11}, respectively) in order to get the d_1 differentials. We prefer to write it as

$$\Sigma^{33} M_6^2 \overset{2,5}{\leftarrow} \Sigma^{40} M_4^1 \leftarrow \Sigma^{48} M_4^1 \leftarrow \Sigma^{64} M_5^0,$$

ignoring the filtration increases, which we think of as being implicit. In fact, the corresponding Φ's are $\Phi^{2^{t+1}-t-2}$, $t \geq 1$ starting with the domain of the first arrow. By Theorem 13.16, this sequence equals $\Sigma^{64} M_4^0 \oplus \Sigma^{32} \mathcal{E}'_{2,5}$.

We now restrict to $\widetilde{\mathcal{A}}_7$, as in (13.1). Rows 4, 6, and 8 in (13.1) simplify in a manner similar to that just described for row 2. With previous $\mathcal{E}'$'s omitted, they become $\Sigma^{128} M_5^0 \oplus \Sigma^{96} \mathcal{E}'_{3,6}$, $\Sigma^{192} M_4^1 \oplus \Sigma^{160} \mathcal{E}'_{3,6}$, and $\Sigma^{256} M_6^0 \oplus \Sigma^{224} \mathcal{E}'_{4,7}$. In each case, the M term is W_3^{64a}. This doesn't work quite so well in rows 3, 5, and 7. The requirement in Theorem 13.16 that $k + 1 + i = e + 3$ is crucial.

Now (13.1) has simplified to the following, with all $\mathcal{E}'$'s omitted.

$$\begin{gathered}
V_7 \overset{1,7}{\leftarrow} \Sigma^8 M_4^0 \leftarrow \Sigma^{16} M_4^0 \leftarrow \Sigma^{32} M_4^0 \\
\leftarrow \Sigma^{64} M_4^0 \\
\Sigma^{65} M_7^2 \overset{2,6}{\leftarrow} \Sigma^{72} M_4^1 \leftarrow \Sigma^{80} M_4^1 \leftarrow \Sigma^{96} M_4^1 \\
\leftarrow \Sigma^{128} M_5^0 \\
\Sigma^{129} M_5^2 \overset{2,7}{\leftarrow} \Sigma^{136} M_4^1 \leftarrow \Sigma^{144} M_4^1 \leftarrow \Sigma^{160} M_4^1 \\
\leftarrow \Sigma^{192} M_4^1 \\
\Sigma^{193} M_7^3 \overset{3,7}{\leftarrow} \Sigma^{200} M_4^2 \leftarrow \Sigma^{208} M_4^2 \leftarrow \Sigma^{224} M_4^2 \\
\leftarrow \Sigma^{256} M_6^0
\end{gathered}$$

Theorem 13.16 applies to the combination of rows 3 and 4, yielding $\Sigma^{128} M_4^0 \oplus \Sigma^{64} \mathcal{E}'_{2,6}$, and to the combination of rows 7 and 8, yielding $\Sigma^{256} M_5^0 \oplus \Sigma^{192} \mathcal{E}'_{3,7}$. Now, ignoring $\mathcal{E}'$'s and combining some rows, we obtain

$$\begin{gathered}
V_7 \overset{1,7}{\leftarrow} \Sigma^8 M_4^0 \leftarrow \Sigma^{16} M_4^0 \leftarrow \Sigma^{32} M_4^0 \leftarrow \Sigma^{64} M_4^0 \leftarrow \Sigma^{128} M_4^0 \\
\Sigma^{129} M_8^2 \overset{2,7}{\leftarrow} \Sigma^{136} M_4^1 \leftarrow \Sigma^{144} M_4^1 \leftarrow \Sigma^{160} M_4^1 \leftarrow \Sigma^{192} M_4^1 \leftarrow \Sigma^{256} M_5^0.
\end{gathered}$$

Theorem 13.16 applies to the second row, yielding $\Sigma^{256} M_4^0 \oplus \Sigma^{128} \mathcal{E}'_{2,7}$. Appending $\Sigma^{256} M_4^0$ to the first row, we obtain $\mathcal{E}'_{1,7}$ of Definition 4.18. We obtain that $\mathcal{E}'_{1,7}$ equals

$$\begin{aligned}
I_7 \oplus \Phi^4 \Sigma^8 M(32)\big|_{16} \oplus \Phi^8 \Sigma^{16} M(16)\big|_{32} \\
\oplus \Phi^{16} \Sigma^{32} M(8)\big|_{64} \oplus \Phi^{32} \Sigma^{64} M(4)\big|_{128} \oplus \Phi^{64} \Sigma^{128} M(2)\big|_{256},
\end{aligned}$$

where $M(2^i) = ko_*(M(2^i))$ and $M\big|_x$ is the portion of M in grading less than x. Comparing with Definition 4.18, note that, e.g., $\Phi^4\Sigma^8 ko_*(M(32))|_{16}$ is identical to "$ko_*(M(32))$ in gradings 8 through 15." Here I_k is as in Definition 7.1. Figure 4.20 illustrates the case $k = 4$.

The spectral sequence behaves for any k in a manner which generalizes what we displayed here for $k = 7$. The general tableau is in (11.2), and an arrow with target $\Sigma^p M^i_\ell$ is labeled with $(i, i + \ell - 3)$. The sequences which form all $\mathcal{E}'_{e,\ell}$ with $e \geq 2$ in $\widetilde{\mathcal{A}}_k$ are described in the following result.

Theorem 14.5. *For every odd positive integer p and $t \geq 0$ satisfying $2^{t+3}(p+1) \leq 2^{k+1}$, there is a sequence satisfying Theorem 13.16,*

$$W^{2^{t+3}p+1} \leftarrow W_0^{2^{t+3}p+8} \leftarrow W_1^{2^{t+3}p+16} \leftarrow \cdots \leftarrow W_{t-1}^{2^{t+3}p+2^{t+2}} \leftarrow W_t^{2^{t+3}(p+1)}, \tag{14.6}$$

which forms $W_{t+1}^{2^{t+3}(p+1)} \oplus \Sigma^{2^{t+3}p}\mathcal{E}'_{\alpha(p)+1,\alpha(p)+t+2}$. Every W_i^{8n} with

$$0 \leq i \leq \begin{cases} \nu(n) & \alpha(n) > 1 \\ \nu(n) - 1 & \alpha(n) = 1 \end{cases}$$

fits into exactly one of these sequences. If $i = \nu(n)$, then $t = \nu(n - 2^i)$ and $p = (n - 2^i)/2^t$, while if $i < \nu(n)$, then $t = i$ and $p = \frac{n}{2^i} - 1$.

Example 14.7. *If $n = 20$, then*

- *$i = 0$ has $t = 0$, $p = 19$, and the sequence is $W^{153} \leftarrow W_0^{160}$, forming $W_1^{160} \oplus \Sigma^{152}\mathcal{E}'_{4,5}$,*
- *$i = 1$ has $t = 1$, $p = 9$, and the sequence is $W^{145} \leftarrow W_0^{152} \leftarrow W_1^{160}$, forming $W_2^{160} \oplus \Sigma^{144}\mathcal{E}'_{3,5}$, and*
- *$i = 2$ has $t = 4$, $p = 1$, and the sequence is*

  $$W^{129} \leftarrow W_0^{136} \leftarrow W_1^{144} \leftarrow W_2^{160} \leftarrow W_3^{192} \leftarrow W_4^{256},$$

  forming $W_5^{256} \oplus \Sigma^{128}\mathcal{E}'_{2,7}$.

(11.2) can be used to see that these sequences are as follows. They are obtained from (13.1) using Theorem 13.16.

$$\Sigma^{153}M_4^4 \overset{4,5}{\leftarrow} \Sigma^{160}M_6^1$$
$$\Sigma^{145}M_5^3 \overset{3,5}{\leftarrow} \Sigma^{152}M_4^2 \leftarrow \Sigma^{160}M_5^1$$
$$\Sigma^{129}M_7^2 \overset{2,7}{\leftarrow} \Sigma^{136}M_4^1 \leftarrow \Sigma^{144}M_4^1 \leftarrow \Sigma^{160}M_4^1 \leftarrow \Sigma^{192}M_4^1 \leftarrow \Sigma^{256}M_5^0.$$

This example illustrates how the subscripts of W^{8n} are successively increased until it becomes an M_4^i, at which point it is melded into another sequence, unless n is a 2-power, in which case it melds into the sequence (4.19) which forms $\mathcal{E}'_{1,k}$. We are left with just $\mathcal{E}'_{1,k}$ and all the $\mathcal{E}'$'s which were left behind. Finally, there are the differentials among the $\mathcal{E}'$'s described in Theorem 4.10, which will be justified in the second paragraph after Figure 14.13.

Proof of Theorem 14.5. Using (11.2), the sequence becomes, omitting $\Sigma^{2^{t+3}p}$,

$$\Sigma M_{4+t}^{\alpha(p)+1} \leftarrow \Sigma^8 M_4^{\alpha(p)} \leftarrow \cdots \leftarrow \Sigma^{2^{t+2}} M_4^{\alpha(p)} \leftarrow \Sigma^{2^{t+3}} M_{\nu(p+1)+4}^{\alpha(p+1)-1}.$$

This satisfies the requirement in Theorem 13.16 because $\alpha(p+1)+\nu(p+1) = \alpha(p)+1$. ■

14.2. Justification of differentials. The main ingredient in justifying the differentials is the generalization of what was done in Section 9 and Theorem 10.4 to pass from differentials in $ku^*(K_2)$ obtained in [11, Theorem 3.1] to differentials among ku_* summands as illustrated in Figure 9.13. We will postpone temporarily consideration of differentials involving the summand V_k of lowest grading. In (10.9), we showed how the theorem of [11] could be interpreted in ku^* summands as

$$d^{2^{t+1}-(t+1)}(b_t(Y_{2^t(a+1)-1,k})) = v^{2^{t+1}-(t+1)}\tau_t(Y_{2^t a,k}).$$

If $\mathrm{Sq}^1(\alpha) = \beta$ in $H^*(K_2)$, a v-tower in the formation of $ku^*(K_2)$ arises from β, while a v-tower in the formation of $ku_*(K_2)$ arises from α. The ku^* differentials in Figure 9.9 are $d^2(b_1(Y_{1,4})) = v^2\tau_1(Y_{0,4})$ and $d^5(b_2(Y_{3,4})) = v^5\tau_2(Y_{0,4})$. The dual differentials in ku_* go in the opposite direction on the α classes associated to the corresponding β classes. For example, dual to the d^5 from 57 to 68 is a d_5 from 67 to 56. See Figure 9.4. This is consistent with (9.10) since it gives a v-tower of height 5 in $(ku^*(K_2))^\vee$ on a class of grading 60, and on a class in $ku_{56}(K_2)$.

This always works, leading to a generalization of Figure 9.13. Suppose $\mathrm{Sq}^1(\alpha_2) = \beta_2$ and $\mathrm{Sq}^1(\alpha_1) = \beta_1$ with $|\alpha_2| = 2x_2-1$ and $|\alpha_1| = 2x_1$, and there is a ku^* differential from the β_1 v-tower to the β_2 v-tower. The differential hits in grading $2x_1+2$, giving a v-tower of height x_2-x_1-1 on a class in $(ku^*(K_2))^\vee$ of grading $2x_1+4$. The differential in $ku_*(K_2)$ gives a v-tower of height x_2-x_1-1 on a class of grading $2x_1$, consistent with (9.10).

We can translate from the ku notation used to label the columns of Figure 9.13 to the ko notation explained prior to (11.2). The contributions to Σ of y_1^2, y_1q, z_j, and M_j are 8, 9, 2^{j+2}, and 2^j, respectively. Also, v_1q and z_j add 2 and 1, respectively, to the superscript of M. In the notation of (10.9) and Definition 14.1, $Y_{2a,k} \leftrightarrow W^{2^{k+1}-8a}$ and $Y_{2a+1,k} \leftrightarrow W^{2^{k+1}-8a+1}$. Then (10.9) implies the following proposition, adapting to ku the notation in (13.1) and Definition 14.1. For example, the columns of Figure 9.13 are now labeled with the W version of (11.3).

Proposition 14.8. *A $d_{2^{t+1}-(t+1)}$ ku_*-differential will go from a $W^{2^{t+2}a}$ summand to the $W^{2^{t+2}(a-1)+1}$ summand.*

We begin illustrating how the description of the spectral sequence, especially the differentials, in Subsection 14.1 follows from Proposition 14.8 using $\mathcal{E}'_{3,6}$ in the sixth row of (13.1). After desuspending, this is

$$\Sigma M_6^3 \overset{3,6}{\leftarrow} \Sigma^8 M_4^2 \quad \Sigma^9 M_4^4 \overset{4,5}{\leftarrow} \Sigma^{16} M_5^2 \quad \Sigma^{17} M_5^4 \overset{4,6}{\leftarrow} \Sigma^{24} M_4^3 \quad \Sigma^{25} M_4^5 \overset{5,6}{\leftarrow} \Sigma^{32} M_7^1. \tag{14.9}$$

In Figure 14.10, we show, for each of the four arrows in (14.9), the two charts combined, without increasing filtration, in both the ko and ku context. For the ku context, M_k^i refers to $\mathrm{Ext}_{E_1}(\Sigma^{2i-2^k}M_k, \mathbb{Z}_2)$, analogous to those in Figure 9.8. We use black for the W^{16a-7} chart and red for W^{16a}. We use big dots to indicate the classes that map across under

$ko_*(K_2) \xrightarrow{c} ku_*(K_2)$. We insert differentials in the ku spectral sequence implied by Proposition 14.8, and then the differentials in the ko spectral sequence implied by those. After presenting the figure, we will comment on some of the implications.

Figure 14.10. d_2 **differentials** ($ko_* \xrightarrow{c} ku_*$)

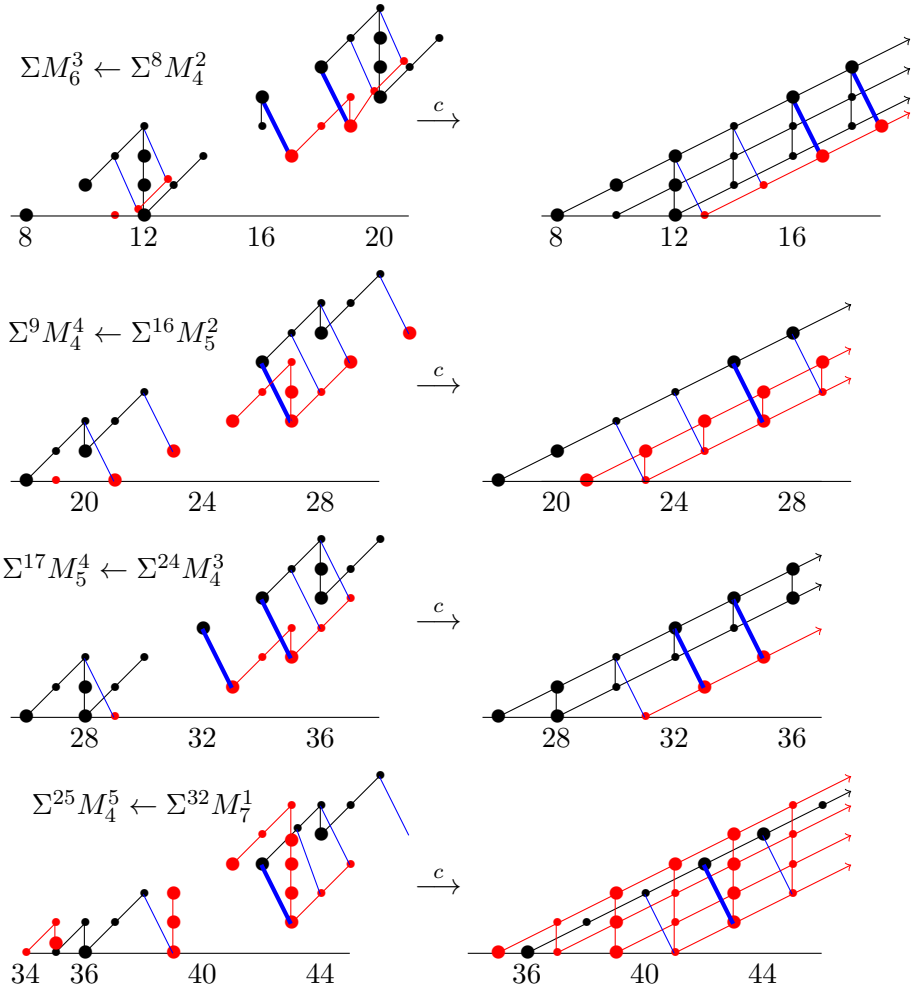

First we note that the classes which map across are exactly those not in $\mathrm{im}(\eta)$. This follows from (12.10). In each of the four situations, there is at least one differential in the ku spectral sequence in which both classes involved in the differential are in $\mathrm{im}(c)$. That implies the corresponding differential in the ko spectral sequence. We indicate these differentials with thicker lines. Other differentials in the ko spectral sequence are implied by naturality with respect to the action of η, v_1^4, or the generator of ko_4.

Now, in each of the four cases, we elevate by 1 the filtration of all classes in the W^{8a} chart (the red classes) so that the d_2 differentials look like d_1's. We did not do this in our ku work in [11], but it will be useful for subsequent comparisons with ko charts. Insert η extensions from α to β if $d_1(v_1\alpha) = 2\beta$. This follows from (12.2). This comparison with ku is the justification for the

filtration shift in (14.2), which applies to the second and fourth situations in Figure 14.10.

In Figure 14.11, the top left chart contains the result of the first ko chart of Figure 14.10 in black and the result of the second ko chart of Figure 14.10 in red. The top right chart in Figure 14.11 is the analogue of this for the first two ku charts in Figure 14.10. We use big dots for classes that map across under $\xrightarrow{c}$. We insert differentials in the ku chart implied by Proposition 14.8. They will appear as a d_4 rather than a d_5 because we increased the filtration of the source classes. Then we insert differentials in the ko chart forced by the morphism c and the ku differentials, again indicating with darker lines the ku differentials that pull back to ko differentials. Then we insert differentials implied by the inserted differentials and naturality with respect to η, v_1^4, and the generator of ko_4. The bottom half of Figure 14.11 does the analogous thing for the third and fourth charts of Figure 14.10.

Figure 14.11. d_5 differentials (look like d_4)

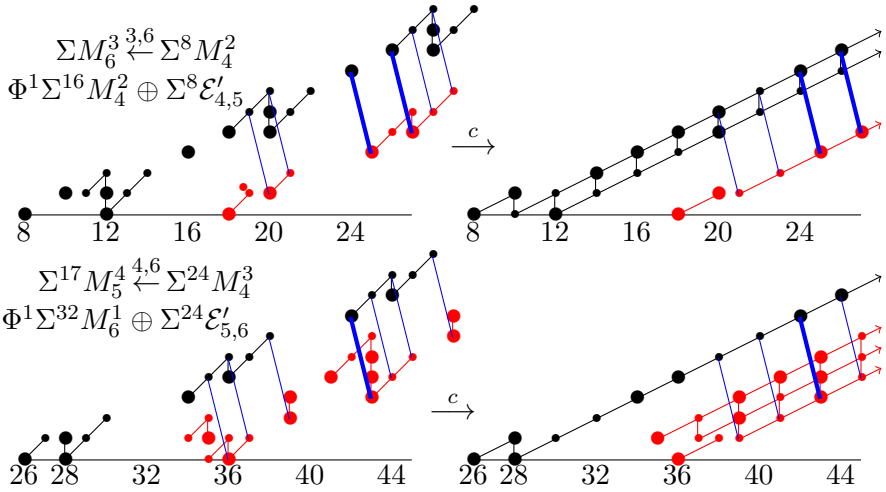

We increase filtrations of v_1^4-periodic red classes in the ko charts of Figure 14.11, remove classes involved in differentials, and insert η extensions implied by (12.2), obtaining Figure 14.12, in which the top (resp. bottom) half of Figure 14.11 is in black (resp. red). Step 2 (14.3) says that the lower chart in Figure 14.11, after simplification, is $\Phi^4\Sigma^{32} M_5^1 \oplus \Sigma^{16}\mathcal{E}'_{4,6}$. The $\Phi^4\Sigma^{32} M_5^1$ appears in Figure 14.12 as all red elements in filtration ≥ 4. Our charts also include $\Sigma^{24}\mathcal{E}'_{5,6}$, which was dropped in the transition from (14.2) to (14.3).

If we did the same for the ku charts, we would have, among other things, a v-tower arising from $(12, 0)$ and v-towers connected by h_0 ($\cdot 2$) arising from $(35, 1)$ and $(37, 1)$ (or $(35, 4)$ and $(37, 4)$, if we increased filtrations analogously to ko). See Figure 14.11. The classes in the ko chart which map across to these v-towers are indicated by big dots in Figure 14.12. There are d_{11} differentials[3] in the ku spectral sequence from the $(37, 1)$ v-tower to the $(12, 0)$ v-tower implied by Proposition 14.8. The classes in the ko chart in $(43, 7)$ and $(42, 15)$, being not in $\mathrm{im}(\eta)$, map across to classes involved in a differential in the ku spectral sequence. Thus there is a differential in the

[3]They are d_{12} in Proposition 14.8, but d_{11} here due to the filtration shift.

ko spectral sequence from $(43, 7)$ to $(42, 15)$, and the other differentials in Figure 14.12 are implied by naturality, as before.

Figure 14.12. Forming the result of (14.9)

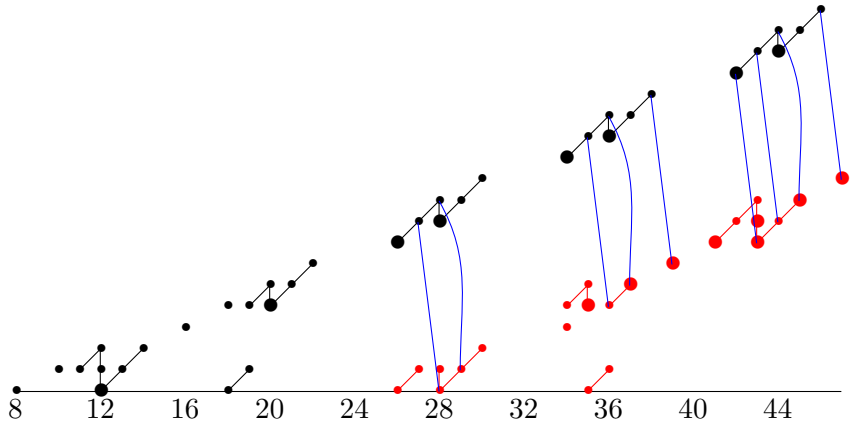

After increasing filtrations of all remaining red classes of filtration ≥ 4 by 7, and removing classes involved in differentials, we obtain Figure 14.13. This is just $\mathcal{E}_{3,6}$, $\Sigma^8\mathcal{E}_{4,5}$, $\Sigma^{16}\mathcal{E}_{4,6}$, $\Sigma^{24}\mathcal{E}_{5,6}$, and $\Phi^{11}\Sigma^{32}M_4^1$, with $\mathcal{E}$'s as in Figure 4.11, except that the classes in $\mathcal{E}'_{3,6}$ which support differentials (into $\mathcal{E}'_{2,6}$) have not been removed. Figure 14.12 is the following analogue of (14.4) except that we have included all the ε''s.

$$((\Sigma M_6^3 \cup_{d_1} \Phi^1\Sigma^8 M_4^2) \leftarrow \Phi^4\Sigma^{16}M_4^2) \leftarrow \Phi^4\Sigma^{32}M_5^1$$

It corresponds to the case $e = 3$, $\ell = 6$, $k = 4$, $i = 1$ of Theorem 13.16, and, if the Σ^{160} is included, the case $t = 2$, $p = 5$ case of (14.6). The main point of the work we have been doing here is how the differentials are implied by the ku differentials in Proposition 14.8.

Figure 14.13. Final result of (14.9)

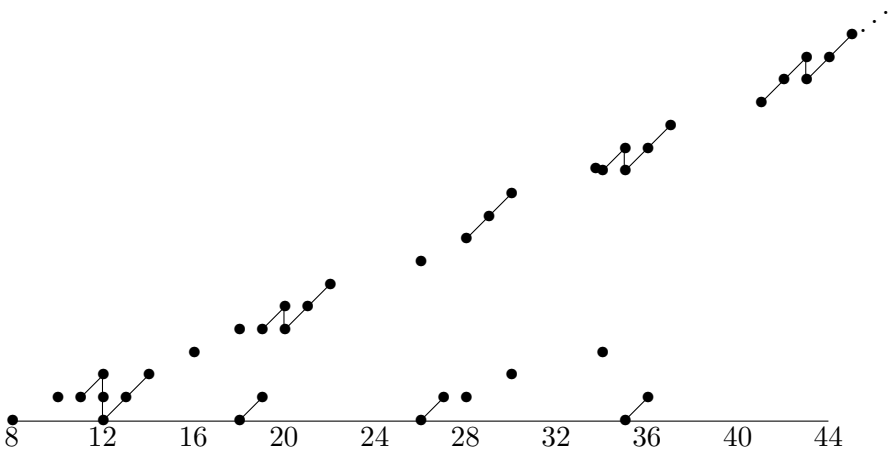

The behavior described in the detailed example just completed will continue regarding how differentials in the ko_* spectral sequence are implied by the $d_{2^{t+1}-(t+1)}$ ku_* differentials of Theorem 14.8, as t increases. It will

always be the case, as in nicely illustrated in Figure 14.11, that the potential differentials go stably from M_k into $\Sigma M_{k'}$ with at least one of k and k' equal to 4 and the other ≥ 4. The generator of $ko_3(M_k)$ is not in $\mathrm{im}(\eta)$ and hence maps across to $ku_3(M_k)$, and similarly for the generator of $ko_2(\Sigma M_{k'})$. Proposition 14.8 says that there will be a differential between the ku classes, and hence there will be a differential between the ko classes. Other differentials in the ko spectral sequence are implied by the action of η, v_1^4, and the generator of ko_4.

This completes the proof that the description of the spectral sequence given in Subsection 14.1, which implies Definition 4.8, is implied by Proposition 14.8. Also, the differentials in Theorem 4.10 follow since, in the notation of the preceding paragraph, a stable element in $ko_3(M_k)$ and $Q \in ko_2(\Sigma M_{k'})$ which satisfy $d_r(P) = Q$ yield differentials on nonzero classes $d_r(\eta P) = \eta Q$ and $d_r(\eta^2 P) = \eta^2 Q$, and all the differentials stated in Theorem 4.10 have v_1^{4i} equal to one of these. This is nicely illustrated in Figure 14.12.

Additional differentials can be ruled out using the action of η and v_1^4. Edges $\mathcal{E}_{e,\ell}$ tend to have less v_1^4 periodicity than edges above them. For example, in $\widetilde{\mathcal{A}}_6$ as shown in Figure 3.4, a conceivable differential on the class in $(74, 1)$ is ruled out by the action of v_1^4. The only possible short edges are shown in Figure 4.11, and the structure of longer edges is already suggested in Figures 4.12, 4.13, 4.14, and 4.15. Note that the lower edge of the chart of an edge, such as the circled elements in Figure 4.12, is v_1^4 periodic throughout the range of the chart, but the upper edge of the chart of an edge, such as the big dots in Figure 4.12, ceases to be v_1^4 periodic at each 2-power.

The upper edge $\mathcal{E}_{1,k}$ was discussed near the end of Section 13. It was stated there that we would "justify the placement of the $\Sigma^{2^i} M_4^0$'s in the sequence of Definition 4.18." In Sections 9 and 12, we gave a fairly complete treatment of the obtaining of the $\mathcal{A}_4$ chart, including the upper edge. Everything generalizes, but two things lacking there were the implication from ku_* differentials to ko_* differentials, as we have been doing for the lower edges in this section, and a thorough approach to the arrangement of summands, as in (13.1). The summands for $\widetilde{\mathcal{A}}_4$ are the first row of (13.1) with V_7 changed to V_4. The ku analogue of V_4 was derived in Figure 9.11 and appears in the right half of Figure 14.14, which shows the morphism c from $V_4 \leftarrow \Sigma^8 M_4^0$ to its ku analogue. We use big dots for classes that map across under c, the ones not in $\mathrm{im}(\eta)$. The differential in the ku chart was derived in Figure 9.12, and is reproduced in Figure 14.14, which incorporates the implied differentials in the ko chart.

Figure 14.14. c **for early part of** $\widetilde{\mathcal{A}}_4$

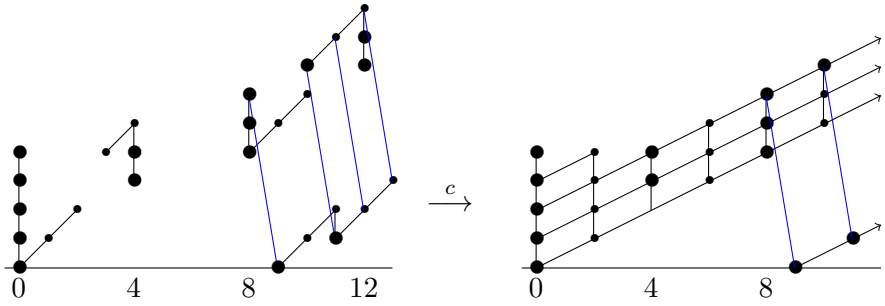

There is an η extension from grading 11 in the resulting chart, which is shown in the right side of Figure 12.4, in which filtrations have been increased to improve the picture. The second arrow of (13.1) results in $\Sigma^8\mathcal{E}'_{2,3} \oplus \Sigma^{16}M_4^0$ pictured in Figure 12.6 and in Figure 12.9 with a filtration shift. The differential from 17 to 16 in forming $\mathcal{E}_{1,4}$ in the ko spectral sequence, pictured in Figure 12.9, is implied by the d_9 in Figure 9.13. This all generalizes, showing how the upper edge is formed to yield Definition 4.18.

14.3. Justifying extensions. Finally, we prove Theorem 4.21, the exotic extensions. Recall that $\mathscr{A}_k$ denotes the ku_* version of $\mathcal{A}_k$, and $\widetilde{\mathscr{A}_k} = \Sigma^{-2^{k+1}}\mathscr{A}_k$. The extensions from $\Sigma^{2^\ell}\mathcal{E}_{2,\ell}$ into $\mathcal{E}_{1,k}$ stated in Theorem 4.21(1) follow from the exact sequence (12.10) and the extensions in $\widetilde{\mathscr{A}_k}$. The first extension for a fixed ℓ occurs in grading $3 \cdot 2^{\ell-1} + 2$, so grading $2^{\ell-1} + 2$ for $\mathcal{E}_{2.\ell}$. This is where the first lightning flash occurs for $\mathcal{E}'_{2,\ell}$. This can be seen in grading 26 and 50 in Figure 3.3 and in Figures 4.11 and 4.12. One can compare with the ku chart in Figure 1.2. We illustrate in Figure 14.15, in which the groups along the top are in $\mathcal{E}_{1,5}$, and those along the bottom are in $\Sigma^{2^\ell}\mathcal{E}_{2,\ell}$. The extension in ko is implied by the exact sequence.

Figure 14.15. Extensions from $\Sigma^{2^\ell}\mathcal{E}_{2,\ell}$ **into** $\mathcal{E}_{1,5}$

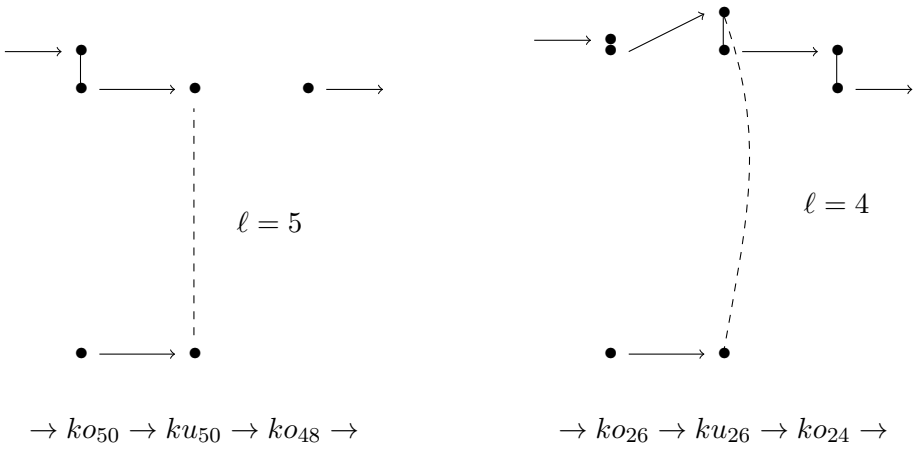

It always happens this way: the only two possibilities for the groups in the exact sequence are illustrated in Figure 14.15, and the ku extension

is implied by [11, Definition 1.5 and Theorem 1.23]. On the other hand, classes x in $\mathcal{E}_{2,\ell}$ in grading $2^{\ell-1}-8\Delta+2$ with $\Delta>0$ have $v_1^{4\Delta}x$ of filtration greater than that of the class in $2^{\ell-1}+2$ which supported the extension, so they cannot support an extension. That there are no other extensions into the upper edge is true because extensions cannot hit into elements x satisfying $\eta x\neq 0$, nor into elements already divisible by 2 (since this could be accounted for by renaming), nor into periodic elements along the lower portion of the upper edge. Because of the very nice form of the upper edge, one can verify that this rules out everything except for a possible extension from $\Sigma^{2^k}\iota_4$, where ι_4 is the bottom class of $\mathcal{E}_{2,k}$, into the last element of the only complete lightning flash in $\widetilde{\mathcal{A}}_k$, an element x such that v_1^4x is hit by a differential. But both of these elements in $ko_{2^k+4}(K_2)$ are in the image from $ku_{2^k+6}(K_2)$, where there is no extension.

To prove the extensions in part (2) of Theorem 4.21, we first note that for $e\geq 2$ all nonzero groups in $\mathcal{E}_{e,\ell}$ in grading $j\equiv 6 \bmod 8$ are $\mathbb{Z}_2$ groups, annihilated by η, and related to one another under v_1^4 periodicity. They pull back to $ku_{j+2}(K_2)$, where there are extensions between the pull-back elements, as can be seen from the inductive structure of the $\widetilde{\mathscr{A}_k}$'s, implying the extension from $\Sigma^{2^{\ell+1-e}}\mathcal{E}_{e+1,\ell}$ to $\mathcal{E}_{e,\ell}$.

There are two differences between the $\mathbb{Z}_2$'s in 2 mod 8 and those in 6 mod 8. In 6 mod 8, all classes are related by v_1^4 and are in $\ker(\eta)$, so they pull back to $ku_{*+2}(K_2)$ in (12.10). In grading 2 mod 8, they are related by v_1^4 until the next 2-power in Definition 4.8 or Theorem 7.6. The break points can also be thought of as the position a fraction $1/2^t$ along the edge for some $t\geq 1$. Also, in 2 mod 8 the classes are not in $\mathrm{im}(\eta)$, so they map across to $ku_*(K_2)$.

In grading 2 mod 8, the only things that can possibly extend into the last half of $\mathcal{E}_{e,k}$ are (the last half of) $\mathcal{E}_{e+d,k}$ for some $d>0$. The only things that can extend into the second quarter of it are (the last half of) $\mathcal{E}_{e+d,k-1}$ for some $d>0$. Similarly, for second eighth, $\mathcal{E}_{e+d,k-2}$, etc. However, if $d>1$, this portion of $\mathcal{E}_{e+d,\ell}$ will have already extended into $\mathcal{E}_{e+d-1,\ell}$. We illustrate this in a schematic Figure 14.16. It shows the edges beneath $\mathcal{E}_{2,7}$ and the key places where they drop their filtration in grading 2 mod 8 (halfway, one quarter, etc.). Extensions in grading 2 mod 8 occur from the second half of edges (where the lightning flashes start in $\mathcal{E}'$) into the edge immediately above them. Other portions of edges have their periodicity in 2 mod 8 end prior to that of the portion of the edge above them. The extensions are implied by the extensions in $ku_*(K_2)$ between the corresponding classes.

Figure 14.16. Schematic of edges under $\mathcal{E}_{2,7}$ in grading 2 mod 8

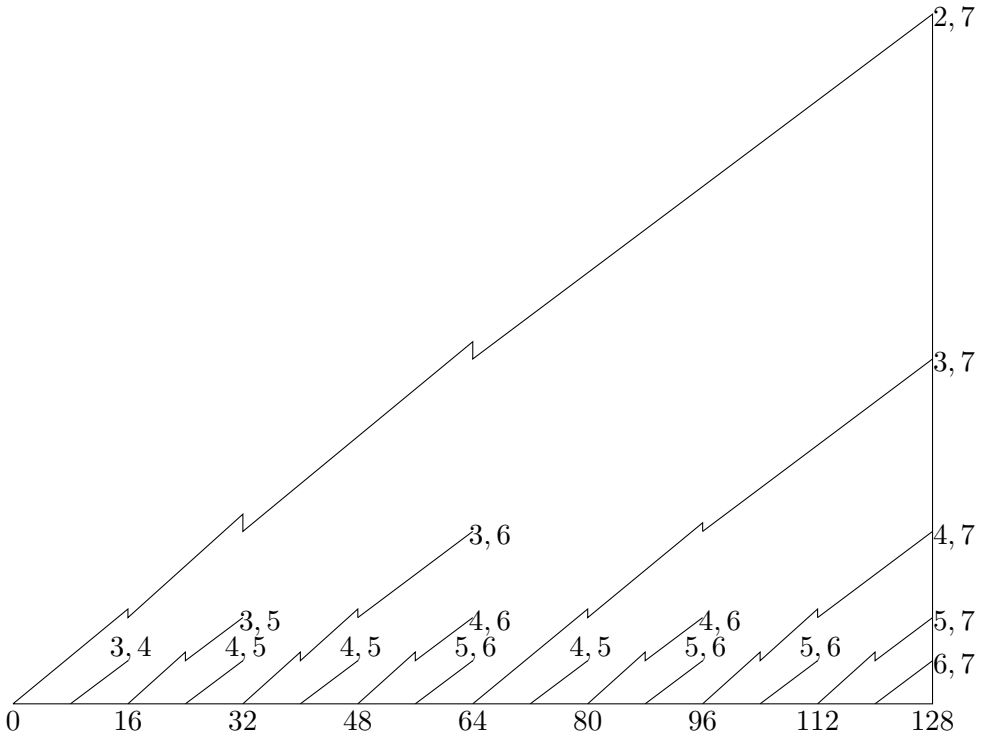

There is no extension from the last class in $\mathcal{E}_{e,e+d}$ when $e \equiv 3 \bmod 4$ because either there is nothing into which to extend, or else it would extend into an element x satisfying $\eta x \neq 0$.

Many extensions also follow from the following fact ([9, near (2.2)]) about Toda brackets and differentials in the Adams spectral sequence:

$$\text{if } d_r(\langle \alpha, 2, \eta \rangle) = \beta\eta, \text{ then } 2\alpha = \beta. \tag{14.17}$$

This bracket represents $v_1\alpha$; the generator of the $\mathbb{Z}/4$ in a lightning flash is obtained from the bottom class via this bracket. The situation in Figure 14.18 appears frequently, implying $2\alpha = \beta$. Often the classes $\alpha\eta$ and $\alpha\eta^2$ will be hit by differentials, but that doesn't matter.

Figure 14.18. Charts implying $2\alpha = \beta$

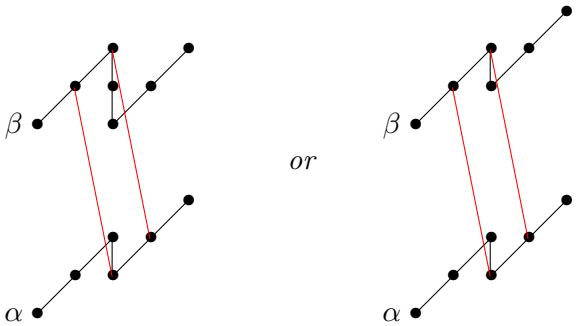

All other possible extensions can be ruled out by v_1^4 periodicity, as we have been using, the fact that $2\eta = 0$, and comparing with ku. Perhaps the

most subtle of these is illustrated by the situation involving $\mathcal{E}_{3,8}$ and $\Sigma^{64}\mathcal{E}_{4,8}$ in grading $64+12$. Using Figure 4.14, we illustrate the problem in Figure 14.19, in which $\mathcal{E}'_{3,8}$ has the lightning flashes, which should have much higher filtration, and the worrisome extension question involves classes A and B, indicated by big dots. The problem is that $v_1^4 B = 0$ (due to the differential) and A is not in $\mathrm{im}(\eta)$, so we cannot use v_1^4 or η to detect the non-extension..

Figure 14.19. $\mathcal{E}'_{3,8}$ and $\Sigma^{64}\mathcal{E}'_{4,8}$

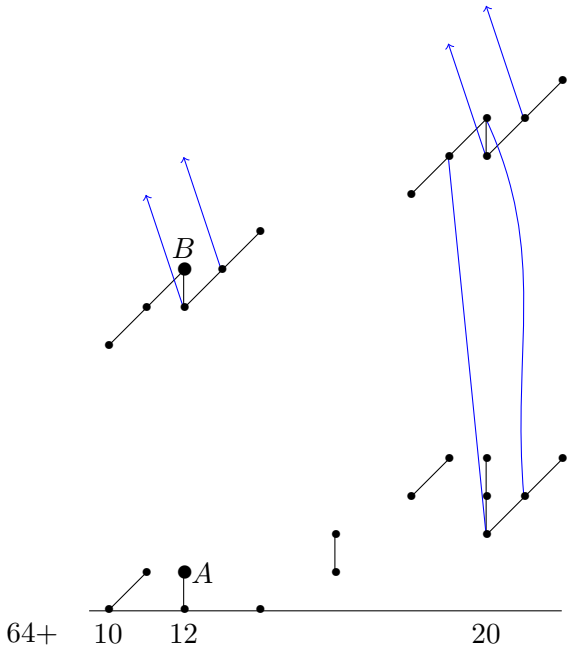

However, A pulls back to $ku_{*+2}(K_2)$, since $\eta A = 0$, and there is no extension on the pullback element, as the ku analogue of $\mathcal{E}_{4,8}$ begins as in Figure 14.20, with the first extension occurring on the element in grading 16. So $2A = 0$.

Figure 14.20. Beginning of ku analogue of $\mathcal{E}_{4,k}$

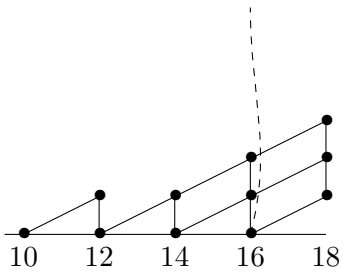

15. Proof for $z^i\mathcal{B}_{k,\ell}$

In this section, we prove Theorem 5.5. We have defined a ku version, $B_{k,\ell}$, of $\mathcal{B}_{k,\ell}$ via summands in Definition 10.2 and shown in Theorem 10.3 that these summands are what are required along with the A_k's to fill out the E_1-module $H^*(K_2)$, and we showed in Theorem 10.4 that each $B_{k,\ell}$ is closed

under the differentials of [11, Theorem 3.1]. It is worth noting, but perhaps not necessary, to point out that $B_{k,\ell}$ corresponds to $B_k z_\ell \oplus y_1^{2^{k-1}-1} q S_{k,\ell} \oplus y_k B_k Z_k^\ell$ in [11].

Most of our discussion will deal with the case $i = 0$ in $z^i \mathcal{B}_{k,\ell}$. We will comment briefly on the effect of i at the end of this section. In (11.5), we gave a general description of the corresponding ko summands, but we feel that the following explicit example, the summands for $\widetilde{\mathcal{B}}_{5,9}$, is useful in understanding the proof.

$$\begin{array}{cccc}
\Sigma M_7^5 \leftarrow \Sigma^8 M_4^4 & \Sigma^9 M_4^6 \leftarrow \Sigma^{16} M_5^4 & \Sigma^{17} M_5^6 \leftarrow \Sigma^{24} M_4^5 & \Sigma^{25} M_4^7 \leftarrow \Sigma^{32} M_6^4 \\
\Sigma^{33} M_6^6 \leftarrow \Sigma^{40} M_4^5 & \Sigma^{41} M_4^7 \leftarrow \Sigma^{48} M_5^5 & \Sigma^{49} M_5^7 \leftarrow \Sigma^{56} M_4^6 & \Sigma^{57} M_4^8 \leftarrow \Sigma^{64} M_{11}^0 \\
\Sigma^{65} M_{11}^2 \leftarrow \Sigma^{72} M_4^1 & \Sigma^{73} M_4^3 \leftarrow \Sigma^{80} M_5^1 & \Sigma^{81} M_5^3 \leftarrow \Sigma^{88} M_4^2 & \Sigma^{89} M_4^4 \leftarrow \Sigma^{96} M_6^1 \\
\Sigma^{97} M_6^3 \leftarrow \Sigma^{104} M_4^2 & \Sigma^{105} M_4^4 \leftarrow \Sigma^{112} M_5^2 & \Sigma^{113} M_5^4 \leftarrow \Sigma^{120} M_4^3 & \Sigma^{121} M_4^5 \leftarrow \Sigma^{128} M_7^1
\end{array} \tag{15.1}$$

If ℓ is increased by 1, the superscripts in the first two rows are increased by 1, except for the last term, whose subscript is increased by 1, while the last two rows remain unchanged except that the subscript of the first term (of the second half) is increased by 1.

What can be observed here, and is true in general using (11.5), is that $\widetilde{\mathcal{B}}_{k,\ell}$ has 2^k summands of which (a) the first half agree with those that form $\mathcal{E}_{\ell-k+1,\ell}$ and everything under it in $\widetilde{\mathcal{A}}_\ell$, and (b) the second half agree with the second half of $\widetilde{\mathcal{A}}_{k+1}$ except that the first summand is $\Sigma^{2^{k+1}+1} M_{\ell+2}^2$ instead of $\Sigma^{2^{k+1}+1} M_{k+2}^2$.[4] (Comparison of (15.1) and (13.1): first half of (15.1) with superscripts of all but last summand decreased by 2 equals Σ^{-192} of last two rows of (13.1), while (b) last two rows of (15.1) equals rows 3 and 4 of (13.1) except for the first (and last) summand.)

Part (2) of Theorem 5.5 follows readily from observation (a) above. The differentials among the summands which form $\mathcal{E}_{\ell-k+1,\ell}$ are the same regardless of whether the summands are appearing in $\widetilde{\mathcal{A}}_\ell$ or in $\widetilde{\mathcal{B}}_{k,\ell}$. There are two differences. One is that in $\widetilde{\mathcal{B}}_{k,\ell}$ there is not an edge $\mathcal{E}_{\ell-k,\ell}$ to be hit by the differentials in grading 4 and 5 mod 8 that occurred in $\widetilde{\mathcal{A}}_\ell$. The other has to do with what happens to the $\Sigma^{2^{k+1}} M_{\ell+2}^0$ at the end of the sequence of summands being considered. In neither case does it contribute to $\mathcal{E}_{\ell-k+1,\ell}$. In both cases, it has its subscript decreased $k-1$ times by differentials into lightning flashes in this batch of summands. In $\widetilde{\mathcal{A}}_\ell$, it continues to have its subscript decreased by differentials into lightning flashes formed by earlier edges. In $\widetilde{\mathcal{B}}_{k,\ell}$, it combines with part of the $\Sigma^{2^{k+1}+1} M_{\ell+2}^2$ which occurs at the beginning of the second half of the list of summands forming $\widetilde{\mathcal{B}}_{k,\ell}$ to form part (3) of Theorem 5.5 in a way that we shall discuss shortly.

We explain now why the filtration of $\Sigma^{2^{k+1}} M_{\ell-k+3}$, which is formed after the last summand of the first half of $\widetilde{\mathcal{B}}_{k,\ell}$ has its subscript reduced $k-1$ times, is increased by $2^k - k - 1$, as claimed in part (1) of the theorem. The first quarter of the summands of $\widetilde{\mathcal{B}}_{k,\ell}$ will have truncated the top part of the initial $\Sigma M_{k+2}^{\ell-k+1}$ chart $k-2$ times resulting stably in lightning flashes with initial classes in position $(8i+2, 4i-\ell+1)$. ⟦The initial class of ΣM_{k+2}^0 is in $(2,0)$, so stably the initial classes of $\Sigma M_{k+2}^{\ell-k+1}$ are in $(8i+2, 4i-(\ell-k+1))$, and the $k-2$ truncations of the top reduce the second component by $k-2$.⟧ Stably the last step in forming

[4] There is a difference in the last summand, too, $\Sigma^{2^{k+2}} M_{k+2}^1$ versus $\Sigma^{2^{k+2}} M_{k+3}^0$, which does not affect this part of the analysis.

$\Sigma^{2^{k+1}}M_{\ell-k+3}$ will be as depicted in Figure 15.2, where the lightning flash is the one just described, and the generator of the $\mathbb{Z}/2^{\ell-k+1}$'s in $\Sigma^{2^{k+1}}M_{\ell-k+3}$ will be the big dot. Since the generator of the $\mathbb{Z}/2^{\ell-k+1}$'s in $\Sigma^{2^{k+1}}M_{\ell-k+3}$ are in position $(2^{k+1}+3+8j, 2-\ell+k+4j)$, which must equal $(8i+3, 4i-\ell+1)$, we obtain that the difference in filtrations is $4i-\ell+1-(2-\ell+k+4j) = 2^k-k-1$, since $2^{k+1}+8j = 8i$.

Figure 15.2. Last step in forming $\Sigma^{2^{k+1}}M_{\ell-k+3}$

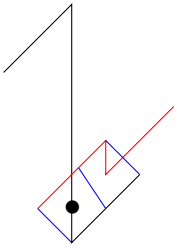

As noted earlier, the second half of the summands of $\widetilde{\mathcal{B}}_{k,\ell}$ agree with those of the second half of $\widetilde{\mathcal{A}}_{k+1}$ except that the first summand is $\Sigma^{2^{k+1}+1}M^2_{\ell+2}$ instead of $\Sigma^{2^{k+1}+1}M^2_{k+2}$.[5] The edge $\Sigma^{2^{k+1}}\mathcal{E}_{2,k+1}$ is formed from $\Sigma^{2^{k+1}+1}M^2_{k+2}$ by interactions with $\Sigma^{2^i}M^1_4$'s formed from the summands which follow it in $\widetilde{\mathcal{A}}_{k+1}$. The leftover parts of those summands form the edges under $\Sigma^{2^{k+1}}\mathcal{E}_{2,k+1}$. The same interactions will occur with $\Sigma^{2^{k+1}+1}M^2_{\ell+2}$, forming something that will contribute to $\Sigma^{2^{k+1}}C_{0,k}$ in part (3) of Theorem 5.5. The leftover parts from the subsequent summands will be the same here as they were in $\Sigma^{2^{k+1}}\mathcal{E}_{2,k+1}$, as stated in part (3) of the theorem.

The $\Sigma^{2^{k+1}+1}M^2_{\ell+2}$ is interacted with by $k-1$ $\Sigma^{2^i}M^1_4$'s, so that stably it is $\Sigma^{2^{k+1}+1}M_{\ell-k+3}$. Stably there must be differentials from this isomorphically to the $\Sigma^{2^{k+1}}M_{\ell-k+3}$ formed in the paragraph preceding Figure 15.2. As described in the paragraph preceding Figure 5.11 and illustrated there, we apply $(v_1^4)^{-1}$ to obtain additional differentials. To see that these differentials are d_{2^k}, we observe that the bottoms of the towers in the lower half of Figure 5.11 are like those of $M^2_{\ell+2}$, while those of the top half are those of $M^0_{\ell-k+3}$ with filtrations increased by 2^k-k-1. Noting that larger subscript of M causes smaller filtration of generators, we obtain that the difference in filtrations of generators is

$$2^k-k-1-(\ell-k+3)-(-(\ell+4)) = 2^k.$$

Since the differentials are d_{2^k} and $M_{\ell-k+3}$ has its filtrations increased by 2^k-k-1, all classes in $M_{\ell-k+3}$ of filtration $\le k$ will not be hit. Nor will the η-pairs along the upper edge until grading $2^{k+2}+2$, when the final truncation in the second half of the summands of $\widetilde{\mathcal{B}}_{k,\ell}$ will have occurred.

This covers parts (1), (3), and (4) of Theorem 5.5 when $i=0$, completing the proof in this case, except for some fine tuning.

- We explain the last sentence of part (3) by means of an example. In $\widetilde{\mathcal{B}}_{4,9}$, we have $\Sigma^{32}C_{0,4}$, which is the big dots in the bottom half of Figure 5.11, and the edges under $\Sigma^{32}\mathcal{E}_{2,5}$ together with differentials involving those subedges. You should compare the chart for $\mathcal{E}_{2,5}$ in Figure 4.11 with $C_{0,4}$. Upper edge elements of $\mathcal{E}_{2,5}$ inject. However, the classes in grading 27 and 28 indicated by big dots in Figure 4.11 are hit by differentials from $\Sigma^{16}\mathcal{E}'_{3,5}$.

[5]The difference in the last summand noted in the previous footnote affects $\mathcal{E}_{1,k+1}$ but not $\mathcal{E}_{2,k+1}$.

The meaning of the last sentence of part (3) of Theorem 5.5 is that the corresponding elements of $\Sigma^{32}C_{0,4}$ are also hit by differentials from $\Sigma^{48}\mathcal{E}'_{3,5}$.

- We explain Remark 5.6 via an example, $\widetilde{\mathcal{B}}_{3,7}$. The first half of the summands are
$$\Sigma M_5^5 \leftarrow \Sigma^8 M_4^4 \quad \Sigma^9 M_4^6 \leftarrow \Sigma^{16} M_9^0.$$
After the indicated d_2 differentials and a filtration shift of the second half, the picture will be as in Figure 15.3, where the portion from the first d_2 is in black and the second in red. The class in $(21, 4)$ is in the $\Sigma^{16}M_6^0$ part of $\Sigma^{16}C_{0,3}$, while the class in $(20, 3)$ is in the $\mathcal{E}'_{5,7}$ part of $\widetilde{\mathcal{B}}_{3,7}$.
- The exotic extensions in part (4) of the theorem follow from (14.17) and the differential from the next-to-top element of one tower to the top of another, like the ones from grading 52 and 60 in Figure 5.11. The extension and the exotic η extension of Remark 5.7 are nicely visualized in Figure 15.4. With P_3 the usual stunted real projective space, Figure 15.4 illustrates the easily-proved result that the cofiber of $P_3 \wedge bo \xrightarrow{2} P_3 \wedge bo$ equals $\Sigma^4 M \wedge bo \vee H$, where M is the mod-2 Moore spectrum and H a mod-2 Eilenberg MacLane spectrum. The diagram shows just the first few gradings of the cofiber sequence, and indicates the gradings both in the cofiber sequence and the corresponding elements in Figure 5.11 if filtrations of the bottom part were increased to make the d_{16} differential look like a d_1.

Figure 15.3. Result from first half of summands of $\widetilde{\mathcal{B}}_{3,7}$

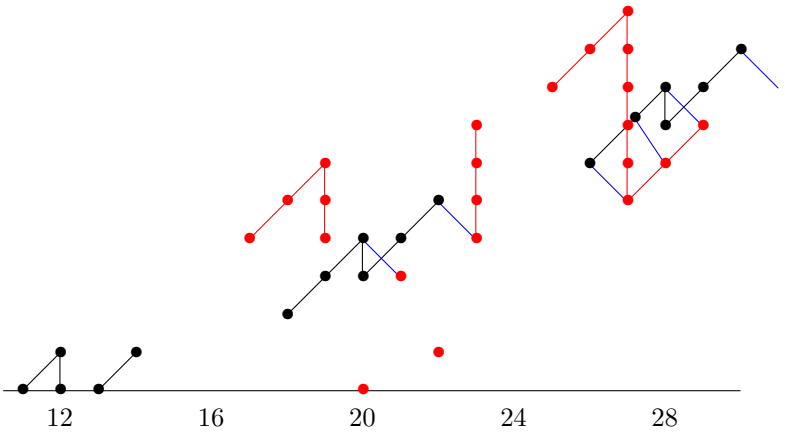

Figure 15.4. Cofiber of 2 on $P_3 \wedge bo$ equals $\Sigma^4 M \wedge bo \vee H$

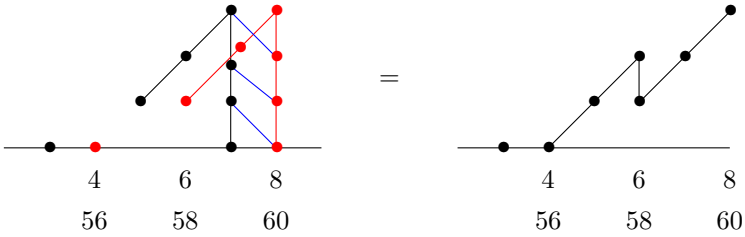

So far in this section, we have been dealing with $z^0\widetilde{\mathcal{B}}_{k,\ell}$. For $z^i\widetilde{\mathcal{B}}_{k,\ell}$, all summands are obtained from the corresponding summands of $\widetilde{\mathcal{B}}_{k,\ell}$ by increasing superscripts by i. The effect on edges $\mathcal{E}_{e,\ell}$ with $e > 1$ (which is all that is relevant for $\widetilde{\mathcal{B}}_{k,\ell}$) is to increase both subscripts by i. To see this, we first observe that all summands, except the last, in the tableau for $\mathcal{E}_{e+1,\ell+1}$ are obtained from those of $\mathcal{E}_{e,\ell}$ by increasing

all superscripts by 1. This is nicely illustrated in (13.1), in which rows 3 and 4 are the summands for $\mathcal{E}_{2,6}$, while rows 7 and 8 are the summands for $\mathcal{E}_{3,7}$. That the different possibilities for the last summand do not affect the edge is discussed in and around Figure 13.2 and (13.10).

The $\Sigma^{2^{k+1}} M^0_{\ell+2}$ and $\Sigma^{2^{k+1}+1} M^2_{\ell+2}$ in the middle of the tableau for $\widetilde{\mathcal{B}}_{k,\ell}$ are responsible for parts (1), (3), and (4) of Theorem 5.5. If both superscripts are increased by i, the filtration shift $(2^k - k - 1)$ required in forming Figure 15.2 is unchanged since both charts have their filtrations changed by the same amount.

The paragraph following Figure 15.2 explains that $C_{0,k}$ is formed from $\mathcal{E}'_{2,\infty}$ because the second half of the summands of $\widetilde{\mathcal{B}}_{k,\ell}$ (except the first) are the same as the first 2^{k-1} summands of $\Sigma^{2^{k+1}} \mathcal{E}_{2,\infty}$. Increasing the superscripts to form $z^i \widetilde{\mathcal{B}}_{k,\ell}$ causes the summands to be the same as those of $\Sigma^{2^{k+1}} \mathcal{E}_{2+i,\infty}$, which is relevant in Definition 5.3. The other thing relevant there is the function h_k, which is determined by the upper edge of the stable chart, which will be i units lower.

16. The exact ko_*-ku_* sequence

In this section, we discuss how the exact sequence (12.10) relating $ko_*(K_2)$ and $ku_*(K_2)$ can be used to justify the consistency of our results, and also to obtain additional information about $ko_*(K_2)$. There are three things that make these comparisons somewhat cumbersome.

(1) $ku_*(K_2)$ contains filtration-0 elements due to free E_1-module summands that are not part of free $A(1)$-module summands. These played a significant role in [11], and also play a significant role in analyzing the exact sequence (12.10). In Proposition 16.1, we explain exactly where these classes occur in terms of the $A(1)$-module summands with chart M^i_k, which we also denote here as M^i_k.

(2) We perform much shifting of filtrations in our determination of $ko_*(K_2)$. This is done to improve the appearance of the charts and to make η extensions easier to see. This causes the ko- and ku-charts to not match up as nicely as one might like.

(3) When elements of $ko_*(K_2)$ are involved in the homomorphism η and also in a differential in the ASS of $ko_*(K_2)$, that can cause ambiguity regarding filtration of classes.

Proposition 16.1. *The free E_1-module summands of the $A(1)$-module M^i_k have generators in grading*

$$\begin{aligned} &8j+2 \quad \text{if} \quad i = 4j+1 \\ &8j+3 \quad \text{if} \quad i = 4j+2 \\ &8j+4 \quad \text{if} \quad k+i = 4j+6 \\ &8j+5 \quad \text{if} \quad k+i = 4j+7. \end{aligned}$$

The $A(1)$-module NU in Figure 12.1, which is used in forming the charts V_k, has a single free E_1-module summand, with generator in grading 11.

Proof. The result for M^0_k is immediate from [13, Figure 2.3]. For each M^i_k, it is just a matter of drawing the $A(1)$-module that matches the Ext chart. We illustrate with M^1_9. The Ext charts for M^0_9 and M^1_9 are shown in Figure 16.2, and then the $A(1)$-module yielding the Ext chart for M^1_9 is in Figure 16.3.

Figure 16.2. Ext charts for M_9^0 and M_9^1.

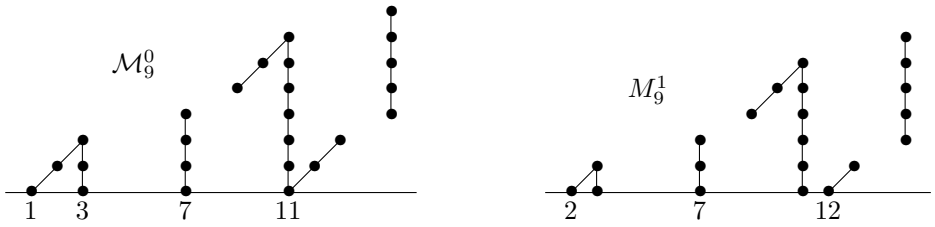

Figure 16.3. M_9^1.

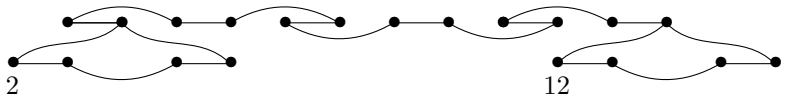

■

Our main example of the exact sequence (12.10) will be for $\widetilde{\mathcal{A}}_3$. In Figure 16.4, we present the ko and ku versions from Figure 3.1 and [8, Figure 2]. The tableau for $\widetilde{\mathcal{A}}_3$, from (11.2), is

$$V_3 \leftarrow \Sigma^8 M_4^0 \quad \Sigma^9 M_4^2 \leftarrow \Sigma^{16} M_5^0.$$

By Proposition 16.1, the ku version $\widetilde{\mathscr{A}_3}$ will have additional filtration-0 classes in gradings 3, 12, and 13, which have been incorporated into Figure 16.4.

Figure 16.4. $\widetilde{\mathcal{A}}_3$ and $\widetilde{\mathscr{A}_3}$.

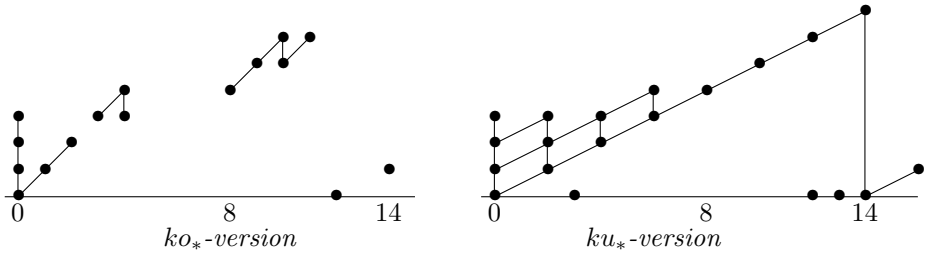

One convenient way of seeing how the exact sequence (12.10) can be used to relate $ko_*(X)$ and $ku_*(X)$ is to draw $ko_*(X) \oplus ko_*(\Sigma^2 X)$, with differentials for the action of η. What is left after the differentials should be $ku_*(X)$. We have done this for $\widetilde{\mathcal{A}}_3$ in Figure 16.5. In order to illustrate difficulty (3) listed at the beginning of this section, we have also included the classes involved in the d_7-differential from $\Sigma^8 \mathcal{E}'_{2,3}$ to $\mathcal{E}'_{1,3}$.

Figure 16.5. Forming $\widetilde{\mathscr{A}_3}$ from $\widetilde{\mathcal{A}}_3 \oplus \Sigma^2 \widetilde{\mathcal{A}}_3$.

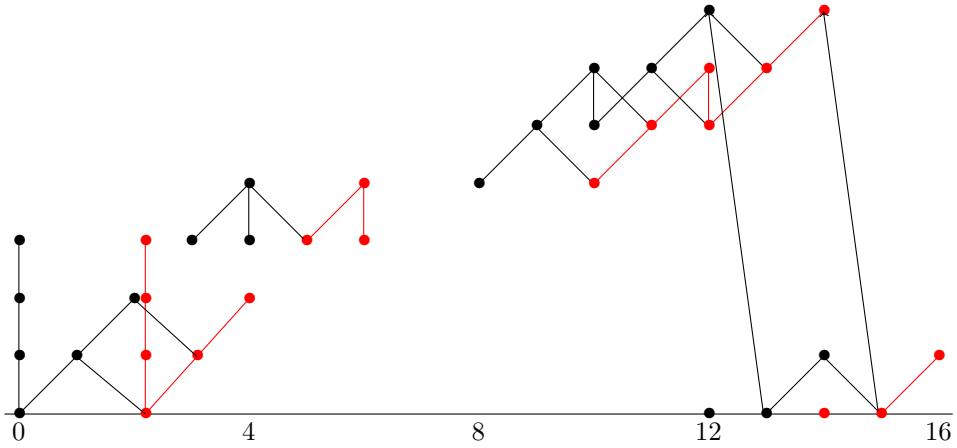

The classes which remain in the left half of Figure 16.5 agree with the left half of the ku chart in Figure 16.4 except for the filtration of the class in grading 3. The class in $(3,3)$ in $\widetilde{\mathcal{A}}_3$ was initially in filtration 0, but had its filtration increased to 3 for reasons discussed prior to Figure 12.3, so this is an example of difficulty (2) in the ko-ku comparison.

In the right side of Figure 16.5, note that two classes in grading 13 are hitting the top class in 12, one due to an Adams differential and the other due to the η homomorphism. If we had removed the classes involved in the Adams differential, it would have looked like the ku class in grading 13 should have filtration 6. But if we had removed the Ext classes involved in the η homomorphism first, then a filtration-0 class in 13 would be left, which is where it should be in the ku chart. Similarly, one class in grading 14 can be considered to have either filtration 1 or 7, depending on whether the η is considered before or after the Adams differential.

So you can see that the exact sequence works, but care is required. For our final example, we consider $\mathcal{B}_{3,4}$, but in much less detail. We compare Figures 5.1 and 5.2. Proposition 16.1 will add filtration-0 $\mathbb{Z}_2$'s to Figure 5.1 in grading 68, 70, 74, 78, 84, 90, 94, 98, and 100.

We make the following observations:

- The lightning flash in the middle of Figure 5.2 plus its double suspension with η differential exactly gives the v-tower from $(81,0)$ in Figure 5.1, but with filtration 4 larger.
- One justification for the filtration increases of the middle lightning flash and the high η pair in Figure 5.2 is that the last two classes in the middle lightning flash and the high η pair are both in $\mathrm{im}(v_1^4)$. This is not the case in the ku situation for parity reasons.
- One way to see that η is nonzero on the class in $(88,0)$ in Figure 5.2 is that the element in grading 89 must be in $\mathrm{im}(\eta)$ because it must map trivially in (12.10) since the ku group is 0 in grading 89.
- If the high η pair in 89 and 90 are lowered to filtration 1 and 2 and the η inserted on the class in $(88,0)$, the analogue of the analysis like that in Figure 16.5 is straightforward.

17. Consequences for Spin manifolds

In this section, we review the relationship of $ko_*(K_2)$ to Stiefel-Whitney classes and immersions of Spin manifolds, and prove Theorem 1.1, building on work done by the author and W.S.Wilson in [12].

The generalized homology theory associated to the Thom spectrum MSpin has the property that $\mathrm{MSpin}_n(K(\mathbb{Z}_2,t))$ is the set of cobordism classes of pairs (M,x), where M is an n-dimensional Spin manifold and $x \in H^t(M,\mathbb{Z}_2)$. ([3]) By [1], localized at 2, *bo* is a split summand of MSpin, and so $ko_n(K(\mathbb{Z}_2,t))$ is a direct summand of $\mathrm{MSpin}_n(K(\mathbb{Z}_2,t))$. In particular, all of the elements in our calculation of $ko_n(K_2)$ give cobordism classes of pairs, an n-dimensional Spin manifold M together with an element of $H^2(M;\mathbb{Z}_2)$.

The following result was proved in [11, Theorem 1.2].

Theorem 17.1. *Let $h : ko_*(X) \to H_*(X;\mathbb{Z}_2)$ denote the Hurewicz homomorphism. There exists an n-dimensional* Spin*-manifold M with nonzero dual Stiefel-Whitney class $\overline{w}_{n-t}(M)$ if and only if there exists an element $\alpha \in ko_n(K(\mathbb{Z}_2,t))$ such that $\langle \chi\,\mathrm{Sq}^{n-t}\,\iota_t, h_*(\alpha)\rangle \neq 0$.*

Here χ is the antiautomorphism of the Steenrod algebra, and ι_t is the fundamental class in $H^t(K(\mathbb{Z}_2,t);\mathbb{Z}_2)$.

Dual Stiefel-Whitney classes are important because if $\overline{w}_c(M) \neq 0$ for an n-manifold M, then M cannot be immersed in $\mathbb{R}^{n+c-1}$. Thus we have the following corollary of our new result, Theorem 1.1.

Corollary 17.2. *The values of n for which there exists an n-dimensional* Spin *manifold that does not immerse in $\mathbb{R}^{2n-3}$, detected by Stiefel-Whitney classes, are exactly all 2-powers ≥ 8.*

Proof of Theorem 1.1. It was shown in [12, Theorem 1.2] that a necessary condition for existence of an n-dimensional Spin-manifold M with $\overline{w}_{n-t}(M) \neq 0$ is $\chi\,\mathrm{Sq}^{n-t}\,\iota_t \notin \mathrm{im}(\mathrm{Sq}^1,\mathrm{Sq}^2)$, and in [12, Theorem 1.3] it was shown that $\chi\,\mathrm{Sq}^{n-2}\,\iota_2 \notin \mathrm{im}(\mathrm{Sq}^1,\mathrm{Sq}^2)$ if and only if n or $n-1$ is a 2-power ≥ 8. It was shown in [7] that $\chi\,\mathrm{Sq}^{2^{e+1}-1} = \mathrm{Sq}^{2^e}\,\mathrm{Sq}^{2^{e-1}}\cdots\mathrm{Sq}^1$ and $\chi\,\mathrm{Sq}^{2^{e+1}-2} = \mathrm{Sq}^{2^e}\,\mathrm{Sq}^{2^{e-1}}\cdots\mathrm{Sq}^2$.

Thus $\chi\,\mathrm{Sq}^{2^{k+1}-2}\,\iota_2 = \iota_2^{2^k}$. The bottom class of $\mathcal{A}_k$ is dual to ι^{2^k}. This follows from Definition 10.2 and the definition of $\widehat{A}_k^o$ in Section 11. Since the bottom class of $\mathcal{A}_k$ supports a nonzero subgroup of $ko_{2^{k+1}}(K_2)$ for $k \geq 2$, its generator gives the desired element α in Theorem 17.1 when $t = 2$.

On the other hand, for $k \geq 2$, the class of lowest grading in our $A(1)$-module $\mathcal{M}_{k+2}$ equals $\chi\,\mathrm{Sq}^{2^{k+2}-1}\,\iota_2$ mod decomposables. This follows from [13, Theorem 2.2] since

$$\mathrm{Sq}^{2^{k+1}}\cdots\mathrm{Sq}^1\,\iota_2 = u_{k+2},$$

a multiplicative generator of $H^*(K_2)$. By Definition 10.2 and its adaptation to $\widehat{A}_k^o$, $\mathcal{M}_{k+2}$ occurs at the end of $\widehat{A}_k^o$. Its class of lowest grading supports a differential. To see this, note that in Definition 4.18, $\mathcal{M}_{k+2}$ becomes the $\Sigma^{2^{k+1}}M_4^0$ at the end of the sequence defining $\mathcal{E}'_{1,k}$. ($\mathcal{M}_{k+2}$ has an additional $\Sigma^{2^{k+1}}$ since $\mathcal{E}'_{1,k}$ is for $\widetilde{\mathcal{A}}_k$, while $\widehat{A}_k^o$ is for $\mathcal{A}_k$.) In forming (4.19), $\Sigma^{-2^{k+1}}\mathcal{M}_{k+2}$ started as $\Sigma^{2^{k+1}}M_{k+2}^0$ but had its bottom cut down by differentials $k-2$ times, turning it into $\Sigma^{2^{k+1}}M_4^0$. Because of the differential on the class arising from $\chi\,\mathrm{Sq}^{2^{k+2}-1}\,\iota_2$, we deduce that when $n = 2^{k+2}+1$ with $k \geq 2$, there is no class that works as α in Theorem 17.1 with $t = 2$. The case $k = 1$ follows from the differential from grading 9 to 8 in Figure 12.11.

Using $\widetilde{\mathcal{A}}_4$ as an example, in Figure 4.20 the class in grading 33 is the class supporting the differential discussed here. It started as the $\Sigma^{32}M_6^0$ at the end of the first row of (13.1) but became M_4^0 after differentials into the $\Sigma^{25}M_4^3$ preceding it and into the resultant of the arrow preceding that. Its filtration was increased several times. ■

18. $ko^*(K_2)$

In this section, we state results regarding $ko^*(K_2)$ and several duality relationships. As we did for $ku^*(K_2)$ in [11], we depict charts with ko-cohomology grading increasing from right to left.

Definition 18.1. *We define $\mathcal{A}_k^*$ for $k \geq 2$ and $(z^i\mathcal{B}_{k,\ell})^*$ for $1 \leq k < \ell$ to be the ko-cohomology charts obtained by applying $\mathrm{Ext}_{A(1)}(\mathbb{Z}_2, -)$ to the $A(1)$-modules $\widehat{A}_k^o$ and $z^i\widehat{B}_{k,\ell}^o$ defined in Section 11, and incorporating differentials and extensions in the ASS, and filtration increases of the sort used above. Also $\widetilde{\mathcal{A}}_k^* = \Sigma^{-2^{k+1}}\mathcal{A}_k^*$ and $(z^i\widetilde{\mathcal{B}}_{k,\ell})^* = \Sigma^{-2^{\ell+2}}(z^i\mathcal{B}_{k,\ell})^*$. We define $\mathcal{A}_1^*$ by incorporating d_2 differentials into $\mathrm{Ext}_{A(1)}(\mathbb{Z}_2, U \oplus N)$, similarly to Figure 12.11.*

The proof of the following analogue of Theorem 1.3 is identical to that of Theorem 1.3, which appeared in Section 11.

Theorem 18.2. *There is an isomorphism of ko^*-modules*

$$ko^*(K_2) \approx \bigoplus_{k\geq 1}\bigoplus_{i\geq 0} \Sigma^{2^{k+2}i}\mathcal{A}_k^* \oplus \bigoplus_{1\leq k<\ell}\bigoplus_{i,j\geq 0} \Sigma^{2^{k+2}i+2^{\ell+3}j}(z^{\alpha(j)}\mathcal{B}_{k,\ell})^*$$

plus a trivial ko^*-module.

The next two results, which, with Theorem 18.2, determine $ko^*(K_2)$, are proved in Section 19.

Theorem 18.3. *For any i, there is an isomorphism of ko^*-modules*

$$(z^t\widetilde{\mathcal{B}}_{k,\ell})^* \approx (z^{4i-\ell-t}\widetilde{\mathcal{B}}_{k,\ell})_{2^{k+2}+8i+4-*}, \tag{18.4}$$

where $z^i\widetilde{\mathcal{B}}_{k,\ell}$ is as determined in Theorem 5.5.

The value of i is irrelevant since $(z^{r+4}\widetilde{\mathcal{B}}_{k,\ell})_{*+8} \approx (z^r\widetilde{\mathcal{B}})_*$. One would usually choose i so that $0 \leq 4i-\ell-t \leq 3$. Since $ko^* = ko_{-*}$, the right hand side of (18.4) is a ko^*-module. Since we picture $ko^*(-)$ charts with gradings increasing from right to left, the charts on both sides of (18.4) will look the same. For example, the charts in Figure 5.10 for $i = 1, 2, 3$ can be interpreted as charts of $(z^t\mathcal{B}_{3,4})^*$ for $t = 3, 2, 1$ if the indicated gradings x are replaced by $52 - x$.

Theorem 18.5. *For $t \geq 1$ and $\varepsilon \in \{1, 2\}$, $\widetilde{\mathcal{A}}_{2t+\varepsilon}^*$ is $(2^{2t+\varepsilon+1} + 8t + 4)$-dual to the chart described as follows. Let $e = 2t+2-\varepsilon$ and $\ell = 4t+1$, and $T = 2^{2t+\varepsilon+1}+8t-2$. For $e \leq e' \leq 4t$, let $D = 2^{\ell-e+2} - 2^{\ell-e'+2}$ and let $\Sigma^D\mathcal{E}_{e',\ell}^T$ be a modified version of $\Sigma^D\mathcal{E}'_{e',\ell}$ which extends the sequence of lightning flashes or portions thereof through grading T. The chart is formed from these together with all edges under them with second subscript $< \ell$, and including differentials and extensions among these edges and subedges as described in Theorems 4.10 and 4.21. There are additional differentials on the added lightning flashes with $e' < e$ on classes in grading 4 or 5 mod 8. There are additional classes x and y in positions $(T-1, 0)$ and $(T, 0)$, respectively, and also an element $\eta x = 2y$, with $d_2(x) \neq 0$. Finally, all of the new classes (except y and those in $\mathcal{E}_{e,\ell}^T$) have exotic extensions into the classes above them.*

For $k \leq 2$, $\widetilde{\mathcal{A}}_k^*$ does not quite fit the theorem. In Figures 18.7, 18.8, and 18.9, we display $\mathcal{A}_1^*$ and $\widetilde{\mathcal{A}}_k^*$ for $2 \leq k \leq 5$. Keep in mind that $\widetilde{\mathcal{A}}_k^*$ is always suspended by odd multiples of 2^{k+1} in $ko^*(K_2)$ if $k \geq 2$.

We illustrate the theorem with $\widetilde{\mathcal{A}}_5^*$. It is 84-dual to a chart which we now describe. For comparison, use Figure 18.9 with grading x replaced by $84 - x$. Start with $\mathcal{E}'_{5,9}$ in Figure 4.15 with its last lightning flash completed and followed by one more (in grading 74 to 78). The classes in Figure 4.15 with big dots are hit by differentials, but the ones with circles do not support differentials. Next we add $\Sigma^{32}\mathcal{E}'_{6,9}$, $\Sigma^{48}\mathcal{E}'_{7,9}$, and $\Sigma^{56}\mathcal{E}'_{8,9}$ (use Figure 4.11 with these replaced by $\Sigma^{40}\mathcal{E}'_{2,5}$, $\Sigma^{56}\mathcal{E}'_{3,5}$, and $\Sigma^{64}\mathcal{E}'_{4,5}$)[6] extended through grading 78, which means that the latter two must have lightning flashes completed, and one additional lightning flash added to $\Sigma^{40}\mathcal{E}'_{2,5}$ in grading 74 to 78. Big dots and circles in these will all take effect. Also add subedges of all of these with second subscript < 9, but do not extend them. Add classes x and y as in Theorem 18.5, and insert differentials and extensions as in Figure 18.6, in which the $\mathcal{E}_{5,9}$ part should be 11 higher.

Figure 18.6. Forming the end of the 84-dual of $\widetilde{\mathcal{A}}_5^*$

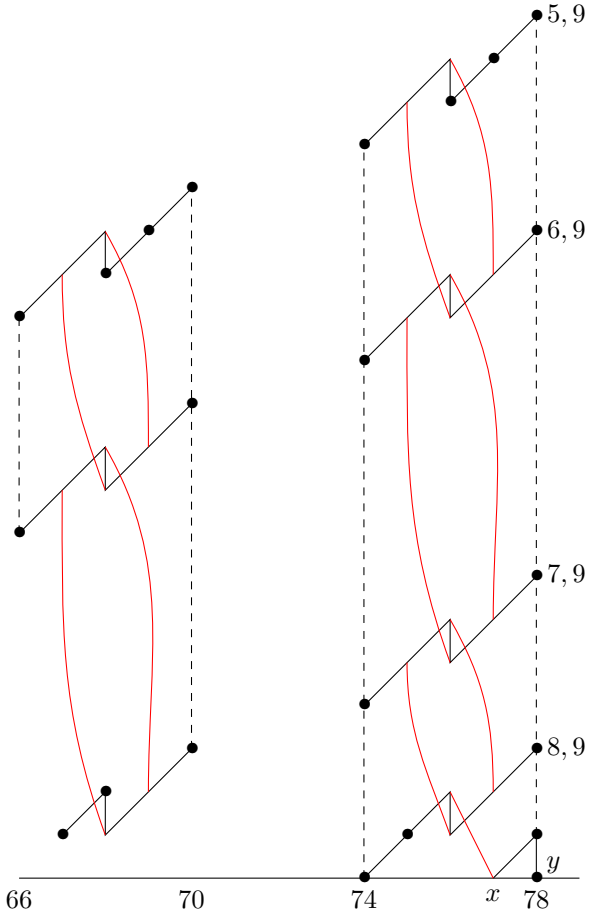

[6]The extra Σ^8 is due to increasing subscripts by 4.

Figure 18.7. Charts for $k \leq 3$

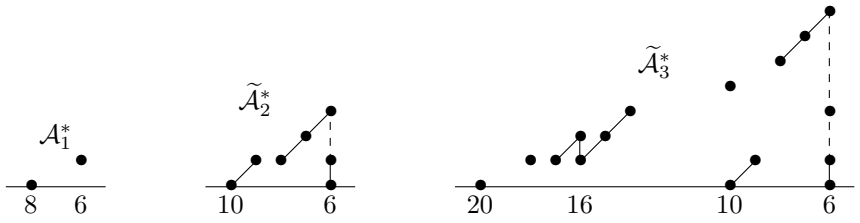

Figure 18.8. $\widetilde{\mathcal{A}}_4^*$

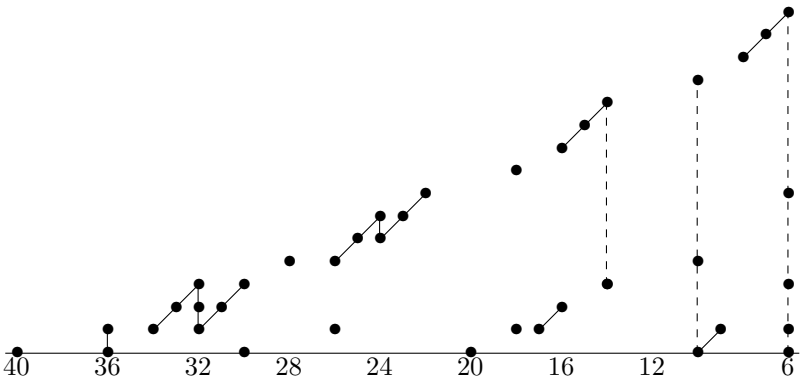

Figure 18.9. $\widetilde{\mathcal{A}}_5^*$

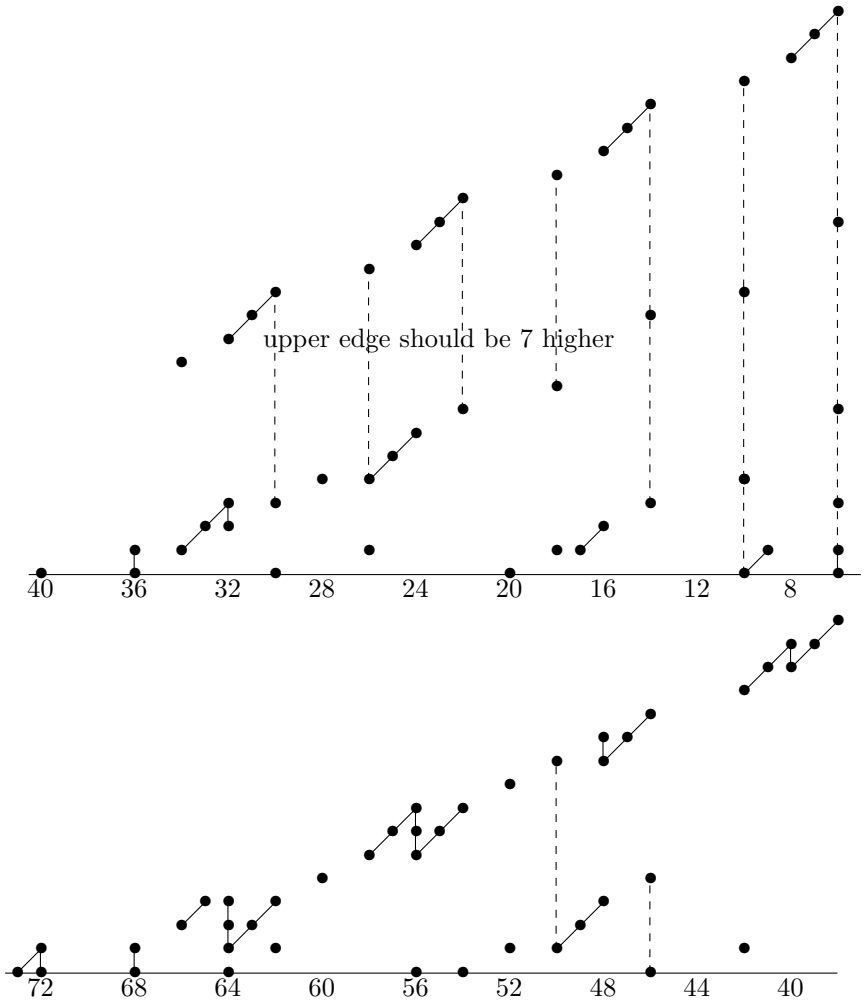

We close this section by discussing Theorem 1.4, which establishes duality between $ko_*(K_2)$ and $ko^*(K_2)$. Here is the proof of the theorem. Note that [14, Corollary 9.3] says that $R = ko$ satisfies the hypothesis of [8, Theorem 3.1] with $a = 6$, while $X = K_2$ has $ko_*(X)$ torsion-free by our calculation or by [2], implying Theorem 1.4 by [8, Theorem 3.1].

Similarly to an observation in Section 9, the actions of $\cdot 2$ and η in the Pontryagin dual appear backwards from the usual interpretation. The duality in Theorem 1.4 applies to each A_k. For example compare Figures 3.3 and 18.9. The actual A_5 would have gradings of each increased by 64. The generator g of $(ko^6(\widetilde{\mathcal{A}}_5^*))^\vee$ is the class in filtration 31. Then $2^5 g$ is the class in filtration 0, and $\eta^2 g \neq 0$. This corresponds to the class in position $(0, 0)$ in Figure 3.3. At the other end of the charts, the class g' in $(66, 0)$ in Figure 3.3 of order 4 with $\eta g' \neq 0$ corresponds to the class in $(72, 1)$ in the Pontryagin dual of Figure 18.9.

The duality in Theorem 1.4 also applies to each $z^t \widetilde{\mathcal{B}}_{k,\ell}$. Combining Theorems 1.4 and 18.3 yields

$$(z^t \widetilde{\mathcal{B}}_{k,\ell})_* \approx (z^t \widetilde{\mathcal{B}}_{k,\ell})^{*+6} \approx (z^{4i-\ell-t} \widetilde{\mathcal{B}}_{k,\ell})_{2^{k+2}+8i-2-*}. \tag{18.10}$$

This gives duality relations among $z^t \widetilde{\mathcal{B}}_{k,\ell}$ charts. For example, for $1 \leq t \leq 3$, let $i = 2$ and obtain

$$(z^t \widetilde{\mathcal{B}}_{3,4})_* \approx (z^{4-t} \widetilde{\mathcal{B}}_{3,4})_{46-*},$$

an isomorphism as ko_*-modules, using the dual action of ko_* on the right hand side. Refer to Figure 5.10. You can observe that the charts for $z\widetilde{\mathcal{B}}_{3,4}$ and $z^3\widetilde{\mathcal{B}}_{3,4}$ are 46-dual, and the chart for $z^2\mathcal{B}_{3,4}$ is 46-self-dual. Note how the exotic $\cdot 2$ and η extensions between gradings 32 and 34 in $z^2\widetilde{\mathcal{B}}_{3,4}$ are dual to the nice part of the chart between gradings 12 and 14. Using (18.10) with $\ell = 2\ell'$ and $t = 2i - \ell'$, we obtain the following generalization.

Proposition 18.11. *If ℓ is even and $t \equiv \frac{\ell}{2} \bmod 2$, then $z^t\widetilde{\mathcal{B}}_{k,\ell}$ is $(2^{k+2}+4t+2\ell-2)$-self-dual.*

19. Proofs of $ko^*(K_2)$ theorems

In this section, we prove Theorems 18.3 and 18.5. We begin by recalling from [13] results about $\mathrm{Ext}_{A(1)}(\mathbb{Z}_2, -)$ applied to the $A(1)$-modules in the splitting of $H^*(K_2)$.

For $k \geq 4$, let $\widetilde{\mathcal{M}}_k = \Sigma^{-2^k}\mathcal{M}_k$ be the $A(1)$-module introduced early in Section 11, and for $r \geq 0$ let M_k^{r*} denote the chart obtained by applying $\mathrm{Ext}_{A(1)}(\mathbb{Z}_2, -)$ to $\Sigma^{-4D}z_J\widetilde{\mathcal{M}}_k$, where $z_J\widetilde{\mathcal{M}}_k = z_{j_1}\cdots z_{j_r}\widetilde{\mathcal{M}}_k$ is a module defined in [13, Definition 3.3] and $D = \prod 2^{j_i}$. In Figure 19.1, we repeat [13, Figure 4.1], which shows M_k^{0*} for $5 \leq k \leq 7$, illustrating what we hope is an obvious pattern.

Figure 19.1. M_k^{0*}

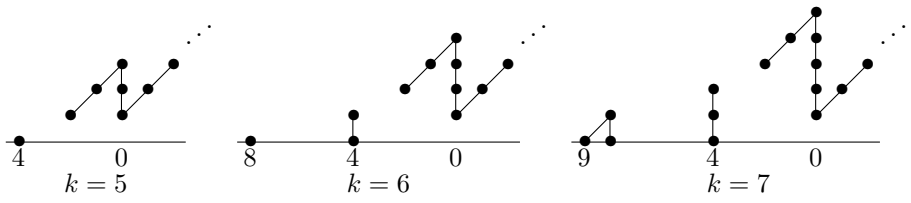

In [13, Proposition 2a] it is shown that M_k^{r*} is formed from M_k^{0*} by increasing all filtrations by r and extending to the left using v_1^4-periodicity. See Figure 19.2 for M_5^{2*}, formed from the left chart in Figure 19.1. Clearly $M_k^{(r+4)*} = \Sigma^8 M_k^{r*}$.

The tableau for $(z^t\widetilde{\mathcal{B}}_{k,\ell})^*$ is obtained from that of $z^t\widetilde{\mathcal{B}}_{k,\ell}$ by applying $*$ to all the summands, reversing the order of the list of summands, and reversing the direction of the arrows. For example, the first (of four) rows of $(\widetilde{\mathcal{B}}_{5,9})^*$ is obtained from (15.1) to be

$$\Sigma^{128}M_7^{1*} \leftarrow \Sigma^{121}M_4^{5*} \quad \Sigma^{120}M_4^{3*} \leftarrow \Sigma^{113}M_5^{4*}$$
$$\Sigma^{112}M_5^{2*} \leftarrow \Sigma^{105}M_4^{4*} \quad \Sigma^{104}M_4^{2*} \leftarrow \Sigma^{97}M_6^{3*}.$$

The following result says that if $i + j + k \equiv 0 \bmod 4$, then the charts M_k^i and M_k^{j*} are $(2(i + j + k) - 5)$-dual. We illustrate in Figure 19.2.

Figure 19.2. Dual M_5's.

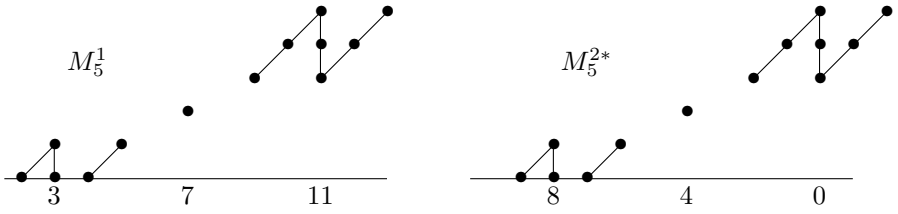

Proposition 19.3. *Let $S = i+j+k$. If $S \equiv 0 \bmod 4$, then $(M_k^i)_x \approx (M_k^{j*})^{2S-5-x}$.*

Proof. First note that M_k^{0*} leaves filtration 0 in the same way that M_k^i does when $k+i \equiv 0 \bmod 4$, by Figures 13.7 and 19.1. Since they have the same k, hence the same maximal heights, we deduce that if $k+i \equiv 0 \bmod 4$, then M_k^i and M_k^{0*} (drawn cohomologically) are isomorphic up to grading. Next note that M_{5+4t}^3, M_{6+4t}^2, M_{7+4t}^1, and M_{8+4t}^0 all leave filtration 0 in grading $11+8t$, while, for any k, M_k^{0*} does so in grading 0. With $S = 8+4t$ and $x = 11+8t$, $2S-5-x = 0$, so the gradings in the proposition work if $i \le 3$. Increasing i by 4 adds 8 to where M_k^i leaves filtration 0, so the proposition is true if $j = 0$.

If the proposition is true for (i,j,k), then it is true for all (i',j,k) with $i' \equiv i \bmod 4$, since increasing i by 4 suspends M_k^i by 8. Let (i,j,k) be arbitrary with $i+j+k \equiv 0 \bmod 4$. The proposition is true for $(i',0,k)$ with $i' \equiv i+j \bmod 4$ and $i' > j$. Since changing (i,j) from $(i',0)$ to $(i'-j,j)$ increases filtration by j in both M_k^i and M_k^{j*}, the proposition is true for $(i'-j,j,k)$ and hence also for (i,j,k). ∎

The proof of Theorem 18.3 follows from combining Proposition 19.3 with the observation preceding it about the tableau for $z^t\widetilde{\mathcal{B}}_{k,\ell}$. The details are a bit delicate, so we provide two examples.

The first four terms of the tableau for $(z^t\widetilde{\mathcal{B}}_{5,9})^*$ are

$$\Sigma^{128}M_7^{(1+t)*} \leftarrow \Sigma^{121}M_4^{(5+t)*} \quad \Sigma^{120}M_4^{(3+t)*} \leftarrow \Sigma^{113}M_5^{(4+t)*}.$$

By Proposition 19.3, this is isomorphic to

$$(M_7^{8-t})_{155-*} \leftarrow (M_4^{7-t})_{148-*} \quad (M_4^{9-t})_{147-*} \leftarrow (M_5^{7-t})_{140-*}.$$

This could also written as

$$(\Sigma M_7^{8-t})_{156-*} \leftarrow (\Sigma^8 M_4^{7-t})_{156-*} \quad (\Sigma^9 M_4^{9-t})_{156-*} \leftarrow (\Sigma^{16} M_5^{7-t})_{156-*},$$

which are the first four terms of the tableau for $(z^{3-t}\widetilde{\mathcal{B}}_{5,9})_{156-*}$ (see (15.1)), consistent with Theorem 18.3.

For a more general verification, we compare dual terms in (11.5). The $(2i+1)$st term in the first half of the tableau for $(z^t\widetilde{\mathcal{B}}_{k,\ell})^*$ is

$$\Sigma^{8(2^{k-1}-i-1)+8}(M_{4+\nu(2^{k-1}-1-i+1)}^{\alpha(2^{k-1}-1-i+1)-1+t})^* = \Sigma^{2^{k+2}-8i}(M_{4+\nu(i)}^{k-2-\alpha(i-1)+t})^*.$$

Since $\alpha(i) = \alpha(i-1)+1-\nu(i)$, Proposition 19.3 implies that this equals

$$(M_{4+\nu(i)}^{-k-t+\alpha(i)+1+4j})_{2^{k+2}-8i+8j+3-*}, \tag{19.4}$$

where j is chosen so that $-k-t+\alpha(i)+1+4j \ge 0$. The $(2i+1)$st term in the first half of the tableau for $(z^{4j-\ell-t}\widetilde{\mathcal{B}}_{k,\ell})_{2^{k+2}+8j+4-*}$ is

$$(\Sigma^{8i+1}M_{4+\nu(i)}^{\ell-k+\alpha(i)+1+4j-\ell-t})_{2^{k+2}+8j+4-*}.$$

With a little manipulation, this equals (19.4).

Proof of Theorem 18.5. It is easy to verify, using Proposition 19.3, that the tableau for $\widetilde{\mathcal{A}}_{2t+\varepsilon}^*$ is $(2^{2t+\varepsilon+1}+8t+4)$-dual to that of $\mathcal{E}'_{2t+2-\varepsilon,4t+1}$, except at the right end. We illustrate with $\widetilde{\mathcal{A}}_5^*$. We write each row of the tableau for $\mathcal{E}'_{5,9}$ directly beneath that of $\widetilde{\mathcal{A}}_5^*$, and observe the 84-duality, since $84 = 65 + (2\cdot 12 - 5)$.

$$\begin{array}{cccc} \Sigma^{64}M_7^{0*} \leftarrow \Sigma^{57}M_4^{4*} & \Sigma^{56}M_4^{2*} \leftarrow \Sigma^{49}M_5^{3*} & \Sigma^{48}M_5^{1*} \leftarrow \Sigma^{41}M_4^{3*} & \Sigma^{40}M_4^{1*} \leftarrow \Sigma^{33}M_6^{2*} \\ \Sigma M_7^5 \overset{5,9}{\leftarrow} \Sigma^8 M_4^4 & \Sigma^9 M_4^6 \overset{6,7}{\leftarrow} \Sigma^{16} M_5^4 & \Sigma^{17} M_5^6 \overset{6,8}{\leftarrow} \Sigma^{24} M_4^5 & \Sigma^{25} M_4^7 \overset{7,8}{\leftarrow} \Sigma^{32} M_6^4 \end{array} \tag{19.5}$$

$$\begin{array}{cccc} \Sigma^{32}M_6^{0*} \leftarrow \Sigma^{25}M_4^{3*} & \Sigma^{24}M_4^{1*} \leftarrow \Sigma^{17}M_5^{2*} & \Sigma^{16}M_5^{0*} \leftarrow \Sigma^{9}M_4^{2*} & \Sigma^{8}M_4^{0*} \leftarrow V_5^* \\ \Sigma^{33}M_6^{6} \overset{6,9}{\leftarrow} \Sigma^{40}M_4^{5} & \Sigma^{41}M_4^{7} \overset{7,8}{\leftarrow} \Sigma^{48}M_5^{5} & \Sigma^{49}M_5^{7} \overset{7,9}{\leftarrow} \Sigma^{56}M_4^{6} & \Sigma^{57}M_4^{8} \overset{8,9}{\leftarrow} \Sigma^{64}M_{11}^{0} \end{array} \tag{19.6}$$

The chart V_k^* is formed from $\mathrm{Ext}_{A(1)}(\mathbb{Z}_2, \mathbb{Z}_2 \oplus \Sigma^{-8}NU)$ with d^{k+1} differentials, similarly to V_k discussed early in Section 12. The module NU is shown in Figure 12.1, and $\mathrm{Ext}_{A(1)}(\mathbb{Z}_2, \Sigma^{-8}NU)$ is easily calculated to be the black part of Figure 19.7, which includes $\mathrm{Ext}_{A(1)}(\mathbb{Z}_2, \mathbb{Z}_2)$ in red, and a d^6 differential, relevant for V_5^*. The right side of Figure 19.7 shows the result after filtrations are increased to make the differential a d^1. Except for the classes in grading 6 and 7, it looks like a Moore spectrum $M(2^{k-1})$. The η extension from -2 to -3 follows from (12.2).

Figure 19.7. Forming V_5^*

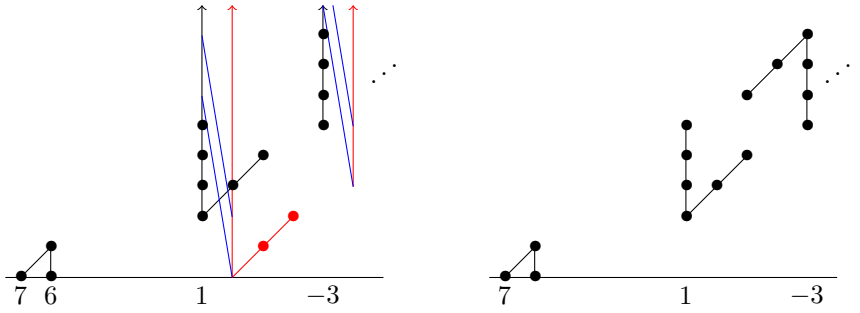

We illustrate the proof using $k = 5$, but the argument clearly generalizes. It seems easiest to use the gradings of $\mathcal{E}'_{5,9}$ and dualize $(84 - *)$ the gradings of $\widetilde{\mathcal{A}}_5^*$. Until the end part of their tableaux (V_5^* or $\Sigma^{64}M_{11}^0$), the charts and differentials in forming $\widetilde{\mathcal{A}}_5^*$ and $\mathcal{E}'_{5,9}$ are the same. In Figure 19.8, we compare V_5^* (with the dual gradings) and $\Sigma^{64}M_{11}^0$. Note especially that their lower edges agree in grading ≥ 83.

Figure 19.8. Comparing V_5^* and $\Sigma^{64}M_0^{11}$

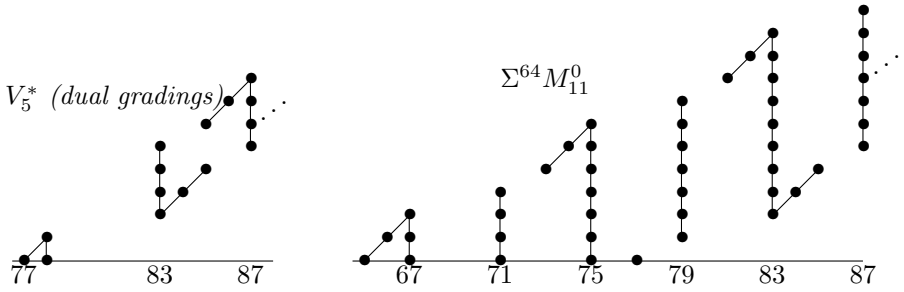

In forming $\mathcal{E}'_{5,9}$, the $\Sigma^{64}M_{11}^0$ will be modified four times, to $\Phi\Sigma^{64}M_{10}^0$, then $\Phi^3\Sigma^{64}M_9^0$, then $\Phi^7\Sigma^{64}M_8^0$, and finally $\Phi^{15}\Sigma^{64}M_7^0$, by having its lower edge hit a lightning flash with a d^1. These lightning flashes are first $\Sigma^{57}M_4^8$, then the result of the $\overset{7,9}{\leftarrow}$ preceding it, then the result of the first two arrows of the second row of (19.6), and finally the result of the arrows in the second row of (19.5). This hitting into lightning flashes will also take place in forming $\widetilde{\mathcal{A}}_5^*$, each time reducing the $M(2^4)$ by one 2-power, until after four such d^1's, it has vanished (except for the classes in 77 and 78).

The difference between forming $\mathcal{E}'_{5,9}$ and $\widetilde{\mathcal{A}}^*_5$ is that prior to grading 83 these four stable lightning flashes, which in forming $\mathcal{E}'_{5,9}$ were interacting with parts of the modifications of $\Sigma^{64}M^0_{11}$, have nothing to interact with in forming $\widetilde{\mathcal{A}}^*_5$. So they are present in $\widetilde{\mathcal{A}}^*_5$, as extensions of sequences of lightning flashes that were modified in forming $\mathcal{E}'_{5,9}$. Beginning in grading 82, they are terminated. The differentials and extensions among these lightning flashes follow for many reasons: v_1^4-periodicity from earlier ones, comparison with ku, or Toda bracket arguments.

■

20. Appendix: Notation and some terminology

In this appendix, we list our specialized notation and a few items of terminology, in roughly alphabetical order.

A_k	§1	summand of $ku^*(K_2)$
$\mathcal{A}_k$	§1	ko_* analogue of A_k
$\widetilde{\mathcal{A}}_k$	§2, Thm.4.1	$\Sigma^{-2^{k+1}}\mathcal{A}_k$
$\mathscr{A}_k$	§1, §12	ku_* analogue of A_k
$\widetilde{\mathscr{A}_k}$	§13.3	$\Sigma^{-2^{k+1}}\mathscr{A}_k$
$\mathcal{A}^*_k$	Def.18.1	ko^* analogue of A_k
$\widetilde{\mathcal{A}}^*_k$	Def.18.1	$\Sigma^{-2^{k+1}}\mathcal{A}^*_k$
$\widehat{A}_k$	Def.10.2	E_1-submodule of $H^*(K_2)$ corresponding to A_k
$\widehat{A}^o_k$	§10	$A(1)$-module analogue of $\widehat{A}_k$
$A(1)$	§10	subalgebra of Steenrod algebra generated by Sq^1 and Sq^2
$\alpha(n)$	§1	number of 1's in binary expansion of n
ASS	§1	2-primary Adams spectral sequence
B_k	§1	summand of $ku^*(K_2)$
$B_{k,\ell}$	§4	summand of $ku^*(K_2)$ corresponding to two B_k's and $S_{k,\ell}$
$\mathcal{B}_{k,\ell}$	§1, §4	ko_* analogue of $B_{k,\ell}$
$\widetilde{\mathcal{B}}_{k,\ell}$	§4	$\Sigma^{-2^{\ell+2}}\mathcal{B}_{k,\ell}$
$\widehat{B}_{k,\ell}$	Def.10.2	E_1-submodule of $H^*(K_2)$ corresponding to $B_{k,\ell}$
$\widehat{B}^o_{k,\ell}$	§10	$A(1)$-submodule of $H^*(K_2)$ corresponding to $\mathcal{B}_{k,\ell}$
$b_i(M)$	§9	ith generator or v-tower from bottom of an E_1-module M
c	§11	complexification $ko \to ku$
C_k	Def.10.1	a certain E_1-submodule of $H^*(K_2)$
$C_{i,k}$	Def.5.3	a chart which appears in $z^i\widetilde{\mathcal{B}}_{k,\ell}$
d^r	§8	differential in ASS for $ku^*(K_2)$, increasing y by r
d_r	§8	differential in ASS for $ku_*(K_2)$, increasing y by r
$\mathcal{E}_{e,\ell}$	§3, Thm.7.6	edges which form $ko_*(K_2)$ and $ko^*(K_2)$
$\mathcal{E}'_{e,\ell}$	Def.4.8	pre-edges: $\mathcal{E}_{e,\ell}$ prior to certain differentials
E_1	§8	subalgebra of Steenrod algebra generated by Q_0 and Q_1
E_2 page	§7, §9	the initial stage of a spectral sequence
η	§2	nonzero element of ko_1 (corresponds to Hopf map)

$f_b(i)$	Thm.7.6, Table 1	function telling how many classes hit by differentials
Φ^i	Def.14.1	increases filtration of a chart by i
Γ_k	§9	exterior algebra on $\{y_i : i \geq k\}$
h_0, h_1	§11	elements in Ext corresponding to 2 and η
h_k	Def.5.3	a height function
$H^*(-)$	§8	cohomology with $\mathbb{Z}_2$ coefficients
I_k	Def.7.1	$\mathcal{E}_{1,k}$ in grading < 8
$J(k,i)$	Def.10.1	a useful function
K_2	§1	Eilenberg-MacLane space $K(\mathbb{Z}_2, 2)$
ko_*	§1	connective KO homology
ko^*	§1	connective KO cohomology
ku_*	§1	connective KU homology
ku^*	§1	connective KU cohomology
$K_{t,\varepsilon}(x,y)$	Def.7.4	charts depicted in Figure 7.5
$L(8a)$	§13.1	label of $W^{8a-7} \leftarrow W^{8a}$
$L_{t,\varepsilon}(x,y)$	Def.7.1	charts depicted in Figure 7.2
Λ_k	§8	exterior algebra on $\{z_i : i \geq k\}$
$\lg(i)$	Thm.7.3	$[\log_2(i)]$
lightning flash	§1	a frequently-occurring chart with 6 classes
M_k	§8	E_1-modules from [11]
M_k	§9	ku^* chart for the module M_k
$\mathcal{M}_k$	§10	$A(1)$-module corresponding to M_k
$\widetilde{\mathcal{M}}_k$	§10	$\Sigma^{-2^k}\mathcal{M}_k$
M_k^i	§3	ko_* chart for $\widetilde{\mathcal{M}}_k$ with filtrations decreased by i
M_k^i	§15	$A(1)$-module with chart M_k^i
M_k^i	§13.2	ku analogue of the chart M_k^i
M_k^{i*}	§18	ko-cohomology analogue of M_k^i
$\widehat{M}_4^s$	Def.4.5	M_4^s with 0 or 1 classes adjoined
stably M_k	Def.4.7, §13	the behavior of any M_k^i in large gradings
$M(n)$	Def.4.18, §12	mod n Moore spectrum or $ko_*(M(n))$
MSpin	§16	Spin cobordism spectrum
N	Figure 9.5	an E_1-module which admits structure of $A(1)$-module
NU	§10	an $A(1)$-module corresponding to the E_1-module y_1N
$\nu(n)$	§9	the exponent of 2 in n
P	§10	the Poincaré series of a graded vector space
pre-edge	Def.4.8	generic term for $\mathcal{E}'_{e,\ell}$
$M^\vee$	§1, §8, §17	The Pontryagin dual, $\mathrm{Hom}(M, \mathbb{Z}/2^\infty)$, of M
q	§8	an element of $H^9(K_2)$
Q_0	§8	another name for Sq^1
Q_1	§8	the Milnor primitive $\mathrm{Sq}^3 + \mathrm{Sq}^2\,\mathrm{Sq}^1$

R	§6	ko_* in grading 0, 1, and 2
Σ^i	throughout	i-fold suspension, raises grading by i
Sq^i	§10, §13.2, §16	generators of the Steenrod algebra
$S_{k,\ell}$	§1	a factor of summands of $ku^*(K_2)$
$\tau_i(M)$	§9	ith generator or v-tower from top of an E_1-module M
U	§10	$A(1)$-module corresponding to y_1
v	§8	generator of ku^{-2} or ku_2; Bott periodicity element
v-tower	§1, §8	portion of a ku^* or ku_* chart consisting of elements $v^i x$
v_1^4	§3	filtration-4 element of ko_8; Adams periodicity element
V_k	Def.4.18	initial step in forming $\mathcal{E}_{1,k}$
$\overline{w}_i$	Thm.1.1, 17.1	dual Stiefel-Whitney classes
W^n	§13.1	$\Sigma^n M$ term in a tableau
W_i^n	§13.1	W^n with subscript of M decreased by i
χ	§16	the antiautomorphism of the Steenrod algebra
y_1	§8	element of $H^4(K_2)$
y_k	§9	$y_1^{2^{k-1}}$
$Y_{j,k}$	§9	term in C_k containing y_1^j as factor
$\mathbb{Z}_2$	§1	group of order 2
z_j	§8, §9	an element of $H^{2^{j+2}+2}(K_2)$
$z_{i,j}$	§9	$z_i^2 z_{i+1}\cdots z_{j-1}$
Z_k^ℓ	§9	$z_k z_{k+1}\cdots z_{\ell-1}$
$z_J\mathcal{M}_k$	§10	$= z_{j_1}\cdots z_{j_r}\mathcal{M}_k$ is an $A(1)$-module from [13]
z^i	§4	product of i distinct $\Sigma^{-2^{j+2}} z_j$'s
$z^i\mathcal{B}_{k,\ell}$	§1, §4, §10	chart like $\mathcal{B}_{k,\ell}$ but built from M_b^{a+i}
$z^i\widetilde{\mathcal{B}}_{k,\ell}$	§4, §10, §14	$\Sigma^{-2^{\ell+2}} z^i\mathcal{B}_{k,\ell}$
$z^i\mathcal{B}^*_{k,\ell}$	§17	ko^* analogue of $z^i\mathcal{B}_{k,\ell}$
$z^i\widetilde{\mathcal{B}}^*_{k,\ell}$	§17	ko^* analogue of $z^i\widetilde{\mathcal{B}}_{k,\ell}$
$z(n)$	Def.10.1	$\prod z_{j_i}$ where $n = \sum 2^{j_i}$

References

[1] Anderson, Donald W.; Brown, Jr., Edgar.H.; Peterson, Franklin P. The structure of the Spin cobordism ring, *Annals of Math* **86** (1967) 271–298. MR0219077, Zbl 0156.21605.

[2] Anderson, Donald W.; Hodgkin, Luke. The K-theory of Eilenberg-MacLane complexes, *Topology* **7** (1968) 317–329. MR0231369, Zbl 0199.26302

[3] Atiyah, Michael F. Bordism and cobordism, *Math Proc Camb Phil Soc*, **57** (1961) 200–208. MR0126856, Zbl 0104.17405

[4] Browder, William. Torsion in H-spaces, *Annals of Math*, **74** (1961) 24–51. MR0124891, Zbl 0112.14501

[5] Clement, Alain. Integral cohomology of finite Postnikov towers, thesis, Univ of Lausanne (2002), available online.

[6] Davis, Donald M. Generalized homology and the generalized vector field problem, *Quar Jour Math Oxford* **25** (1974) 169–193. MR0356053

[7] ———, The antiautomorphism of the Steenrod algebra, *Proc Amer Math Soc* **44** (1974) 235–236. MR0328934, Zbl 0256.55016

[8] Davis, Donald M.; Greenlees, John P.C. Gorenstein duality and universal coefficient theorems, *Jour Pure Appl Alg* **227** (2023) paper 107265, 12 pp. MR4513876, Zbl 1512.55020, doi:10.1016/j.jpaa.2022.107265

[9] Davis, Donald M.; Mahowald, Mark. v_1-periodic homotopy of $Sp(2)$, $Sp(3)$, and S^{2n}, Lecture Notes in Math, 1418, *Springer-Verlag* (1990) 219–237. MR1048189, Zbl 0708.55009.

[10] Davis, Donald M.; Ravenel, Douglas C.; Wilson, W. Stephen. The connective Morava K-theory of the second mod p Eilenberg-MacLane space, *Jour Pure Appl Alg* (2026) doi:10.1016/j.jpaa.2026.108171 arXiv:2206.14035

[11] Davis, Donald M.; Wilson, W. Stephen The connective K-theory of the Eilenberg-MacLane space $K(\mathbb{Z}_p, 2)$, *Glasgow Math Jour* **66** (2024) 188-220. Zbl 1539.55014, doi:10.1017/50017089523000423.

[12] ———, Stiefel-Whitney classes and immersions of orientable and Spin manifolds, *Topology and Appl* **307** (2022) paper 107780, 14 pp. MR4365043, Zbl 1487.57040, doi:10.1016/j.topol.2021.107780.

[13] ———, The connective KO-theory of the Eilenberg-MacLane space $K(\mathbb{Z}_2, 2)$, I, the E_2 page, *Jour Htpy Related Str*, **20** 2025 511–521, MR4984184, Zbl 08123841, doi:10.1007/s40062-025-00379-4, arXiv:2410.23094.

[14] Mahowald, Mark; Rezk, Charles. Brown-Comenetz duality and the Adams spectral sequence, *Amer Jour Math* **121** (1999) 1153–1177. MR1719751, Zbl 0942.55012.

[15] Wilson, W. Stephen. A new relation on the Stiefel-Whitney classes of Spin manifolds, *Ill Jour Math* **17** (1973) 115–127. MR0310883, Zbl 0246.57012

Department of Mathematics, Lehigh University, Bethlehem, PA 18015, USA
dmd1@lehigh.edu